EXPERIMENTAL TESTS OF ELECTROWEAK THEORIES

AT MARK-J

by

HE SHENG CHEN

Submitted to the Department of Physics
in Partial Fulfilment of the

Requirement for the
Degree of

DOCTOR OF PHILOSOPHY

at the

MASSACHUSETTS INSTITUTE OF TECHNOLOGY

June 1984

Signature of Author Signature redacted
Department of Physics
June 1984

Certified by Signature redacted
Samuel C.C. Ting
Thesis Supervisor

Accepted by Signature redacted
George F. Koster
Chairman, Department Graduate Committee

EXPERIMENTAL TESTS OF ELECTROWEAK THEORIES

AT MARK-J

by

HE SHENG CHEN

Submitted to the Department of Physics
in partial fulfilment of the requirement for the
Degree of Doctor of Philosophy in Physics in June 1984

ABSTRACT

The reactions of electron-positron annihilation into lepton pairs have been measured with MARK-J detector at PETRA in the c.m. energy range from 12 GeV to 46.8 GeV. The data are in good agreement with the standard electroweak model of Glashow, Weinberg and Salam. The other alternative models are also compatible. The limits on the parameters of these models have been found. A model-independent fit to MARK-J lepton data gives the weak neutral current coupling constants $g_V^2 = 0.009 \pm 0.036$ AND $g_A^2 = 0.307 \pm 0.045$. Leptons are still point-like particles with radii less than 10^{-16}cm at the 95% C.L..

The data of reaction $e^+e^- \to \gamma\gamma$ are in good agreement with the predictions of Quantun Electrodynamics in the above energy range.

The lepton data and $e^+e^- \to \gamma\gamma$ data are also used to search for an excited electron, scalar electron, photino, zino and X particles. None of these particles have been found and mass limits on the particles and the preon mass scale have been obtained.

Thesis Supervisor: Samuel C. C. Ting
Title: Thomas Dudley Cabot Institute Professor of Physics

ACKNOWLEDGMENTS

In 1977, The Chinese Academy of Science and Professor Samuel C. C. Ting started a collaboration at the MARK-J experiment. This is the first large Scientific collaboration between China and Western countries. I would like to thank the foresighted collaboration for having given me an opportunity to learn experimental high energy physics.

It is my great pleasure to thank my thesis supervisor, Professor Ting for his invaluable help, advice, guidance and encouragement during my stay at DESY and MIT. Professor Ting, with his deep understanding of physics, sharp judgement and outstanding leadership made the experiment possible, and to obtain first rate results. His criticism and advice have proven instrumental in the effort and preparation leading to this thesis.

Very special thanks are extended to Professors James Branson and Min Chen. I have greatly benefitted from their excellent understanding of high energy physics and data analyses. Many thanks to them also for numerous good suggestions and helps during the preparation of the thesis. I wish to thank Prof. Branson for careful reading of the thesis.

I would like to thank Prof. U. Becker and Dr. J. Burger for their lectures at Beijing in 1979. Thanks to Prof. Becker also for his helpful advice and suggestions for the thesis. I would like also thank Miss S. Marks for her gentle helps, excellent english lectures, and for her efficient management in the experiment.

Professors H. Newman and A. Bohm have all helped me a great deal at times when help was needed most, with instructive physics discussions and infinite helps.

I wish to thank all of members of MARK-J collaboration for their parts in bringing this thesis to fruition, in particularly, D. Barber, M. Capell, R. Clare, E. Deffer, M. Demarteau, B.Z. Dong, P. Duinker, M. Fukushima, G. Herten, P. Kuijer, C. Mana, G.G.G. Massaro, I. Mirza, M. Pohl, F.P. Poschmann, J.P. Revol, S.Rodriguez, M. Rohde, H. Rykaczewski, D. Teuchert, K.L. Tung, C.C. YU and C.C. Zhang for helpful discussions and their cooperations. I wish to thank Drs. R.Y. Zhu, J. Salicio, Mr. B.X. Yang and D.Z. Jiang for Monte Carlo simulations, which are an important procedure to obtain any physics results at high energy experiments.

Thanks to Drs. G. Swider and M. White for their patient reading of the thesis and numerous advices.

I would like to thank The Chinese Academy of Science and The Institute of High Energy Physics, Beijing, for their support and concern. I also would like to thank my chinese colleagues at DESY, in particularly, Prof. X.W. Tang, for their encouragement and help.

I would like to thank The National Institute of Nuclear and High Energy Phsics, Amsterdan and The Fundamenteel Onderzoek der Materie, The Netherlands, for their support during part of my stay at DESY.

I would like to thank the DESY directorate for their hospitality during my stay at DESY. My thanks to The PETRA Machine Group for the excellent performance of PETRA.

I wish to thank Ms. S. Burger, R. Meisel, P. Slade and G. Zomerland for the adiministrative assistance.

CONTENTS

CHAPTER I INTRODUCTION

The unification of all of the interactions in Nature is always one of the ultimate goals of Science. Several thousands years ago, the ancient Chinese and Greek philosophers had attempted to give their unified explanations for all of Nature phenomena.

In 1865, J.C. Maxwell unified the electric interaction and the magnetic intraction as the electromagnetic interaction, describing them by the Maxwell field equations.

For a long time, the theory of the electromagnetic interaction, Quantum Electrodynamics (QED), was the only successful quantum field theory which could be renormalized and calculated. The various predictions of QED have been tested very precisely by numerous experiments, some of which have reached the accuracies better than one part in a million.

In 1934, E. Fermi, in analogy to QED, established the theory of β-decay, the first theory of the weak interaction. In 1958, R. Marshak presented the V-A theory, which describes the low energy phenomena of the weak charged current. But the theory has the divergence problems when higher energy phenomena are calculated, and can not be renormalized.

In the last decades, particle physics has obtained tremendous achievements in the unification of the electromagnetic interaction and the weak interaction. S.L. Glashow (1961)[17] and A. Salam (1964)[17] incorporated two kinds of the neutral currents, the electromagnetic current and the weak neutral current, and invented the $U(2)\times U(1)$ model. S. Weinberg (1967)[17] incorporated the idea of the spontaneous breakdown of the local gauge symmetry into the $SU(2)\times U(1)$ model, found a mechanism for the mass generation of the intermediate vector bosons and speicified the relative strength between the weak charged current and the weak neutral current. The quark-parton model established by the electron deep inelastic scattering and the discoveries of the J and upsilon resonances and the τ lepton gave an opportunity to unify the two interactions.

One of main predictions of the theory, the weak neutral current, was discovered in 1973. Afterwards, numerous neutrino scattering experiments and electron-deuteron scattering experiments were carried out. The results showed that the low q^2 weak interaction phenomena to be in excellent agreement with the predictions of the SU(2)×U(1) theory.

The electron-positron storage ring PETRA started running at the end of 1978. The e^+e^- experiments provided the first opportunity to test the electroweak theories at large q^2 and without the complications from the interal structure of hadrons in the lepton-hadron collisions. Evidence of the neutral weak boson Z° was found almost two years before it was finally discovred in pp collisions. The weak coupling constants have been measured precisely in pure lepton reactions.

This thesis reports the physics results on the test the electroweak theories and the search for new particles by using the reactions:

$$e^+e^- \rightarrow e^+e^- \tag{1-1}$$

$$e^+e^- \rightarrow \mu^+\mu^- \tag{1-2}$$

$$e^+e^- \rightarrow \tau^+\tau^- \tag{1-3}$$

$$e^+e^- \rightarrow \gamma\gamma \tag{1-4}$$

at the MARK-J experiment.

Chapter II briefly describes the e^+e^- storage ring PETRA. Chapter III contains a brief description of the MARK-J detector, and a detailed discussion about the calibration of the shower counters. Chapter IV describes electroweak theories in the reactions of e^+e^- annihilation into lepton pairs. Chapter V reports the results on the four reactions, and compares them with the predictions of electroweak theories. Chapter VI contains results on the new particle searches which are important for particle physics to go beyond the stardard model.

CHAPTER II PETRA

THE PETRA (Positron Election Tanden Ringbeschleuniger Anlage) electron-positron collider[3] at DESY (Deutsches Elektronen Synchrotron) in HAMBURG, FEDERAL REPUBLIC of GERMANY is shown in Fig. 2.1. The ring with a circumference of 2.3 kilometers has four interaction regions. Electrons are injected into DESY from LINAC I, accelerated to 7 Gev and then injected in two bunches into PETRA. Positrons come from LINAC II and are accumulated in PIA (Positron Intensity Accumulator) before being injected into PETRA. Once in PETRA the two bunches of electrons and two bunches of positrons are, then accelerated to high energies and are made to collide.

PETRA began operating in the fall of 1978, and remains as the world's highest energy e^+e^- colliding beam machine. The initial physics runs were at center of mass energies of 13 GeV and 17 GeV. In the spring of 1979 additional RF cavities were installed, and the center of mass energy reached 30 GeV. As more RF cavities were installed, the maximum energy was raised to 36.7 GeV. In February 1981 additional focussing quadrapoles, so called mini-β, were installed 4 meters from the interaction regions. These quadrupoles decrease the β at the intersection regions, thus increasing the luminosity. Since the installation of those mini-β quadrupoles, the maximum luminosity has been $1.6\text{x}10^{31}$ $cm^{-2}sec^{-1}$, with $650nb^{-1}$ per day. Since the fall of 1982, PETRA energies were increased again. The center of mass energy of 46.78GeV was reached in April of 1984. An integrated luminosity of about $120pb^{-1}$ mostly at energies above 30 GeV, has produced a very large sample of events.

CHAPTER III MARK-J DETECTOR

3.a THE GENERAL DESCRIPTION

MARK-J detector consists of two functional parts: a fine grain calorimeter to measure energies and directions of electrons, photons, and hadrons and a magnetized iron spectrometer to identify muons over large solid angle and measure their momenta. Fig. 3.1 is the side view of the detector, and fig. 3.2 is the end view of the detector. Fig. 3.3 shows the radial layers of the detector. The vertex detector and the calorimeter cover the range from a polar angle $\theta = 12°$ to $168°$. The outer drift chambers cover from $\theta = 25°$ to $155°$. Except for small gaps in the four corners, the detector covers the full azimuthal angle ϕ around the beam direction.

Particles leaving the intersection region pass first through a five millimeter thick beampipe of an outer diameter of 19.0 cm. The beampipe diameter is large enough to allow synchnotron radiation to pass unobstructed through the detector. Then they pass through the vertex detector, consisting of a four layer array of drift tubes which surround the beampipe and cover the azimuth angles from 12° to 168° (fig. 3.4). They are used to distinguish charged particles from neutral particles, and to reconstruct the event vertex along the beam direction to an accuracy of 2 mm. In Bhabha scattering, the drift tube tracks are also used to determine the precise directions of electrons and positrons. Fig. 3.5 is the vertex distribution of Bhabha events reconstructed from the vertex detector with $\sigma = 0.85$cm.

Particles then pass through the electromagnetic shower counters (labeled A, B, C), consisting of 18 radiation lengths of lead-scintillator sandwich. Since every shower counter is viewed by one phototube at each end, the longitudinal position (Z) of the particle trajectories can be detemined by comparing the relative pulse heights from each end of the counter. The timing information provides another measure of the longtudinal position. Since A counters are closest to the beam pipe, their TDC signals are sometimes contaminated by various backgrounds . In addition to the normal TDC, a high threshold TDC is also employed for each A counter phototube. This rejects most of the background and improves the resolution of TDC position of A counters tremendously. Each phototube of the A, B, and C counters has two ADC's. One covers a small pulse height range and is sensitive to the lower energy hits. The other one has a large measurement range which can handle the hits with very high energies, especially the hits of Bhabha events. Such a design of the MARK-J calorimeter enables very high resolutions in the energy and position calculation.

Following the electromagnetic calorimeter are the inner drift chambers of the muon spectrometer (labeled S, T, U, V). Additional energy measurements for hadrons are provided by 4 layers of scintillation counters (labeled K) imbedded in the magnetized iron of the toroidal magnet. Penetrating particles passing through the iron are detected and the momentum analyzed by drift chambers half way through (labeled Q) and outside (labeled P, R) of the magnet. The time of flight trigger counters(labeled D, E) define a fiducial region inside the spectrometer in such a way that the acceptance is uniform and independent of the muon charge up to $\cos\theta = 0.8$.

A more complete description of the detector may be found in reference 1,2 and 5. More than five years of data taking shows that the design of MARK-J detector gives not only very high accuracy of the position, energy and momentum measurements, but also good performance despite the large machine backgrounds at the highest PETRA energies. The MARK-J detector maintains very high efficiency of data taking and typically accumulates the highest luminosity among the experiments of PETRA.

3.b THE CALIBRATION OF SHOWER COUNTERS

In the MARK-J detector both the event identification and the energy measurement depends on the detailed response of the calorimeter counters. The directions of motion of hadrons and photons are calculated from the ADC and TDC of the calorimeter counters. Moreover, because there are insensitive regions in the four corners of the vertex detector, one must use the TDC and ADC information alone to calculate the directions of electrons and positrons in some of the Bhabha scattering events. The Physics at MARK-J experiment requires very precise measurements of the positions and the energies of the electrons, photons and hadrons. For instance, one would like to measure the electroweak interference in Bhabha scattering, which makes only 3% changes in the differential cross section at $\theta = 90°$. Thus the calibrations of the calorimeter counters are very important for the MARK-J data analysis.

Before the MARK-J detector was installed , one quardrant of the complete A, B, C and K counter assembly was calibrated by test beam at CERN[1].

During data taking the performance of the counters changes somewhat. For instance, due to the synchrotron radiation the scintallaters are getting yellow, thus their attenuation lengths, gains and the velocity of the light may change. The performance of phototubes and electronics may change due to the variation of the temperature and other factors. Although such changes are usually relatively small, one must calibrate each counter individually from time to time to keep the high precision of the energy and position calculation.

During normal data taking there is a special cosmic ray trigger to record the minimal ionization pulse heights of cosmic ray muons. For every two or three weeks of data taking, off-line analysis collects those events and calculates the minimal ionization line of each counter to determine gain of each phototube. The calibration programs also select a sample of Bhabha events which have only two back-to-back clean drift tube tracks from the same period of data. Comparing the hit positions extrapolated from the drift tube tracks with those calculated from the ADC and TDC values, one can calibrate the attenuation length and the TDC time zero of each counter, and adjust the ratio of the gains of two phototubes of each counter without changing the energy of the hit. Finally, we use those calibration results to do off-line analysis for the same period of data. The calibration procedure has kept the energy and position calculations at MARK-J calorimeter very precise in more than five years of data taking, and for the large energy range from 12 GeV to 47 GeV.

The Bhabha event samples are also used to improve several important corrections in the energy and position calculation, e.g. the pulseheight dependence of the TDC's, the saturation correction of phototubes and so on. Furthermore, some empirical relations for the ADC and Z-position dependence of the attenuation length and the speed of light in the scintallator were fit to make these corrections more precise.

After the above calibration procedures, very good energy and position resolutions are achieved in MARK-J experiment. Fig. 3.6 shows the TDC position resolution of B counters. The width (σ) from the fitting of the Gaussian distribution is 1.87 cm. Fig. 3.7 shows the ADC position resolution of B counters with σ = 2.00 cm. Fig. 3.8 shows the high threshold TDC position resolution of A counters with σ = 1.78 cm. The final Z-position to be used in data analysis so-called ZBEST, is a weighted average of the ADC position and TDC position (for A counters, high threshold TDC information is also used). The weights depend on the details of the hits and the quality of the information from the counters , e.g. the timing zero of TDC's , the pulseheight, ... etc, and also vary with the type of counters. Fig. 3.9 shows the resolution of ZBEST. It has σ = 1.64 cm from the Gaussian distribution fit. The energy resolution of electrons in Bhabha scattering at c.m. energy 35 GeV is shown in fig. 3.10. It has σ = 8.5 % of the beam energy with a small radiative tail at the lower energy end. Fig 3.11 is a similar plot for the photons in the reaction of $e^+e^- \rightarrow \gamma\gamma$ at the same c.m. energy. Comparing the two energy resolution distributions, one can see that electrons have a better energy resolution than photons have, but electrons have also a long radiation tail at lower energies.

Fig. 3.12 is the FWHM resolution of electron energy as a function of $\cos\theta$ at the c.m. energy 35 GeV. It shows that in the whole angular range of $|\cos\theta| < 0.9$, the energy resolution of the MARK-J detector is uniform and the FWHM of the electron energy distribution is about 17%. When the $|\cos\theta|$ is larger than 0.9, the energyresolution gets worse, mainly due to the saturation of the phototubes and the energy leaks at the edges of counters. These phenomena are much less significant at c.m. energy below 20 GeV. Fig. 3.13 is the FWHM resolution of electron energy as a function of the c.m. energy. The error bars contain the statistical error only. One can see that the FWHM resolution is about 20% over the large energy range from 14 GeV to 47 GeV. The fluctuation in the energy resolution is less than 5% during last five years of data taking.

In conclusion, based on the good design and the careful calibration from time to time, MARK-J calorimeter obtains very good energy and position resolutions over the whole energy range of PETRA. Such excellent performance gives MARK-J experiment an unique opportunity to test the electroweak theories very precisely.

3.c THE LUMINOSITY MEASUREMENT

The luminosity in MARK-J intersection is monitored by measuring the rate of Bhabha events in the central A counter (fig. 3.1) and a small angle luminosity monitor. We assume that at present energies and small q^2 the absolute rate of the Bhabha scattering process is well described by QED and it can be used as an absolute monitor. Nevertheless, one has to take proper account of radiative corrections, because the measured rate of Bhabha scattering receives contributions from all orders in the perturbation expansion of QED. Futhermore, given the finite energy and position resolution of the detector, some events in which a hard photon is radiated are also detected and attribued to Bhabha scattering. Thus it is necessary to calculate the contribution to the total cross section to order α^3. The program from Berends and Kleiss is used in all the necessary calculations.

Before the mini-β quadrupoles were installed in the MARK-J intersection region, there were two arrays of lead glass counters (labeled G) located 5.8 m from the intersection point, which measured Bhabha events at small θ angle (30 mrad). Comparing G counters luminosity with the luminosity measured from A counters, gave an independent check of the luminosity at the MARK-J detector. We find that they agree within 3% (see fig. 3.14).

CHAPTER IV ELECTROWEAK THEORIES IN $e^+e^- \to \ell^+\ell^-$

The reactions of Bhabha scattering (1-1) and μ pair production (1-2) were classical tests of Quantum Electrodynamics for a long time, and were found to be in very good agreement with the predictions of QED[6]. The elecltron and muon are found to be point-like particles. Since PETRA runs at the highest energies in the world, these tests could be extented to higher energies and higher precision. Studying the reaction of tau pair production (1-3), MARK-J first proved that tau particle is also a point-like particle, and is well described by QED[1,50].

The weak interaction is also involved in those reactions, since every exchanged photon can be replaced by a neutral weak intermediate boson Z°. Their Feynman diagrams are shown at figs. 1a and 1b. According to The SU(2)×U(1) model, the electromagnetic interaction and the weak interaction are unified. To describe the reactions (1-1), (1-2) and (1-3), we include both the electromagnetic current and the weak neutral current by using the Hamiltonian[15,18]

$$H_t = -4\pi\alpha\bar{e}\gamma_\lambda e\,\frac{1}{s}\,\bar{\ell}\gamma^\lambda\ell - \frac{2G_F}{\sqrt{2}}[\bar{e}\gamma_\lambda(g_V+g_A\gamma_5)e\,\frac{m_z^2}{m_z^2-s}\,\bar{\ell}\gamma^\lambda(g_V+g_A\gamma_5)\ell] \qquad (4\text{-}1)$$

for $\ell = \mu,\ \tau$, and

$$H = H_t+4\pi\alpha\bar{\ell}\gamma_\lambda e\,\frac{1}{q^2}\bar{e}\gamma^\lambda\ell - \frac{2G_F}{\sqrt{2}}[\bar{\ell}\gamma_\lambda(g_V+g_A\gamma_5)e\,\frac{m_z^2}{m_z^2-q^2}\bar{e}\gamma^\lambda(g_V+g_A\gamma_5)\ell] \qquad (4\text{-}2)$$

for $\ell = e$, where g_V and g_A are the coupling constants of the weak neutral current to leptons and $G_F = 1.02\times10^{-5}/m_p{}^2$. In general the cross sections of the three reactions contain three terms:

$d\sigma_{qed}/d\cos\theta$, $\quad d\sigma_{interference}/d\cos\theta$, $\quad d\sigma_{qed}/d\cos\theta$.

which are proportional to

$\propto \alpha^2/s$, $\qquad \propto \alpha\, G_F$, $\qquad \propto G_F{}^2 s$.

At present PETRA energies, compared with the electromagnetic interaction, the effects of the weak neutral current itself are still very small and negligible. But the size of the interference term relative to QED contribution is of order $(G_F/\alpha)s$ and rises with s, the square of c.m. energy. At the highest energies of PETRA, the interference term in the three reactions is measurable. The differential cross scetion of Bhabha scattering and the production cross sections of μ pair and τ pair are sensitive to the value of $g_V{}^2$. The charge asymmetries of μ pair and τ pair productions are sensitive to the value of $g_A{}^2$.

The weak neutral current has been extensively studied in neutrino scattering experiments[39] and in electron deuteron scattering experiments[40]. The results are in very good agreement with the predictions of GWS $SU(2)_L \times U(1)$ theory at low q^2 and low c.m. energy. The value of $\sin^2\theta_W$ have been measured in these experiments. A combined fit to the results of the ν-nucleon and electron-deuteron scattering experiments gives[16] $\sin^2\theta_W = 0.234 \pm 0.013$.

The study of the electroweak interference in e^+e^- collision is very important for the test of the electroweak theories. The test can be done at very high q^2 and c.m. energy($\approx$ 2000 GeV^2) with purely leptonic reactions(1-1), (1-2) and (1-3) which are free of the complications of strong interactions which enter in the electron-deuteron scattering. The measurement of the weak coupling constants between leptons, and tests of $e - \mu - \tau$ universality in the weak neutral current interactions are very important for electroweak theories.

The reactions $e^+e^- \to \ell^+\ell^-$ can be described in a model-independent way suggested by Hung and Sakurai[15]. They introduced three parameters h_{VV}, h_{VA} and h_{AA} to describe the weak coupling between leptons. At high energies, we must introduce the mass of the $Z°$ as an additional parameter. Since we assume that the lepton universality of the weak neutral current is valid, the parameters are identical for ℓ = e, μ and τ. For the models with a single $Z°$ we can relate the parameters h_{VV}, h_{VA} and h_{AA} to vector and axial vector couplings g_V and g_A measured in neutrino-electron scatttering. If the coupling constant of neutrino to the $Z°$ is given by $c_\nu/2$, then

$$h_{VV} = g_V{}^2/c_\nu{}^2 \qquad (4\text{-}3)$$

$$h_{AA} = g_A{}^2/c_\nu{}^2 \qquad (4\text{-}4)$$

$$h_{VA}^{2} = h_{AA} \cdot h_{VV} = g_V^{2} \cdot g_A^{2} / c_\nu^{4} \tag{4-5}$$

In SU(2)×U(1) models, these parameters are expressible in terms of the weak mixing angle $\sin^2\theta_W$, T_{3L} and T_{3R}, the third components of the weak isospin of the left-handed and right-handed leptons, in following way

$$h_{VV} = \rho(T_{3L} + T_{3R} + \sin^2\theta_W)^2 \tag{4-6}$$

$$h_{AA} = \rho(T_{3L} - T_{3R})^2 \tag{4-7}$$

$$m_{Z^\circ}^2 = \frac{m_W^2}{\cos^2\theta_W} = \frac{1}{\rho}\,\frac{\pi\alpha}{\sqrt{2}G_F}\,\frac{1}{\sin^2\theta_W\cos^2\theta_W} \tag{4-8}$$

where m_W and m_{Z° are the masses of the charged and neutral weak bosons. The parameter ρ is a ratio of the strength of the weak neutral current interaction to the strength of the weak charged current interaction. A fit to the results of the ν experiments gives[16] $\rho = 1.002 \pm 0.015$.

CHAPTER V EXPERIMENTAL DATA AND COMPARISON WITH ELECTROWEAK THEORIES

5.a BHABHA SCATTERING

Bhabha scattering is one of most important reactions in electron-positron colliding experiments. Besides the continuous test of Quantum Electrodynamics, at PETRA energies it becomes sensitive to the interference between the electromagnetic current and the weak neutral current at large θ angles. Thus the reaction is useful to test electroweak theories. Some of the important electroweak interaction parameters can be determined only by Bhabha scattering at present energies (e.g. the parameter C, see section 5.e.iii). On the other hand, for all electron-positron interaction, the Bhabha scattering at small θ angles is a reference reaction to determine the luminosity of the e^+e^- collisions.

The virtual photon exchanged in Bhabha scattering can be either space-like or time-like. The photons at both channels could be replaced by an intermediate weak neutral boson Z°, i.e. through the weak neutral current. The corresponding Feynman diagrams are shown in fig. 5.1a.

Since the interference effect is relatively small and is not sensitive to the event selection and the acceptance of the detector, we use following two steps to get the predictions of electroweak theories :

1) make a Monte Carlo simulation which includes QED process only to find the QED predictions ;
2) using the formulas of the electroweak theories calculate the effects from the interference and correct the QED predictons bin by bin.

Such a procedure is very flexible for test electroweak theories. One can easily change the parameters of electroweak theories, or switch from one electroweak theory to another without repeating complicated QED event generation and detector simulations.

As the beam energies of PETRA are much larger than the mass of electron, one can use the extreme relativistic limit of the lowest order QED cross section of Bhabha scattering :

$$\frac{d\sigma}{d\Omega} = \frac{\alpha^2}{2s}\left\{ \frac{q'^4+s^2}{q^4} + \frac{2q'^4}{q^2 s} + \frac{q'^4+q^4}{s^2} + \frac{q^4+s^2}{q'^4} + \frac{2q^4}{q'^2 s} + \frac{q'^4+q^4}{s^2} \right\} \quad (5\text{-}1\text{-}1)$$

where $q^2 = -s\cdot\cos^2(\theta/2)$, $q'^2 = -s\cdot\sin^2(\theta/2)$.

Using the Lagrangian (4-2) to include both the electromagnetic interaction and the weak interaction in the framework of the SU(2)×U(1) model, the differential cross section of Bhabha scattering, depending on the weak neutral coupling constant $g_V{}^2$ and $g_A{}^2$ and the mass of Z°, turns out to be:

$$\frac{d\sigma}{d\cos\theta} = \frac{\pi\alpha^2}{2s}\left[\frac{2(t^2+(s+t)^2)}{s^2}A(s) + \frac{s+2t}{s}B(s) + \frac{2(s^2+(t+s)^2)}{t^2}A(t) + \frac{t+2s}{t}B(t) + \frac{4(s+t)^2}{st}D(s,t)\right] \quad (5\text{-}1\text{-}2)$$

where

$$A(s) = 1-4\left[\frac{G_F S}{4\sqrt{2}\pi\alpha}\right]\left[h_{VV} - \frac{G_F S}{4\sqrt{2}\pi\alpha}\left(h^2_{VV} + h^2_{AA} + 2h^2_{VA}\right)\right]$$

$$B(s) = 1-8\left[\frac{G_F S}{4\sqrt{2}\pi\alpha}\right]\left[h_{AA} - \frac{G_F S}{4\sqrt{2}\pi\alpha}\left(h_{VV}h_{AA} + h^2_{VA}\right)\right]$$

$$D(s,t) = 1 - \frac{1}{2\sqrt{2}\pi\alpha}\left[G_F(s)s(h_{VV}(s)+h_{AA}) + G_F(t)t(h_{VV}(t)+h_{AA})\right) + \frac{G_F(s)sG_F(t)t}{(2\sqrt{2}\pi\alpha)^2}\left[(h_{VV}(s)+h_{AA})(h_{VV}(t)+h_{AA}) + 4h_{VA}(s)h_{VA}(t)\right]$$

and $G_F(t) = G_F(1+t/M_{Z°}{}^2)$, $G_F(s) = G_F(1+s/M_{Z°}{}^2)$,

$h_{VV}(t) = h_{VV}(1+t/M_{Z°}{}^2)$, $h_{VV}(s) = h_{VV}(1+s/M_{Z°}{}^2)$,

$h_{VA}(t) = h_{VA}(1+t/M_{Z°}{}^2)$, $h_{VA}(s) = h_{VA}(1+s/M_{Z°}{}^2)$.

Fig. 5.2 gives examples showing the variations of the differential cross section as $g_V{}^2$ and $g_A{}^2$ are changed.

5.a.i The Event Selection

Following criteria have been used to select Bhabha events :

1) two or three electromagnetic showers, where at least two of them have measured energies larger than one third of beam energy;
2) the acollinearity angle between two charged tracks must be

less than 50°.

The energy threshold cut is chosen to be well below the tail of the electron energy resolution curve with r.m.s. width of ≈ 8%, so that the resolution correction is not sensitive to this cut. The acollinearity cut is also chosen at the region where there are only a few events expected and far from the events of background reaction ee → eeee from two photon channels.

To reduce the background from the hadron jets (including the τ events with hadron decays), following two criteria are used to distinguish the electromagnetic shower and the hadron shower :

1) the energy deposited at the hadron calorimeter (K counters) must be less than 5 to 10 %. The detailed cuts depend on both ϕ and θ angles of the track.
2) the number of matched inner drift tube tracks of each shower i.e. the charge multiplicity, must be less than two.

After above cuts, the hadron contamination in the Bhabha sample is very small. At the large θ angles, it is only about 0.5% of Bhabha events. At small θ angle it is negligible. Since all of hadron events are scanned during data analysis, the easiest way to remove those remaining hadrons is to run the Bhabha analysis programs on the hadron sample, detemine the the hadronic background, and finally subtract the accepted events from the $\cos\theta$ distribution of Bhabha events bin by bin .

The background from the τ events where both τ decay to electron are subtracted according to the τ Monte Carlo. It is also in 0.5% level at large θ angles. The background from the reaction of ee → $\gamma\gamma$ is also subtracted according the QED Monte Carlo. This reaction is well understood and described by QED alone (see section 5.d). The cut on the acollinearity angle removes most of the background from the reaction of ee → eeee through two photon channels. The surviving events are also subtracted according to Monte Carlo simulation of the reaction.

5.a.ii The Radiative Corrections and The Detector Simulation

The measured cross section of Bhabha scattering contains all oredrs in the perturbation expansion of QED. Due to the finite energy and position resolution of the detector, a radiative photon which is close to an electron, may not be distinguishable from the electron and treated as one track by off-line analysis. Furthermore, our Bhabha event selection also accepts the $ee\gamma$ events. Thus one has to calculate the radiative corrections carefully before doing any test of electroweak theories. As the c.m. energy increases, the contributions from the radiative corrections increase considerably (see, e.g. fig. 5.4). For large θ which is sensitive to the electroweak interference, the radiative correctins are between 10 - 25%, which is much large than the effect of the electroweak interference (about 2 - 3 %, see, e.g. fig. 5.2) at the same region.

We write the cross section for Bhabha scattering as

$$\frac{d\sigma}{d\Omega} = \frac{d\sigma_o}{d\Omega}\,(1 + \delta(\theta,\phi)) \qquad (5\text{-}1\text{-}3)$$

where $d\sigma_o/d\Omega$ is the lowest order (α^2) QED cross section (5-1-1) and δ represents the radiative correction to order α^3. Following the notation of Berends, we write

$$\delta = \delta_b + \delta_{v1} + \delta_{v2},$$

where the δ_b is due to the real bremsstrahlung and receives contributions from the eight diagrams in fig. 5.3a. The δ_{v1} is due to the virtual bremsstrahlung whose contribution is the interference between the lowest order diagrams and the diagrams in which one closed loop occurs (due to virtual photons, electron-positron pair or muon pair) shown in fig. 5.3b, and the δ_{v2} is the contributions from the vacuum polarization of tau pair and quark pairs (fig. 5.3b), similar to δ_{v1}.

For a real experiment, the calculations of radiative corrections are very complicate. They are not only dependent on the cuts of the analysis used, e.g. the acollinearity angle cut and the energy threshold, but also are sensitive to the geometry and the acceptance of the detector. The Monte Carlo simulation is a powerful tool to do the calculations. Usually, the Monte Carlo simulation contains two parts: the event generation and the detector simulation.

We use the Monte Carlo generation programs developed by F.A. Berends and R. Kleiss[7]. Those programs include the bremsstrahlung and virtual radiative correction to order α^3 (corresponding to δ_b and δ_{v1} respectively). Fig. 5.4 shows the radiative corrections for Bhabha scattering at c.m. energy = 35, 41 and 45 GeV. The cut on acollinearity angle is 50°. The energy threshold is one third of the beam energy, i.e. for electron, positron or possible photon, at least, two of them are inside the detector and with energy larger than one third of beam energy. Since MARK-J detector does not distinguish electron and positron, the angular distribution is folded around $\theta = 90°$ weighted by their cross sections.

The contributions from tau and hadron vacuum polarization (δ_{v2}) were calculated directly according to the formulas given by Berends and Komen[8]. In the calculations the measured R-values of ee $\rightarrow$ hadrons as a function of the energy, including the effects from all of the hadron resonances, were used. The results are shown in fig. 5.5 for c.m. energy = 35, 41 and 45 GEV. After detector simulation, the Monte Carlo prediction will be corrected by these δ_{v2} values point by point.

In the detector simulation programs, MARK-J detector has been completely simulated. Particles are tracked through the detector and the intersection points with counter and chamber planes are calculated. The energy in each counter is determined from tables which give the dependens on the penetration depth, angle, and particle energy. Energy resolution and longitudinal shower fluctuation are also simulated using tabulated informations. Those tables were generated from the test beam taken with electrons and pions at energies from 0.5 to 10 GEV of MARK-J shower counters, from experimental calorimeter studies[9], and from shower Monte Carlo program EGS (Electron Gamma Shower)[10]. Then the counter ADC and TDC information is digitized. Pulse heights are corrected for attenuation in the scintillator and times are corrected for particle flight time, scintillation light transit time, and time slewing due to varying pulse heights. The hits in drift tubes and drift chambers are also digitized. The backgrounds, inefficiency, multiple-hits, cross-talk and δ-rays are also simulated.

An instructive example is the edge effects of shower counters A. Since the cross section of Bhabha scattering is proportional to θ^{-4}

at small θ angle, the Bhabha event acceptance at the edge of A counters affects the luminosity calculation considerably. Fig. 5.6 shows the efficiency function at end of A counters from the Monte Carlo study. Near the edges, the radiative corrections become larger and negative as more photons of lower energy can cause one of the outgoing electrons to recoil outside the counter limits. Thus the acceptance decreases quickly. On the other hand, because of the shower spread and back scattered showers from neighboring counters, the acceptance does not drop sharply at the end of the A counters but shows a tail beyond the geometrical end of counters. Such phenomena were observed in the Bhabha scattering data. Except the edges of the A counters, the Monte Carlo study shows the acceptnace of Bhabha scattering in MARK-J detector is uniform and near 100 %.

The Monte Carlo simulation describtes Bhabha scattering well. Fig. 5.7 is the measured total energy distribution of Bhabha events compared with the prediction of Monte Carlo in the angle range of $|\cos\theta| < 0.85$. Fig. 5.8 is the measured acollinearity angle disitribution of Bhabha events comparing with the prediction of Monte Carlo in the same angle range. Both of them agree well.

5.a.iii Comparison With The Standard Model

MARK-J experiment has accumulated a very high statistics sample of Bhabha scattering events from c.m. energy 12 GEV to 46.8 GeV in total 2164k events. They are combined into four energies: 14, 22, 35, and 43 GeV. All of data points have been corrected by the radiative corrections and the detector acceptance according the Monte Carlo simulation. Thus they can be compared directly with the predictions of the lowest order QED and the electroweak theories.

Figs. 5.9-5.12 are the measured $\cos\theta$ distribution of Bhabha scattering compared with the lowest order QED prediction at the four combined energies. In these and following graphs, the error bars contain both the statistical errors and the systematic error of 3% point by point. Because the effect of the weak interference is only 2-3% even at 43 GEV and the data can not be distinquished them from QED in the logarithmic scale plots, one must introduce the δ-value to see the details, which is defined as :

$$\delta(\cos\theta) = \frac{\sigma_{data}(\cos\theta) - \sigma_{QED}(\cos\theta)}{\sigma_{QED}(\cos\theta)} \qquad (5\text{-}1\text{-}4)$$

Figs. 5.13 and 5.14 are the δ plots of Bhabha scattering for the c.m. energies 35 GeV and 43GeV which have large statistics. The curves are the predictions of the GWS standard model for $g_A{}^2 = 0.25$, $g_V{}^2 = 0.0016$. The QED prediction is the horizontal line, i.e. $\delta = 0$. The data agree with the predictions of GWS standard model obviously. Comparing with fig. 5.2, one can also conclude that the other solution of the g_A and g_V values shown in fig. 5.2 are also excluded, because they predict positive δ values at the large θ angles. As the c.m. energy increases, the data points at large θ angle tend to more negative values, as predicted by GWS standard model.

The fitting of the parameters of weak interactions will discussed at section 5.e.

5.a.iv The QED Cut-off Parameters

As the c.m. energy increases, if electron is no longer a pointlike particle, QED would be breakdown. The cut-off parameter is parameterization of this deviation from QED via a modified photon propagator model[11]. The QED cut-off parameters Λ modified the differential cross section of Bhabha scattering in the following form:

$$\frac{d\sigma}{d\Omega} = \frac{\alpha^2}{2s}\left\{ \frac{q'^4+s^2}{q^4} F_S F_S^* + \frac{2q'^4}{q^2 s}\mathrm{Re}(F_S F_T^*) + \frac{q'^4+q^4}{s^2} F_T F_T^* + \frac{q^4+s^2}{q'^4} F'_S F'^*_S + \frac{2q^4}{q'^2 s}\mathrm{Re}(F'_S F_T^*) + \frac{q^4+q'^4}{s^2} F_T F_T^* \right\}[1+W(\theta)], \qquad (5\text{-}1\text{-}5)$$

where $q^2 = -s\cdot\cos^2(\theta/2)$, $q'^2 = -s\cdot\sin^2(\theta/2)$. $F_S = 1\mp q^2/(q^2-\Lambda_{S\pm}{}^2)$ and $F'_S=1\mp q'^2/(q'^2-\Lambda_{S\pm}{}^2)$ are the form factors of the spacelike photon, and $F_T=1\mp s/(s-\Lambda_{T\pm}{}^2)$ is the form factor of the timelike photon. The $w(\theta)$ is the effect of the weak interference. Since the interference effects have been observed in the various lepton reactions, one has to include this term to find the correct cut-off parameters. Fig 5.15 shows the changes in the $\cos\theta$ distribution for various λ values.

Using the Bhabha scattering data described in the last section, one can fit the cut-off parameters at 95% C.L. lower limit summarized in Tab. 5.1. According to Heisenberg uncertainty principle, one can conclude that if electron was not a pointlike particle, its radius would be less than 10^{-16}cm.

Other experiments at PETRA have obtained the similar results on the Bhabha scattering[12].

In conclusion, the Bhabha scattering data at MARK-J experiment is consistent with the prediction of the GWS standard model. And up to the highest PETRA energy, electron is still a pointlike particle.

5.b MUON PAIR PRODUCTION

The MARK-J detector provides a precise measurement of muon track direction ($\sigma_\theta \approx 2$ mrad.) and charge. The acceptance for muon is 90% and constant over the angle region $|\cos\theta| < 0.8$. The magnet polarity is alternated weekly to average over any asymmetry from the detector itself. Thus MARK-J detector gives the precise measurement of the muon cross section and the charge asymmetry, which are imprortant tests of QED and electroweak theories.

5.b.i Event Selection

A muon pair is identified by the requirement that two minimum ionizing particles penetrate to the outside P or R drift chambers, making a timing coincidence in the D counters and with the vertex less than 10 cm from the intersection region. The acollinearity angle between two muons must be less than 20°. At least one of muons must have a fitted momentum larger than 50% of the beam energy. These cuts reject the backgrounds from cosmic ray muons, the muon pairs from two photon channel, and the muon pairs from τ decays. The detailed discussions about the muon pair selection, Monte Carlo simulation and backgrounds estimation are describted in reference 1, 2 and 42.

A large muon pair sample was accumulated at MARK-J experiment in total 4.3 k events in the energy range from 12 GEV to 46.8 GEV.

5.b.ii The Measurement of The Cross Section

According to QED, the cross section of $e^+e^- \to \mu^+\mu^-$ is given by the pointlike particle cross section

$$\sigma_{point} = 4\pi\alpha^2/3s \qquad (5\text{-}2\text{-}1)$$

In e^+e^- collision experiments, the total cross sections of most reactions are normalized to the pointlike particle cross section. Then it is easy to compare them with the predictions of theories. The electroweak theories predict a small deviation from the pointlike cross section due to the interference between γ and $Z°$

$$R\mu\mu = \sigma_{\mu\mu}/\sigma_{point} = 1-2g_V{}^2+(g_V{}^2+g_A{}^2)^2\chi^2 \qquad (5\text{-}2\text{-}2)$$

where

$$\chi = \frac{1}{4\sin^2\theta_W\cos^2\theta_W}\,\frac{s}{m_{Z°}^2-s} = \frac{\rho G_F m_{Z°}^2}{2\sqrt{2}\pi\alpha}\,\frac{s}{m_{Z°}^2-s} \qquad (5\text{-}2\text{-}3)$$

We have neglected the width of $Z°$ since the c.m. energies at PETRA is much less than the mass of $Z°$. The equation shows that the change in the total cross section of the muon pair production is proportional to the vector coupling constant $g_V{}^2$ and is not sensitive to the axial vector coupling constant $g_A{}^2$.

Fig. 5.16 is measured $R_{\mu\mu}$ as a function of s. The solid line shows the QED prediction, and the dash-dot line is the prediction of GWS standard model corresponding to $\sin^2\theta_W = 0.23$. The data points are consistent with both lines within the statistical errors. The results clearly show that the $g_V{}^2$ is very small and nearly zero, and rule out the vector-like solution (the dashed curve with $g_V{}^2 = 0.25$ and $g_A{}^2 = 0$).

Since the weak interaction contribution is very small, we can use those data to test QED. Similar to the Bhabha scattering, the photon form factors are defined:

$$F_\pm(q^2) = 1\mp q^2/(q^2-\Lambda_\pm{}^2) \qquad (5\text{-}2\text{-}4)$$

where $\Lambda_\pm$ are the cut-off parameters. The form factors will modified the cross section by

$$\sigma = \sigma_{\mu\mu}F_\pm{}^2(s) \qquad (5\text{-}2\text{-}5)$$

Comparing with the data, one finds that at 95% C.L., the lower limit of Λ_- is 209 GeV, and the one of Λ_+ is 335 GeV. This means that muon does not show any structure until energy scale at least 200 GeV and interacts pointlike down at least to a distance of 10^{-16}cm.

5.b.iii Charge Asymmetry And Comparison With The Standard Model

In the muon pair production the scattering angle θ is defined as the angle between the μ^- and the outgoing e^- beam. The forward-backward charge asymmetry is defined by

$$A_{\mu\mu} = \frac{N(\theta<90°) - N(\theta>90°)}{N(\theta<90°) + N(\theta>90°)} \qquad (5\text{-}2\text{-}6)$$

The lowest order QED predicts that the differential cross section of spin 1/2 pointlike particle is proportional to $(1+\cos^2\theta)$, i.e. no charge asymmtery. The higher order terms QED produce a positive charge asymmetry, through the interference of one and two photon exchange graphs and between the initial and final state bremsstrahlung. This asymmetry can be calculated and corrected by the Monte Carlo calculation. The detailed discussions can be found in the references 2 and 42.

The electroweak interference changes the differential cross section of the μ pair production and τ pair production in the form:

$$d\sigma/d\cos\theta = \pi\alpha^2[R_{\mu\mu}(1+\cos^2\theta)+B\cos\theta]/2s \qquad (5\text{-}2\text{-}7)$$

where $B = -4\chi g_A{}^2+8\chi^2 g_A{}^2 g_V{}^2$. The term proportional to $\cos\theta$ produces a charge asymmetry

$$A_{\mu\mu} \simeq -3/2\ \chi g_A{}^2 \qquad (5\text{-}2\text{-}8)$$

This asymmetry is proportional to the $g_A{}^2$. Below the mass of Z°, $\chi > 0$. Thus the asymmetry from the electroweak interference should be negative. According to the GWS standard model, $\sin^2\theta_W = 0.22\pm0.01$, and $M_Z = 94\pm2$ GeV, thus the asymmetry is expected to be $(-8.8\pm0.5)\%$ at c.m. energy 34.6 GeV, and $(-11.2\pm0.5)\%$ at 43 GeV.

The measured angular distribution from muon pair production at 34.6 GeV are shown in fig. 5.17. The solid line is the prediction of the standard model, and the dashed line is the prediction of QED. The data clearly favour the standard model. Fitting the measured angular distributions with the form given in the equations (5-2-7) and (5-2-8) and extrapolating to all solid angles, one obtains an asymmetry value of $(-11.7\pm1.6)\%$, where the asymmetry from QED at 34.6 GeV $A_{\mu\mu}{}^{QED} = (1.4\pm0.1)\%$ has been subtracted. The result agree with the GWS model prediction $A_{\mu\mu} = (-8.8\pm0.4)\%$, and rule out the pure QED explanation with six standard deviations Fig. 5.18 shows the asymmetry value of muon pair production as a function of s at MARK-J experiment. The results agree well with the prediction of GWS standard model and rule out the pure QED explanation.

5.c TAU PAIR PRODUCTION

The τ pair production (1-3) can be detected by measurement of an isolated μ opposite of an electronic or hadronic shower. The detail event selection and the background discussions can be found in the references 1 and 2. A sample of 1.1K τ pairs have been found in the c.m. energies between 12 and 46.8 GeV from MARK-J experiment.

All of discussions about the electroweak interaction in the muon pair production (section 5.b), including all formulas, can be applied to the τ pair production without any change. Fig. 5.19 shows the measured τ production cross section $\sigma_{\tau\tau}$ as a function of $\sqrt{s}$ from the experiment. The results show that τ is also a pointlike particle as the electron and muon. The fitted Λ values are $\Lambda_+ > 170$ GeV and $\Lambda_- > 117$ GeV with 95% C.L.. It means that tau does not show a structure at least up to an energy scale 140 GeV and interacts as if pointlike down to at least a distance of about 10^{-16}cm. This is especially remarkable in view of the fact that τ has a mass is about twice that of the nucleons, which have a complicated structure. Fig. 5.20 shows the angular distribution of the τ pair production at 34.6 GeV. The solid line is the prediction of the GWS standard model, and the dashed line is the prediction of pure QED. The data points again are in favour of the standard model. The fitted tau asymmetry value $A_{\tau\tau} = (-8.5\pm4.8)\%$, consistents with the prediction of standard model $A_W = -8.8\%$.

5.d $e^+e^- \to \gamma\gamma$

The reactoin $e^+e^- \to \gamma\gamma$ provides an important test of QED. At the energy ranges of PETRA and LEP, it remains the only pure QED test which is not affected at lower orders by the weak interaction and the vacuum polarization, in contrast to Bhabha scattering and lepton pair productions. When LEP runs at the energies near the mass of Z°, it would be the only reference reaction which can be use to determine the luminosity. Furthermore, the reaction is also very useful to search for some of new particles (see sections 6.a.iii, 6.b.ii and 6.d). The MARK-J calorimeter with 4π solid angle and 18 radiation lengths of electromagnetic shower counters and drift tubes inside, is very suitable to study the reactions.

Fig. 5.21 shows the corresponding Feynman diagrams of the reaction $e^+e^- \to \gamma\gamma$ in the lowest order. The first diagram shows the virtual intermediate electron state with space-like momentum q, where $q^2 = -s\cdot\sin^2(\theta/2)$. The second one corresponds the exchange of a virtual electron of space-like momentum q', where $q'^2 = -s\cdot\cos^2(\theta/2)$, Two diagrams together obey Bose-Einstein statistics which is required. At the energies of PETRA, the beam energy is much larger than the mass of electron. Thus the differential cross section of the reaction in the extreme relativistic approximation is:

$$\frac{d\sigma}{d\Omega} = \frac{\alpha^2}{s} \frac{1+\cos^2\theta}{\sin^2\theta} \qquad (5\text{-}4\text{-}1)$$

where θ is the angle between the momentum of an outgoing photon and the beam axis.

5.d.i The Event Selection

Following cuts are used to select $\gamma\gamma$ events:

i) Two or three electromagnetic showers, at least two of which have the energies larger than one third of beam energy;

ii) None of these showers has a matched drift tube track;

iii) the acollinearity angle between the two most energetic showers must be less than 50°;

iv) none of them at the corners of the detector (±12°), since the ends of the drift tubes have lower efficiency.

These criteria are very similar to the one of Bhabha scattering. The only difference is the requirement of no-charged tracks. All of $\gamma\gamma$ events which have at least one photon converted in the beam pipe or the walls of drift tubes are rejected by our data analyses.

5.d.ii Monte Carlo Simulation

We use the Monte Carlo generation programs of $e^+e^- \to \gamma\gamma$ developed by Berends and Kleis[13] to do the Monte Carlo simulation. The generation programs include three photon events, i.e. to α^3, whose Feynman diagram is shown in fig. 5.22. Fig. 5.23 shows the radiative correction as a function of $\cos\theta$ according to the Monte Carlo generation. The cuts in the calcualtion are the same as in the section 5.a.ii. It shows that the radiative correction is also increasing as c.m. energy increases, but the mount is relatively smaller compared with Bhabha scattering. The detector simulation uses the results from EGS calculations[10] to simulate the shower development of photons in MARK-J calorimeter. The Monte Carlo gives a good simulation of the reaction. The points at fig. 5.24 are the measured total energy distribution of $e^+e^- \to \gamma\gamma$ events in angular range of $\cos\theta < 0.84$ compared with Monte Carlo simulation. Fig. 5.25 is the measured acollinearity angle distribution of the two photons at the same angular range compared to the prediction of Monte Calro simulation. Both of them agree well with Monte Carlo predictions.

The photon conversions in the beam pipe wall and the walls of the drift tubes have been simulated in Monte Carlo. The Monte Carlo study shows that the acceptance of $e^+e^- \to \gamma\gamma$ events at the MARK-J detector is almost constant at 70% for $|\cos\theta| < 0.9$. The 30% lost are mainly due the cut at the corners of the detector. As $\cos\theta$ increases, the accpetance only slowly decreases a little bit due to the photon conversion rate increases.

The only background in the reaction is from the Bhabha events with both electron and positron drift tube tracks missing. This background has been simulated in Monte Carlo and subtracted from data. Since the drift tubes have a very high efficiency, it is only about 1.5% to 2% of the cross section $ee \to \gamma\gamma$ in the angle range of $|\cos\theta| < 0.9$.

5.d.iii Comparison With QED

MARK-J experiment has accumulated a large sample of $\gamma\gamma$ events at c.m. energy range from 12 GEV until 46.8 GEV, in total 14.2 K event. Thus one can test QED in the reaction with high statistics and in a wide energy range.

Before 1981, the inner drift tube packages were shorter and had small gaps in the center[1]. For this period of data, only the events at the angular range of $0.2 < |\cos\theta| < 0.8$ are used. For the data taken after 1982, all of events with $|\cos\theta| < 0.9$ are used. In following results, all of data points have been corrected by the radiative correction and the detector acceptance according to Monte Carlo simulation. Fig. 5.26 shows the total cross section as a function of c.m. energy. The points are data, the line is the prediction from lowest order QED. They are in good agreement in the whole energy range, from 12 GeV until 46.8 GeV. Fig. 5.27a and 5.27b are the measurements of the differential cross sections of the reaction at c.m. energies = 14 and 22, 35 and 43 GEV respectively. The lines again are the predictions of the lowest order QED. To see this in better detail, the δ-plots are shown in fig. 5.28a and 5.28b for the c.m. energies 35GeV and 43GeV, which have the higher statistics. The definition of δ is in (5-1-4). The error bars in these graphs are statistical errors only. Again the data show good agreement with the predictions of QED.

Another way to test QED is the cut-off parameters. The definitions of cut-off parameters $\Lambda_\pm$ in $e^+e^- \to \gamma\gamma$ are

$$d\sigma/d\Omega = d\sigma_{\gamma\gamma}/d\Omega \; [1\mp q^2/(q^2-\Lambda_\pm{}^2)] \qquad (5\text{-}4\text{-}2)$$

From the above $\cos\theta$ distributions one can fit the lowest limit on the cut-off parameters at 95% C.L., $\Lambda_+ > 46$ GeV, and $\Lambda_- > 65$ GeV.

Other experements at PETRA have done the similar test[14]. Their results also show that QED is correct at the reaction.

In conclusion, Quantum Electrodynamics is correct for the reaction $e^+e^- \to \gamma\gamma$ up to the c.m. energy 46.8 GeV.

5.e THE COMBINED FIT OF THE PARAMETERS OF ELECTROWEAK THEORIES

In this section all lepton data in MARK-J experiment, i.e. the $\cos\theta$ distribution of Bhabha scattering, the total cross sections and the charge asymmetries of muon pair and tau pair productions, are combined to fit various parameters of electroweak interaction theories[2,22,23]. To emphasize the effects of electroweak interference, we use only first eight $\cos\theta$ bins (0.0 - 0.8) in the

$\cos\theta$ distribution of Bhabha scattering to do the fit. In the following fitting we have included the 3% systematic error in the luminosity calculation for all lepton reactions. Due to the uncertainty in the position calculation, a 3% point to point systematic error has been estimated for $\cos\theta$ distribution of Bhabha scattering. For the μ pair production, a 3% of systematic error has been included in the total cross section, and a 1% of systematic error in the charge asymmetry[49]. For τ pair production, a 10% of systematic error has been included in the total cross section, and a 2% for the charge asymmetry. These systematic errors are from the backgrounds in the event selection, the uncertainty of the detector acceptance, the asymmetry of the detector itself, ... etc. . The relatively larger error in the cross section of the τ pair production is mainly due to the uncertainty of the branching ratio to muon decay.

5.e.i The Fitting of $\sin^2\theta_W$ in GWS Stardard Model

In the standard $SU(2)_L \times U(1)$ model of Glashow, Weinberg and Salam[17], the left-handed lepton fields are arranged in the weak iso-doublets, and the right-handed lepton fields in the weak iso-singlets, i.e. $T_{3L} = -1/2$ and $T_{3R} = 0$ for charged leptons. The model also predicts $\rho = 1$, and gives the relations

$$h_{VV} = g_V^2 = (1-4\sin^2\theta_W)^2/4 \qquad (5\text{-}5\text{-}1)$$
$$h_{AA} = g_A^2 = 1/4$$

Thus the only unknown parameter in the model is $\sin^2\theta_W$. Using all of MARK-J lepton data one can fit the value of $\sin^2\theta_W$ according to the relations (4-8) and (5-5-1). The best fit value is $\sin^2\theta_W = 0.278^{+0.066}_{-0.119}$. At 95% C.L., our fit gives $0.120 < \sin^2\theta_W < 0.378$. The χ^2 is 22.0 for 35 degrees of freedom.

The fitting value of $\sin^2\theta_W$ is consistent with the results of the ν experiments and the electron-deuteron scattering experiments.

5.e.ii The Model-Independent Fitting of g_V and g_A

More generally, the model-indepentant fitting of g_V and g_A has been done to the same set of lepton data. We do the fit in the general framework of $SU(2)\times U(1)$ with a single Z° mediating the weak neutral current according to the formula (4-6), (4-7). Since Z° has been observed by the CERN pp collider[19], the mass of Z° has been set to the average measured value 94 GeV. The best fit values from MARK-J data are : $g_V^2 = 0.009\pm0.036$ and $g_A^2 = 0.306\pm0.045$. The χ^2 is 20.5 for 34 degrees of freedom. At 95% C.L., we found $g_V^2 < 0.096$ and $0.199 < g_A^2 < 0.418$. These results rule out the pure QED prediction by 7 standard deviations and clearly prove the existence of electroweak interference in the e^+e^- collisions.

These results are obtained purely from leptonic e^+e^- reactions and can therefore be compared to similar results from ν-electron scattering. The results from both types of experiments have similar precision and agree well with one another. A comparison with ν-electron experiments can also be done in more detail by displaing the results in a diagram on the g_V-g_A plane (fig. 5.29). In the our e^+e^- experiment the allowed region in this plane has a four-fold symmetric contours because only the square of coupling constants can be measured. The results from neutrino scattering alone limits the values to two shaded regions, a vector-like and an axial vector-like solution. Previously, the electron-deuteron scattering data was needed to solve this ambiquity. Now an unique solution can be determined from purely leptonic reactions, as shown in fig. 4.29, therefore avoiding the inherent uncertainties resulting from the use of hadronic targets.

5.e.iii The Fit of Parameter C

Besides the $SU(2)\times U(1)$ model, many alterative models of the electroweak interaction were proposed. These models extent the $SU(2)\times U(1)$ with a larger group $SU(2)\times U(1)\times G$, where G is a group, and predict the different intermediate vector boson spectra with more than one Z°[24]. These models give the predictions at low q^2 similar to the one of standard model. But at higher energies, more Z° species would show up and give completely different predictions. The Hamiltonian of the neutral current for these models is described by

$$2H_{NC} = \frac{-e^2}{q^2}\, j_{EM}^2 + \frac{8G_F}{\sqrt{2}}\, [(j^{(3)} - \sin^2\theta_W j_{EM})^2 + C\cdot j_{EM}^2] \qquad (5\text{-}5\text{-}2)$$

where $j^{(3)}$ is the third component of the weak isospin current, and C is a constant depending upon the group G. For models with single Z, C is zero, while for thoeries with more than one Z° boson, C should be greater than zero. Thus the equation (4-5) becomes

$$h_{VV} = g_V^2 = ((1-4\sin^2\theta_W)^2+16C)/4 \qquad (5\text{-}5\text{-}3)$$

The value C gives the measure of a deviation from the standard model in following way [51]:

$$C = \frac{[\int ds\cdot s\cdot\sigma(e^+e^-\to All)]_{data}-[\int ds\cdot s\cdot\sigma(e^+e^-\to All)]_{GWS}}{16[\int ds\cdot s\cdot\sigma(e^+e^-\to All)]_{GWS}} \qquad (5\text{-}5\text{-}4)$$

At present energies of PETRA, the Bhabha scattering is the reaction which is most sensitive to the g_V and can be used to determine the value of C. To fit the value of C, we assume that $\sin^2\theta_W = 0.23$, and $h_{AA} = g_A^2 = 1/2$. Combining all MARK-J lepton data[53], we find the 95% C.L. upper limit on C to be

$$C < 0.017, \qquad (5\text{-}5\text{-}5)$$

with $\chi^2 = 22.0$ for 35 degrees of freedom. The other experiments at PETRA have obtained similar results[52].

For a given model (i.e. a given group G), one can convert the value of C into a limit on the lowest mass of multiple Z°-bosons. For the modle SU(2)×U(1)×U(1) which predicts one pair of charged gauge bosons and two neutral gauge bosons[20] with masses m_1 and m_2, we have

$$C = \cos^4\theta_W(m_{Z^\circ}{}^2/m_1{}^2 - 1)(1-m_2{}^2/m_{Z^\circ}{}^2) \qquad (5\text{-}5\text{-}6)$$

where M_{Z° is the mass of Z° predicted by the standard model. Similarly, for the model SU(2)×U(1)×SU(2) which predicts two pair of charged gauge bosons and two neutral gauge boson[21], we have

$$C = \sin^4\theta_W(m_{Z^\circ}{}^2/m_1{}^2 - 1)(1-m_2{}^2/m_{Z^\circ}{}^2) \qquad (5\text{-}5\text{-}7)$$

Using the C value obtained in MARK-J experiment, we find the mass limits for the two models. The two contours in fig. 5.30 show the 95% C.L. lower limits on the masses of Z°'s for the two models respectively.

In conclusion, we observe the electroweak interference in the data of Bhabha scattering, μ pair and τ pair productions with the MARK-J experiment. The results are in good agreement with the prediction of $SU(2)_L \times U(1)$ model of Glashow, Weinberg and Salam. Leptons are still pointlike particles with radii less than 10^{-16}cm at 95% C.L.. According to the data, other alternative electroweak models can not be ruled out. We have set the limits on the parameters of these models.

CHAPETR VI SEARCH FOR NEW PARTICLES

The standard model of Glashow, Weinberg and Salam, $SU(2)_L \times U(1)$, is very successful in the description of the electroweak interactions. One of the main question is the existence and the mass of the scalar Higgs meson which plays a crucial role in the spontaneous breakdown of $SU(2) \times U(1)$ and gives the masses to quarks and leptons. The standard model leaves many fundmental parameters arbitrary, e.g. the masses and mixing of the quarks and leptons, the weak mixing angles ... etc. It does not explain why there are three generations of quarks and leptons and what the relation is between them. To find the answers of these questions, one has to go beyond the standard model.

Beyond the standard model, there are two general directions :

i) the existence of new symmetries to relate particles and their interactions, e.g. grand unified theory, supersymmetry.

ii) the existence of subconstituents of particles previously considered as 'elementary'. e.g. composite model.

These models suggest the existence of various new particles. The MARK-J data at PETRA give a unique opportunity to search for the new particles.

6.a SEARCH FOR THE EXCITED ELECTRON e^*

One possible deviation from QED would be the existence of the excited leptons (e^*, μ^* and τ^*). There have been many theoretical discussions as to whether leptons are composite particles so that excited states exist[27]. These excited states should have the same lepton numbers and the same charges as the corresponding leptons, but different masses. A particularly interesting case is the excited electron. The existence of the excited electron of mass between 40 to 50 GEV is one of popular speculations to explain the unusually high rate of hard photons in the decay of $Z^\circ \to e^+e^-$ and $\mu^+\mu^-$[41].

In the electron-positron collision experiments, the excited leptons maybe produced by following ways:

a) the pair production of the excited leptons; This is similar to to the normal fermion pair production by the electromagnetic coupling. Their Feynman diagrams are shown in fig. 6.1a;

b) the production of a lepton and a corresponding excited lepton; Their Feynman diagrams are shown in fig. 6.1b. The coupling between lepton, excited lepton and photon is magnetic.

c) the exchange of a virtual excited lepton between a pair of excited electron at in the reaction of ee $\rightarrow \gamma\gamma$. The Feynman diagrams are shown in fig. 6.1c.

In the first two reactions, the excited leptons would decay to the corresponding lepton and a photon. By comparing the invariant mass distribution of lepton and photon with the prediction of QED, one can search for the excited leptons. On the other hand, one can not directly observe the decay photon in the case c). But the exchange of a virtual excited lepton should change the angular distribution of the reaction products. The advantage of case c) is that one can reach a mass range of the excited lepton which is higher than the c.m. energy of the reaction. In e^+e^- collisions, one usually only uses it to search for the excited electron. As MARK-J experiment has accumulated an integrated luminosity of more than 120 /pb, for c.m. energies up to 46.8GEV, one can extend the search for excited leptons to a higher mass range.

In this section, only the results on the search for an excited electron are reported. The results on the search for excited μ and τ can be found in references 2 and 49.

6.a.i From The Reaction $e^+e^- \rightarrow e^*e^*$

If there is an excited electron with mass less than the beam energy, it would be pair produced in the e^+e^- collision experiments, as the case a) mentioned above. The excited electrons should decay into normal electrons and photons immediately with very short lifetime. Thus an electron-positron pair and two photons will be observed in the final state. We assume that the coupling between e^* and photon is the normal electromagnetic coupling. The total cross section of production is

$$\sigma_{\ell\ell} = \sigma_{\mu\mu}(3\beta-\beta^3)/2 \qquad (6\text{-}1\text{-}1)$$

where $\sigma_{\mu\mu}$ is the QED cross section of point-like particle pair production, and $\beta^2= (\gamma^2-1)/\gamma^2$, where $\gamma = E_{beam}/M_{e^*}$. Since the present energies of PETRA are much smaller than the mass scales of any relevant composite models, we assume that the structure function of the excited electrons equals one.

The event selection to search for $ee\gamma\gamma$ pair production is:

a) There are four and only four energetic tracks which have been found inside the detector;

b) Each of them must be an electromagnetic shower with energy larger than 20% of the beam energy;

c) Two of them must be charged, i.e. matched with drift tube tracks, and the other two must be neutral.

We have selected 90 candidates from all of data with c.m. energy above 32 GeV. For each event, one calculates the invariant masses for every $e\gamma$ pair to find the invariant mass distribution. These events apparently are from the fourth order QED (to α^4). Since the QED Monte Carlo event generations used in PETRA only includes to order of α^3, one can not compare the distribution with QED predictions at present time. But the event rate is very small compared with the predicted rates from the pair production of excited electrons, and there is no peak in the invariant mass dsitribution. The histogram at fig. 5.2 is the invariant mass distribution of $e\gamma$ pairs at 95% C.L. upper limits for data with c.m. energies between 32 GeV and 46.8 GeV. Thus one can still rule out an excited electron in this energy range. Once the fourth order QED Monte Carlo simulation is available, the contribution from the fourth order QED could be subtracted, and the mass limit on the excited electron will be improved slightly.

We have used Monte Carlo simulation to calculate the acceptances of the pair production of excited electrons for various masses of e^*. The typical acceptances of the pair production are between 40% to 60%, depending upon the mass of e^*. Due to the limited energy and position resolutions, the acceptance drops sharply as the mass of e^* falls below 5 GeV. Thus this method is not sensitive to the mass of e^* below 2 GeV. Using the cross section formula (6-1-1) and the acceptances, one can calculate the predictions on the invariant mass distributions. The curve in fig. 6.2 is the predicted rate of $e\gamma$ pairs with a invariant mass equal to the e^* mass as a function of the e^* mass. To calculate the Monte Carlo predictions at each mass of e^*, we use the luminosity integrated for all of data with the beam energy larger than the mass plus 1 GeV. The data clearly rule out the existence of e^* in the mass range between 2.3 GeV and 22 GeV at 95% C.L., which corresponds to the dash-dot line in fig. 6.4. The shaded region III is excluded by the results of $ee\gamma\gamma$ events.

One should point out that the mass limit obtained from e^* pair production is relatively lower compared to other two reactions, but the mass limit is independent of the magnetic coupling λ which is unknown and presumably small.

6.a.ii From The Reaction $e^+e^- \rightarrow ee^*$

In the reaction the coupling of an excited electron to photon and electron is a magnetic interaction[28]:

$$H_I = \frac{e\lambda}{2M_e*} \bar{\Psi}_e*\sigma_{\mu\nu}\Psi_e F^{\mu\nu} + \text{h.c.} \tag{6-1-2}$$

where the M_e* is the mass of excited electron, $F^{\mu\nu}$ is the electromagnetic field tensor, and λ is a measure of the magnetic coupling in units of α. The differential cross section of the reaction is in following form:

$$\frac{d\sigma}{d\Omega} = \frac{\alpha^2\lambda^2}{4M_e^2*}\left[1-\frac{M_e^2*}{s}\right]\left\{\frac{4\sin^2\theta}{(1-\cos\theta)^2}\left[1-\frac{M_e^2*}{2s}\right]+\frac{1}{1-\cos\theta}\,\frac{4M_e^2*}{s-4M_e^2*}+\right.$$
$$\left.+\frac{2\sin^2\theta}{1+\cos\theta}\left[1-\frac{M_e^2*}{s}\right]+\sin^2\theta\left[1-\frac{M_e^2*}{s}\right]+\frac{2M_e^2*}{s}\left[1-\frac{M_e^2*}{s}\right]\right\} \tag{6-1-3}$$

This formula is only valid for $\theta \gg m_e/E_{beam}$. The excited electron should decay into an electron and a photon. The final state of the reaction must be a pair of electrons and a photon. These kind of events are included in our Bhabha scattering sample already, if they do exist. In the Bhabha scattering sample, there are many normal Bhabha scattering events with a radiated photon. One can distinquish two kinds of events by the invariant masses of $e\gamma$. The event from an excited electron decay should have one of $e\gamma$ pairs which has an invariant mass to be near M_{e^*}. Thus their invariant mass distribution would have a significant peak at M_{e^*}. On the other hand, the invariant mass distribution of QED events can be calculated by QED Monte Carlo simulations (see section 5.a.ii).

One $ee\gamma$ sample has been selected from MARK-J Bhabha scattering data between 32 GeV and 46.8 GeV by following additional cuts :

a) the event has two and only two charged tracks and one neutral track;

b) each track must have energy bigger than 10% of beam energy;

c) all of tracks in the event must be in the angular range of $|\cos\theta| < 0.9$ to reduce the background from higher order QED processes.

Those $ee\gamma$ events have been combined into two energies: 3733 events at 35 GeV, and 514 events at 43 GeV. QED Monte Carlo predicts 3829 events for 35 GeV, and 512.5 events for 43 GeV. Fig. 6.3 is the invariant mass distribution (points) of each $e\gamma$ pair in the 43 GeV sample. They agree well with the predictions of QED Monte Carlo simulation (histogram). The bump around 15 GeV corresponds to the geometry cuts of the detector and has been reproduced by QED Monte Carlo quite well.

The reaction of $ee \rightarrow ee^*$ has been also simulated by Monte Carlo calculations to find the acceptances of the reaction for various masses of e^*. Using the acceptances and the cross section formula (6-1-3), the predicted invariant mass distributions of $e\gamma$ pairs for various M_{e^*} have been calculated. Comparing them with the invariant mass distribution of $ee \rightarrow ee\gamma$ in MARK-J data, one can set a lower limit on the e^* mass and coupling λ at the 95% C.L., which is the dashed line in fig. 6.4. The shaded region II is the excluded range of the mass of e^* and the coupling λ. For instance, if one assumes the coupling λ to be larger than 0.1, we can rule out the existence of e^* up to $M_{e^*} = 42.3$ GeV.

6.a.iii From The Reaction $e^+e^- \rightarrow \gamma\gamma$

If there is an excited state of the electron, the reaction $ee \rightarrow \gamma\gamma$ would have an additional channel due to the exchange of an e^*

instead of e. The corresponding Feynman diagrams are shown in fig. 6.1c. The effective interaction Lagrangian is the same as (6-1-2). As a result, both the event rate and the cosθ distribution of photons in the final state would be changed. The differential cross section, depending on λ and on M_e*, becomes:

$$\frac{d\sigma}{d\Omega} = \left(\frac{d\sigma}{d\Omega}\right)_{QED} + \frac{\alpha^2}{2}\{[\frac{\lambda}{M_e*}]^4 [\frac{q^4}{(q^2-M_e^2*)^2} + \frac{q'^4}{(q'^2-M_e^2*)^2}][\frac{s\cdot \sin^2\theta}{4} + M_e^2*] + + \frac{\lambda^4}{2M_e^2*}\frac{s^2\sin^2\theta}{(q^2-M_e^2*)(q'^2-M_e^2*)} + \frac{2\lambda^2}{M_e^2*}[\frac{q^2+s\cdot\sin^2\theta/4}{q^2-M_e^2*} + \frac{q'^2+s\cdot\sin^2\theta/4}{q'^2-M_e^2*}]\} \tag{6-1-4}$$

For example, if we take $\lambda = 1$ and $M_e* = 10$ GEV, the measured $\gamma\gamma$ rate would be 30 times larger at cosθ = 0.25 than measurements shown in Fig. 5.27b. Since the c.m. energies at PETRA are compatible with the mass range where we are looking for the excited leptons, the low energy approxamation can not be used any more.

As mentioned at section 5.d, the total event rate and the cosθ distribution of $e^+e^- \rightarrow \gamma\gamma$ in MARK-J experiment agree well with the QED predictions. Using the formula of (6-1-4), one can find the lower limit contour in the plane of e^* mass and the coupling λ at the 95% C.L., which corresponds to the solid curve at Fig. 6.4. The shaded region I is excluded by the data of ee $\rightarrow \gamma\gamma$. If we take $\lambda = 1$, the lower limit on M_e* is 72 GEV. Other experiments at PETRA have obtained the similar results[29].

In conclusion, combining the results in the three reactions, one can exclude the existence of e^* in the shaded regions I + II + III in the $M_e* - \lambda$ plane shown at fig. 6.4. If an excited electron does exist, its mass must be very large or its magnetic coupling strength must be very small: $M_e*/(m_e\cdot\lambda) >= 10^5$.

6.b SEARCH FOR THE SUPERSYMMETRIC PARTICLES

Supersymmetry (SUSY)[30] is a relativistic symmetry of a Lagrangian field theory which relates the particle fields of different statistics (Fermion-Boson symmetry). It implies that particles have partners with spin differing by 1/2 unit, and these pairs are not neccessarily degenerate in mass. For example, there would be spin-0 leptons and quarks, spin-1/2 photino, gluino, zino and wino, as superpartners of the ordinary leptons, quarks, photon, gluon, Z° and $W^{\pm}$. This introduces a natural way to break the supersymetry spontously without the "higgs" mystery, and also solves the hierarchy problems giving a natural explanation why the weak interaction scale m_W is so different from the Planck mass. It may ultimately lead to the unification of all fundamental interactions, including gravitation.

Though SUSY is a very attractive theory, so far there is no experimental evidence for SUSY models. The SUSY theories does not even have a theoretical lower limit on the magnetude of the spontaneous breaking of the SUSY. The theorists need experiments to set up the limits on the parameters of the models and to guide direction of the theory.

The experimental searches for supersymmetric particles are done for the N=1 model, which has a one to one correspondence between the SUSY multiplets. For leptons and quarks, there are two SUSY scalars corresponding to the left-handed and right-handed components.

The SUSY current is assummed to be conserved and defines a conserved quantum number R. All of ordinary particles have R = 0, while their SUSY partners: photinos, gluinos, spin-0 leptons and quarks, etc. have R=±1. Hence the SUSY particles are produced by normal paticles in associated production. When decaying, the decay products must contain an SUSY particle.

6.b.i Search for Scalar Electron

The supersymmetric partner of the electron is called the scalar electron[43]. These are spin-0 fields s_e and t_e associated with the left-handed and right-handed parts of the Dirac electron fields, respectively. They have equal masses if their interactions with the photino and the goldstino preserve parity. When the energy is higher enough, pairs $s_e{+}s_e{-}$ and $t_e{+}t_e{-}$ can be produced in e^+e^- annihilation in both the space-like channel and the time-like channel. Fig. 6.5 shows the Feynman diagrams. We assume that the mass of the scalar electron is heavyer than the mass of the photino (goldstino). Then the scalar electrons immediately decay to electrons and photinos (goldstinos):

$s_e \rightarrow e^- +$ photino (goldstino).

$t_e \rightarrow e^- +$ antiphotino (antigoldstino).

Photinos(goldstinos) presumably have a small mass and do not interact with the detector. Thus only a pair of electrons with a missing energy would be observed in the final state. Thus we can search for the scalar electron by looking for acoplanar electron pairs.

The differential cross section for producing scalar electrons at an angle θ with a momentum $\beta E_{beam}/c$ is[43]:

$$\frac{d\sigma(e^+e^-\rightarrow s\bar{s}+t\bar{t})}{d\cos\theta} = \frac{\pi\alpha^2\beta^3\sin^2\theta}{4s}\left[1+\left(1-\frac{4}{1-2\beta\cos\theta+\beta^2}\right)^2\right] \qquad (6\text{-}2\text{-}1)$$

where the photino is assumed to be massless particle.

The selection of the candidates of the scalar electron pair production are the following :

a) there are two and only two charged electromagnetic showers, each of them must have the energy more than 20% of the beam energy;

b) the acoplanarity angle must be larger than 30°;

c) the momentum unbalance in the direction perpenticular to the beam axis must be large than 10% of the c.m. energy;

d) the missing momentum must point to the active region of the detector.

Since the photinos, from the scalar electron decay, carry a part of the energy, the electrons in the final state have relatively lower energy. Thus we have lowerd the energy threshold to 20% of the beam energy, instead of one third of the beam energy as in the normal QED process, to increase the acceptance for the scalar electron events. The cuts on the acoplanarity angle and the momentum unbalance reject the electron pairs from Bhabha scattering. The cut d) rejects the $ee\gamma$ and $ee\gamma\gamma$ events in which γ escape along the beam pipe. All of data with c.m. energy between 32 GeV and 46.8 GeV, in total 113/pb, have been used to do the search. We have found no candidate in the data.

A Monte Carlo calculation has been used to find the acceptances for the scalar electron pair production in the MARK-J detector for various scalar electron masses. The acceptance increases as the mass of scalar electron increases. But the cross section of the pair production decreases, and is finally limited by the c.m. energy.

Using the formula (6-2-1) and the acceptances, one can calculate the predicted number of the acoplanar events as a function of the mass of scalar electron. This is shown in fig. 6.6. Since there is not any candidate in the MARK-J data, one can excluded the existence of scalar electrons until a mass of 22.5 GeV.

6.b.ii Search for A Massive Photino

The supersymmetric partner of photon is called the photino (γ). In e^+e^- collisions, a pair of photinos could be produced by the exchange of a scalar electron, as the Feynman diagram shown in fig. 6.7. Although the photino mass is expected to be small, the theory does not firmly exclude the existence of a massive photino. If the photino has a finite mass, it should decay into a photon and a non-observed gravitino(G), the supersymmetric partner of the graviton. The lifetime of the photino can be estimated by[31]

$$\Gamma(\gamma \to \gamma + G) = m_\gamma^5 / 8\pi d^2 \qquad (6\text{-}2\text{-}2)$$

where the parameter d, with a dimension of $(\mathrm{mass})^2$, is the scale of the supersymmetry breaking. We assume that $\sqrt{d}$ is in the order of 100 GeV. Thus our search for photinos is limited at low mass, because only the photon from photino decay can be detected. If massive photinos do exist, the photon pairs from the photino decays should be in the two photon final state sample. We would either observe acoplanar photon pairs for the case where the mass of photino is large, or find the differential cross section of the collinear photon pairs increasing significantly for the case where the mass of photino is below a few GeV.

The differential cross section of massive photino pair productoin in e^+e^- collision is[32] :

$$\frac{d\sigma}{d\cos\theta} = \frac{\pi\alpha^2 s\beta^3}{4[(\Delta M^2+s/2)^2 - s^2\beta^2\cos^2\theta/4]^2} \times \Big\{(\Delta M^2+\frac{s}{2})^2(1+\cos^2\theta) - s[2(\Delta M^2+\frac{s}{2}) - m_\gamma^2 - \frac{s}{4}]\cos^2\theta + \frac{s^2\beta^2\cos^4\theta}{4}\Big\} \qquad (6\text{-}2\text{-}3)$$

where $\Delta M = m_{\tilde{e}}^2 - m_{\tilde{\gamma}}^2$ and $\beta = (1-4m_{\tilde{\gamma}}^2/s)^{1/2}$. The production rate depends upon the mass of photino and the mass of scalar electron. The supersymmetry theory predicts that there are both left-handed and right-handed scalar electrons. We assumed their masses to be the same, thus the cross section (6-2-3) should be multiplied by 2.

At first, we seach for photinos with mass bigger than a few GeV. The selection criteria for the candidates for the massive photino pair production are the following :

a) there are two and only two neutral electromagnetic showers, each of them must have an energy more than 20% of beam energy;
b) they are not at the corners of the detector(±12°);
c) the acoplanarity angle must be large than 30 degrees;
d) the momentum unbalance at the direction perpenticular to the beam axis must be large than 10% of the c.m. energy;
e) the missing momentum must point to the active regions of the detector.

These criteria are similar to the those applied to the scalar electron pair production. The only change is to select the neutral tracks instead of the charged tracks there. The additional cut at the corners is due to the lower effeciency at the ends of the drift tubes. All of $\gamma\gamma$ final state events with c.m. energy between 32 GeV and 46.8 GeV, in total 113/pb, have been used to do the search. We have found no candidate in the data.

The Monte Carlo calculations have been used to find the acceptances for the massive photino pair productions at the MARK-J detector for various masses of photinos. The acceptance increases as the mass of photino increases. But the cross section of the pair production decreases, and is finally limited by the c.m. energy. The acceptance is almost independent upon the masses of scalar electrons, but the cross section of the production is sensetive to it.

Using the formula (6-2-2) and the acceptances, one can calculate the predicted number of the acoplanar photon pair events as the function of the photino mass and the scalar electron mass. The fig. 6.8 is a two dimensional plot of scalar electron mass and photino mass. Since there is not any candidate has been found in MARK-J data, one can excluded the existence of a massive photino in the shaded mass region I at 95% C.L. by the above results.

The above discussions are very similar to section 6.b.i, the search for scalar electrons. Especially, the Monte Carlo acceptances are very similar and no candidate has been found in data. But the conclusion is slightly different: this method does not work in searching for the photinos with mass below a few GeV. The reason is that the cross section of photino pair production (timelike channel only) is much smaller than the one of scalar electron pair, and the predicted acoplanar event rate is also much smaller.

When the mass of photino is below a few GeV, the photon pairs from the photino decay should be collinear, similar to the events from the normal QED process. Thus the differential cross section of $e^+e^- \to \gamma\gamma$ should be changed. The event rates at large θ angle should increase significantly. Thus we use the photon pairs with $\cos\theta$ less than 0.5 from the sample which was used in sectoin 5.d. Only the data between 32 GeV and 37 GeV are used to do the search.

We have also done Monte Carlo calculations to find the acceptances for various masses of photino in this case. According to the cross section formula (6-2-3) and the accpetances, the predicted event rates for the various photino masses and scalar electron masses have been calculated. Comparing them with the data and QED Monte Carlo, one can rule out the existence of photino in region II of the photino mass-selectron mass plane at fig. 6.8 at the 95% C.L.

Combining with the results of the two cases, the existence of a photino in the whole shaded region of fig. 6.8 is excluded at 95% C.L.. For example, if the mass of scalar electron is 50 GeV, one can rule out the existence of a photino with mass between 0.1GeV and 20 GeV. Thus one can conclude that if the massive photino does exist in the energy range of PETRA, it must be very light and not decay into photon before escaping from the detector, or its production rate must be too small because the mass of scalar electron is too large.

The CELLO and JADE experiments have obtained the similar results on the search for the massive photino[46].

6.b.iii Search For Zino

The supersymmetry theory predicts the existence of a neutral spin

1/2 fermion $\tilde{Z}$, zino, as the SUSY partner of the neutral weak boson Z°[44,45]. The mass of zino is presumably smaller than the mass of Z°. The mass of lowest lying zino is expected to be less than half of the Z° mass, i.e. 47 GeV. Such a zino particle would be produced singly in e^+e^- annihilation via the reaction

$$e^+e^- \to \text{photino} + \text{zino}.$$

The zino is expected to decay into

$$\text{zino} \to e\tilde{e} \to ee\tilde{\gamma}\ ,$$
$$\text{zino} \to \mu\tilde{\mu} \to \mu\mu\tilde{\gamma}\ ,$$

where $\tilde{e}(\tilde{\mu})$ is a scalar electron(muon) and is expected to decay to $e(\mu)$ and a photino, which presumably has no interaction with the detector. The corresponding Feynman diagrams are shown in fig. 5.9. The differential cross section of zino production is[45]:

$$\frac{d\sigma}{d\cos\theta} = \frac{\pi\alpha^2}{4}(c_R^2+c_L^2)\ \frac{s\beta}{[(\Delta+s/2)^2-s^2\beta^2\cos^2\theta\ /4]^2}$$
$$\times\{2(\Delta+s/2)^2[1-(m_{\tilde{\gamma}}-m_{\tilde{Z}})^2/s]$$
$$-\beta^2\{(\Delta+s/2)^2(1-\cos^2\theta)+s[2\Delta+s/2+(m_{\tilde{\gamma}}+m_{\tilde{Z}})/2]\cos^2\theta\}$$
$$-\beta^4 s^2\cos^2\theta(1-\cos^2\theta)/4\} \qquad (6\text{-}2\text{-}4)$$

where c_R and c_L equal to 1/2 for the present measured value of $\sin^2\theta_W$. And $\Delta=m_{\tilde{e}}{}^2-(m_{\tilde{\gamma}}{}^2+m_{\tilde{Z}}{}^2)/2$, $\beta=[1-(m_{\tilde{\gamma}}+m_{\tilde{Z}})^2/s][1-(m_{\tilde{\gamma}}-m_{\tilde{Z}})^2/s]$. The differential cross section depends on the masses of the zino, scalar electron(muon) and photino. The lifetime of zino is expected to be very short, of the order of 10^{-16} to 10^{-20} seconds. The branching ratio of the zino decay to $ee\gamma$ ($\mu\mu\gamma$) is about 10%. As mentioned in the section 6.b.i, the lifetime of scalar electrons is also very short. Since there are two missing photinos carrying a large transverse momentum in the reaction, the signature of the observed final state would be an acoplanar pair of electrons (muons). The event selection and the background discussions in the electron channel are exactly the same as section 6.b.i. They will no be repeated here. There was no candidate for a zino decay event found in our data sample.

The acceptnaces for the zino events have been calculated by Monte Carlo simulation for various combinations of zino mass, scalar electron mass and photino mass. The typical acceptance of the zino events is about 20%. Generally, the acceptance drops sharply as the photino mass increases mainly due to the change of the phase space. On the other hand, the acceptance increases as the scalar electron mass increases but the production rate drops sharply at the same time.

Since there is no candidate found at our data sample, one can fit the lower limit on the mass of zino in the zino mass-scalar electron mass plane. The three contours in fig. 5.10 show the results for the photino masses 2, 5 and 10 GeV respectively. The shaded regions are excluded at 95% C.L. .

The JADE experiment has obtained a similar result on the search for the zino[47].

6.c SEARCH FOR PREON

The existence of large number of leptons and quarks, as well as the desire to explain their mass spectrum, are the motivations for the composite models[33]. The composite models assume that leptons and quarks could be made of subconstituents, so called preons, bound together by a new strong force, called metacolor, with in a mass scale Λ. This is analogous to the QCD description of hadrons, formed of quarks bound by a strong color force due to gluon exchanges. Furthermore, the composite models assume that the weak intermediate bosons W^+, W^-, and Z° are also composite on this scale and the observed weak interaction is a remnant of the confining interaction. The composite models can give a prediction of the spectrum of quarks and leptons, and give the correct weak interaction phenomenology.

Many composite models have been proposed, but so far no obviously correct or compelling model has yet emerged. There is not even a consensus on the most fundamental aspect of quark and lepton substructure - the value of the mass scale Λ, which characteres the strength of preon-binding interaction and the physical size of composite states.

The $\cos\theta$ distribution of Bhabha scattering can be used to find the mass scales. If electrons are composite at the energy scale Λ, the strong forces binding their constituents induce a flavor-diagonal contact interactions, whcih have significant effects on the $\cos\theta$

distribution at reaction energies well below Λ[34]. The Lagrangian is a flavor-diagonal, helicity-conserving contact interactions of the form

$$L_{\ell\ell}=\frac{g^2}{2\Lambda}[\eta_{LL}\bar{\Psi}_L\gamma_\mu\Psi_L\bar{\Psi}_L\gamma^\mu\Psi_L+\eta_{RR}\bar{\Psi}_R\gamma_\mu\Psi_R\bar{\Psi}_R\gamma^\mu\Psi_R+2\eta_{RL}\bar{\Psi}_R\gamma_\mu\Psi_R\bar{\Psi}_L\gamma^\mu\Psi_L] \quad (6\text{-}3\text{-}1)$$

where η_{LL}, η_{RR} and η_{RL} can be -1, 0 or 1, corresponding to the different models. The differential cross section of Bhabha scattering, including γ and Z° exchange, is given by

$$d\sigma/d\cos\theta = (\pi\alpha^2/4s)[4A_o+A_-(1-\cos\theta)^2+A_+(1+\cos\theta)^2] \quad (6\text{-}3\text{-}2)$$

where

$$A_o=\left(\frac{s}{t}\right)^2\left|1-\tan\theta_W\cot2\theta_W\frac{t}{t_z}+\frac{\eta_{RL}t}{\alpha\Lambda^2}\right|^2,\quad A_-=\left|1-\tan\theta_W\cot2\theta_W\frac{s}{s_z}+\frac{\eta_{RL}s}{\alpha\Lambda^2}\right|^2,$$

$$A_+=\frac{1}{2}\left|1+\frac{s}{t}+\tan^2\theta_W\left(\frac{s}{s_z}+\frac{s}{t_z}\right)+\frac{2\eta_{RR}s}{\alpha\Lambda^2}\right|^2+\frac{1}{2}\left|1+\frac{s}{t}+\cot^2 2\theta_W\left(\frac{s}{s_z}+\frac{s}{t_z}\right)+\frac{2\eta_{LL}s}{\alpha\Lambda^2}\right|^2,$$

where $t = -s(1-\cos\theta)/2$, $s_z = s-m_z{}^2+im_z\Gamma_z$ and $t_z = t-m_z{}^2+im_z\Gamma_z$. The predicted deviations of $\cos\theta$ distribution from the standard model are shown in fig. 6.11 and 6.12 for different Λ's. Using the Bhabha scattering results of the MARK-J experiment (section 5.a.iii), one can fit the 95% C.L. lower limit value for these Λ's. The table 6.1 summerazes the fitting results. It shows the lower limits of the preon mass scales are of the order of 1 to 2 TeV.

There is a similar result on the preon mass scales from the JADE experiment[47].

6.d SEARCH FOR THE X PARTICLE

One of popular speculations to explain the abnormally high rate of Z° decays into $\ell\ell\gamma$ in the pp collisions[41] is the hypothesis of a new particle[35,36], X, produced in the reaction

$$Z° \rightarrow X + \gamma \quad \text{where } X \rightarrow \ell^+\ell^-$$

whose Feynman diagram is shown in fig. 6.13a. According to these models, the Z° is a composite particle. From the data of the pp collisions, if the X particle does exist, its mass should be between 40 and 50 GeV, and its spin can be either one or zero. The decay channels for a spin 1 particle are expected to be the lepton pairs and quark pairs. For spin 0 particle, there is an additional channel:

two photons. To explain the abundance of the $\ell\ell\gamma$ event, the partial width of $Z \to X + \gamma$ and $X \to$ lepton pairs should be both unusually large. Thus the X particle be could then observed in e^+e^- annihilation into lepton pairs, photon pairs and probably hadrons. Fig. 6.13b and c are the corresponding Feynman diagrams of those reactions. In the Bhabha scattering, the X particle can be exchanged in both s and t channels, but the main contribution is from the interference of the s channel X exchange with the t channel γ exchange. The data of a continuous energy scan in the range 39.79 < c.m. energy < 46.78 GeV taken with the MARK-J detector at PETRA in the reactions

$$e^+e^- \to \text{hadrons}$$
$$e^+e^- \to \gamma\gamma$$
$$e^+e^- \to \mu^+\mu^-$$
$$e^+e^- \to e^+e^-$$

with an integrated luminosity of 12.6 /pb have been studied to seach for the X particle[37].

To enhance the signals from the channel of the proposed X particle and to reduce the backgrounds from QED reactions, we only use the $\gamma\gamma$ data within the angular range of $|\cos\theta| < 0.8$ and the Bhabha scattering data within the angular range of $|\cos\theta| < 0.5$. The event selection has been described in the section 5.a.i and 5.d.i. The selection of μ pairs and hadrons have been described in detail in the references 2 and 42. The R values of these reactions are defined as the ratios of the measured cross sections over the QED point-like particle cross section. The figs. 6.14a-c and fig. 6.15 are the R plots of hadrons, $\gamma\gamma$, μ pair and Bhabha scattering respectively. If the X particle with mass in the range decays into any of these channels, there must be some kind of resonance structure in the R plots of the reactions.

We have done the fitting both for a broad resonance and for a narrow resonance in the first three reactions, which are sensetive to a resonance with a mass in above range. The Breit-Wigner formula has been used to do the fitting of a broad resonance. The results clearly shows that there is no broad resonance in the energy range. Our limit on the integrated cross section and $\Gamma_{ee}\cdot B_i$ increase approximately as $(\Gamma_X/110\mathrm{MeV})^{0.6}$, where the value 110 MeV is the full width of c.m. mass energy spread, and B_i is the decay branching ratio of X particle in i-th channel.

For a narrow resonance searching, we fit the data to a constant R_0 plus a narrow resonance using the formulas from J.D. Jackson and D.L. Scharre[38] which includes both the machine beam width and the radiative corrections. First of all, we do the fit to the data of each reaction individaully. We fit the resonance mass M_X and the 95% C.L. upper limit on the integrated cross section S_i. From S_i, one can calculate $\Gamma_{ee}\cdot B_i\cdot N$ by

$$S_i = \int \sigma_i d\sqrt{s} = 2\pi^2 N\Gamma_{ee}B_i/M_X{}^2 \qquad (6\text{-}4\text{-}1)$$

where N is the number of states of the X particle: N = 3 for spin 1 particle and N = 2 for spin 0 complex conjugate doublet. The results are summarazed in table 6.2. If we assume lepton universality, those results can be combined to find the upper limit of Γ_{ee} by

$$\begin{aligned}(n_\ell\cdot S_\mu+S_\gamma+S_h) &= 2\pi^2 N\Gamma_{ee}(n_\ell B_\mu+B_\gamma+B_h)/M_X{}^2\\ &\simeq 2\pi^2 N\Gamma_{ee}/M_X{}^2 \qquad (6\text{-}4\text{-}2)\end{aligned}$$

where n_ℓ = 6 is the number of lepton types. We also did a simultaneous fit for the three reactions. The 95% C.L. upper limit on Γ_{ee} is 20 KeV. Thus our fit results exclude the existence of the narrow resonance in the mass range between 39.79 and 46.78 GeV.

For the case when $M_X > \sqrt{s}$, it has been suggested[36] that there is a sizeable contribution from a γ-X interference, decreasing slowly as $1/(M_X{}^2-s)$ for increasing values of M_X in Bhabha scattering. In the energy range near the resonance mass, the contribution from the interference is described[36] by

$$\begin{aligned}\delta R_X=\left(\frac{1-\cos\theta}{3+\cos^2\theta}\right)^2\frac{N\alpha_h}{\alpha}\Big\{&\frac{s^2}{(s-M_X^2)^2+M_X^2\Gamma_X^2}\left[2\frac{s-M_x^2}{t}+\frac{\alpha_h}{\alpha}+2\frac{g_V^2-g_A^2}{e^2}\frac{s-M_X^2}{t-M_Z^2}\right]\\ &+\frac{t^2}{(t-M_X^2)^2+M_X^2\Gamma_X^2}\left[2\frac{t-M_X^2}{s}+\frac{\alpha_h}{\alpha}+2\frac{g_V^2-g_A^2}{e^2}\frac{t-M_X^2}{s-M_Z^2}\right]\\ +(2-N)\frac{\alpha_h}{\alpha}&\frac{s}{(s-M_X^2)^2+M_X^2\Gamma_X^2}\frac{t}{(t-M_X^2)^2+M_X^2\Gamma_X^2}\left[(s-M_X^2)(t-M_X^2)+M_X^2\Gamma_X^2\right]\Big\} \qquad (6\text{-}4\text{-}3)\end{aligned}$$

where $\alpha_h = 2\Gamma_{ee}/M_X$. In the fitting, we allow the background R to have a slope as the c.m. energy increases, instead of the constant R_0 in the fitting of the first three reactions. The slope may come from the energy dependence of the detecter accpetance or the systematic errors on the luminosity measurement. The data shown in fig. 6.15 rule out the existence of such scalar doublet particle with $Mx < 49.2$ GeV at 95% C.L..

In conclusion, none of the hypothetical excited electron, supersymmetric particles or composite paticles have been found in the MARK-J experiment up to c.m. energy 46.8 GeV. The mass limits have been set for these particles.

THE FIGURE CAPTIONS

hypothetical resonance, and the dashed curves are the 95% C.L. limits on such a resonance for the reactions:

a) $e^+e^- \rightarrow$ hadrons;

b) $e^+e^- \rightarrow \gamma\gamma$, integrated over $|\cos\theta| < 0.8$;

c) $e^+e^- \rightarrow \mu\mu$.

Fig. 6.15 The measured cross section of $e^+e^- \rightarrow e^+e^-$, integrated over $|\cos\theta| < 0.5$, normalized to the pointlike QED cross section in the energy region from 39.79 GeV to 46.78 GeV. The curve includes the contribution of the hypothetical scalar particle with mass = 49 GeV which has been ruled out by the data at 95% C.L..

REFERENCES

[1] The MARK-J collaboration, "Physics with High Energy Electron-Position Colliding beams with MARK-J Detecter", Physics Reports 63(1980), 339.

[2] The MARK-J collaboration, "A Summary of Recent Experimental Results from MARK-J: High Energy e+e- Collisions at PETRA", MIT LNS Report No.131 (1983), to be published at Physics Reports.

[3] PETRA Proposal (updated version), DESY, Hamburg (February 1976)

[4] U. Becker et al., Nucl. Instruments and Methods, 180(1981) 61.

[5] M.M. White, MIT Ph.D Thesis, 1981, unpublished.

[6] V. Alles-Borelli et al., Nuovo Cimento 7A(1972) 345;
H. Newman et al., Phys. Rev. Lett. 32(1974) 483;
J.-E. Augustin et al., Phys. Rev. Lett. 34(1975) 233;
L.H. O'Neill et al., Phys. Rev. Lett. 37(1976) 395.

[7] F.A. Berends and R.Kleiss, Nucl. Phys. B177(1981) 237,

[8] F.A. Berends and G.J. Komen Nucl. Phys. B115(1976) 114.

[9] H.G. Sanders, Diplomarbeit, Physikalisches Institut, Acchen, Report No. HEP 74/07(1974). unpublished.

[10] R.L. Ford and W.R. Nelson, SLAC Report-210, unpublished.

[11] S.D. Drell, Ann.Phys.(N.Y.) 4(1958) 75,
T.D. Lee and G.C. Wick, Phys.Rev. D2(1970) 1033.

[12] CELLO Coll., H.-J. Behrend et al., Z. Phys. C16(1983) 301.
JADE Coll., W.Bartel et al., Z. Phys. C19(1983) 197.
TASSO Coll., M. Althoff et al. Z. Phys. C22(1984) 13.

[13] F.A. Berends and R. Kleiss, Nucl. Phys. B186(1981) 22, and the programs which they supplied.

[14] CELLO Coll., H.-J. Behrend et al., Phys. Lett. 123B(1983) 127;
JADE Coll., W.Bartel et al., Z. Phys. C19(1983) 197;
PLUTO Coll., Ch. Berger et al. Phys. Lett. 94B(1980) 87;
TASSO Coll., R. Brandelik et al. Phys. Lett. 117B(1982) 365.

[15] P.Q. Hung and J. Sakurai, Phys. Lett. 69B(1977) 323; 88B(1979) 91; Ann. Rev. of Nucl. and Particle Science, 31(1981) 375.

[16] J.E. Kim et al., Rev. Mod. Phys. 53(1981) 221.

[17] S.L. Glashow, Nucl. Phys. 22(1961) 579;
S. Weinberg, Phys. Rev. Lett. 19(1967) 1264 and Phys. Rev. D5(1972) 1412;
A. Salam and J.C. Ward, Phys. Lett. 13(1964), 168;
S.L. Glashow, J.Ilipoulos and L.Maiani, Phys. Rev. D2(1970) 1285.

[18] E.H. de Groot and D. Schildknecht, Phys. Lett. 95B(1980) 128.

[19] UA1 Coll.: G. Arnison et al., Phys. Lett. 126B(1983) 398; 129B(1983) 273;
UA2 Coll.: P. Bagnaia et al., Phys. Lett. 129B(1983) 130.

[20] E.H. de Groot G.J. Gounaris and D.Schildknecht, Phys. Lett. 85B(1979) 399 and Univ. of Bielefeld, BI-TP 79/39.

[21] V. Barger, W.Y. Keung and E. Ma, Wisconsin-Hawaii Reports, No. COO-881-126(1980). COO-881-133(1980) and COO-881-138(1980).

[22] MARK-J Coll.:
D.P. Barber et al., Phys. Lett. 95B(1980) 149;
D.P. Barber et al., Phys. Rev. Lett. 46(1981) 1663.

[23] J.G. Branson, Proceedings of the international Symposium on Lepton and Photon Interaction at High Energies, Bonn, 1981, edited by W. Pfeil.

[24] H. Georgi and S. Weinberg , Phys. Rev. D17(1978) 275.
[25] B. Naroska, DESY 83-111(1983).
[26] CELLO Coll., H.-J. Behrend et al., Z. Phys. C16(1983) 301;
JADE Coll., W.Bartel et al., Z. Phys. C19(1983) 197;
PLUTO Coll., Ch. Berger et al. Z. Phys. C4(1980) 269;
TASSO Coll., M. Althoff et al. Z. Phys. C22(1984) 13.
[27] J.C. Pati and A. Salam, Phys. Rev. D10(1974);
J.C. Pati, Phys. Lett. 98B(1981) 40;
H. Terazawa et al., Phys. Rev. D15(1977);
A. Harari and N.Seeberg, Phys. Lett. 98B(1981).
[28] A. Litke, Ph.D. Thesis, Harvard Univ. 1970(unpublished).
[29] CELLO Coll., H.-J. Behrend et al., Phys. Lett. 114B(1982) 287.
JADE Coll., W.Bartel et al., Z. Phys. C19(1983) 197.
[30] Yu.A. Gol'fand and Likhtman, Pis'ma Zh. Eksp. Teor. Fiz. 13(1971) 452;
J. Wess and B. Zumino, Nulc. Phys. B70(1974) 39;
P. Fayet and S. Ferrara, Phys. Rep. 32C(1977) 249;
P. Fayet, Phys. Lett. 69B(1977) 489;
G.R. Farrar and P. Fayet, Phys. Lett. 76B(1978) 575; 79B(1978) 442.
P. Fayet, Phys. Lett. 84B(1979) 421;
G.R. Farrar and P. Fayet, Phys. Lett. 89B(1980) 191.
[31] N. Cabibbo et al., Phys. Lett. 105B(1981) 155.
[32] J. Ellis and J.S. Hagelin, Phys. Lett. 122B(1983) 303.
[33] For recent reviews , see e.g.
M.E. Peskin, Proc. of 1981 Int. Symp. on Lepton and Photon Interaction at High Energies, Bonn, 1981, edited by W. Pfeil;
L. Lyons, Oxford University Report No. 52/82, 1982.
[34] E.J. Eichten, k.D. Lane and M.E. Peskin, Phys. Rev. Lett. 50(1983), 881.
[35] M. Veltman, Univ. of Michigan preprint UMHE 83-22;
M.j.Duncan and M.Veltman, UMHE 84-1;
G. Gounaris, R. Kogeler and D. Schildknecht, Univ. of Bielefled preprint BI-TP 83/17.
[36] W. Hollik, F. Schrempp and B Schrempp, DESY 84-011.
[37] MARK-J Coll.: B. Adeva at. el., MIT LNS Technical Report No. 134, to be published at Phys. Rev. Lett..
[38] J.D. Jackson and D.L. Scharre, Nuclear Instruments and Methods, 128(1975), 13.
[39] For recent reviews, see e.g.
P.Q. Hung and J.J. Sakurai, Ann. Rev. of Nucl. and Particle Science, 31(1981) 375;
G.Barbiellini, Proc. of 1981 Int. Symp. on Lepton and Photon Interactions at High Energies, ed. W. Pfeil, Bonn 1981, p623.
[40] C.Y. Prescott et. al., Phys. Lett. 77B(1978), 347 and 84B(1979), 524.
[41] UA1 Coll.: G. Arnison et al., CERN-EP/83-162, to be published in Phys. Lett. B.
[42] J.P. Revol, MIT Ph.D Thesis, 1981, unpublished.
[43] G.R. Farrar and P. Fayet, Phys. Lett. 89B(1980) 191.
[44] S. Weinberg, Phys. Rev. Lett. 50(1983) 387.
[45] E. Reya, Phys. Lett. 133B(1983) 245.
[46] CELLO Coll., H.-J. Behrend et al., Phys. Lett. 123B(1983) 127;

JADE Coll., W.Bartel et al., DESY Report 84-016(1984).
[47] JADE Coll., W.Bartel et al., DESY Report 84-038(1984).
[48] S. Yamada, DESY Report 83-100(1983).
[49] MARK-J Coll.: B.Adeva at. el., Phys. Rev. Lett. 48(1982) 1701.
[50] MARK-J Coll.: D.Barber at. el., Phys. Rev. Lett. 43(1979) 1915.
[51] E.H. de Groot and D.Schildknecht, Zeit. fur Phys. C12(1982) 57.
[52] CELLO Coll., H.-J. Behrend et al., Z. Phys. C16(1983) 301;
JADE Coll., W.Bartel et al., Z. Phys. C19(1983) 197;
PLUTO Coll., Ch. Berger et al. Z. Phys. C7(1981) 289;
TASSO Coll., M. Althoff et al. Z. Phys. C22(1984) 13.
[53] A. Bohm, PITHA, 80/9 and Proceedings of The XX Inter. Conf. on High Energy Physics, Madison, 1980.

Table 5.1 The QED Cut-off Parameters of BHabha Scattering

cut-of- parameter	Λ_{S+}	Λ_{S-}	Λ_{T+}	Λ_{T-}	$\Lambda_{S=T\,+}$	$\Lambda_{S=T\,-}$
GeV	138	260	104	75	143	235

Table 6.1 The Preon Mass Scale

	Λ^{+}_{LL}	Λ^{+}_{RR}	Λ^{+}_{AA}	Λ^{+}_{VV}	Λ^{-}_{LL}	Λ^{-}_{RR}	Λ^{-}_{AA}	Λ^{-}_{VV}
η_{LL}	1	0	1	1	1	0	-1	-1
η_{RR}	0	1	1	1	-1	0	-1	-1
η_{RL}	0	0	-1	1	0	0	1	-1
(GeV)	920	920	2250	1710	950	950	940	2350

Table 6.2

95% c.l. limits on integrated cross sections and the product $\Gamma_{ee} \cdot B_i$ for narrow resonances.

Final states from e^+e^- annihilation	$\int \sigma_i dE$ (MeV • nb)	$n(2J+1) \cdot \Gamma_{ee} \cdot B_i$ (keV)
1) hadrons	34	8.7
2) $\gamma\gamma$	15	3.7
3) $\mu\mu$	21	4.5
SUM	$n(2J+1) \cdot \Gamma_{ee} \cdot (B_h + B_{\gamma\gamma} + 6B_{\mu\mu}) \sim n(2J+1) \cdot \Gamma_{ee} < 39$ keV	
4) hadrons, $\gamma\gamma$, $\mu\mu$ (simultaneous fit)	$\int (\sigma_h + \sigma_{\gamma\gamma} + 6\sigma_{\mu\mu})\, dE < 77$	$n(2J+1) \cdot \Gamma_{ee} < 20$ keV

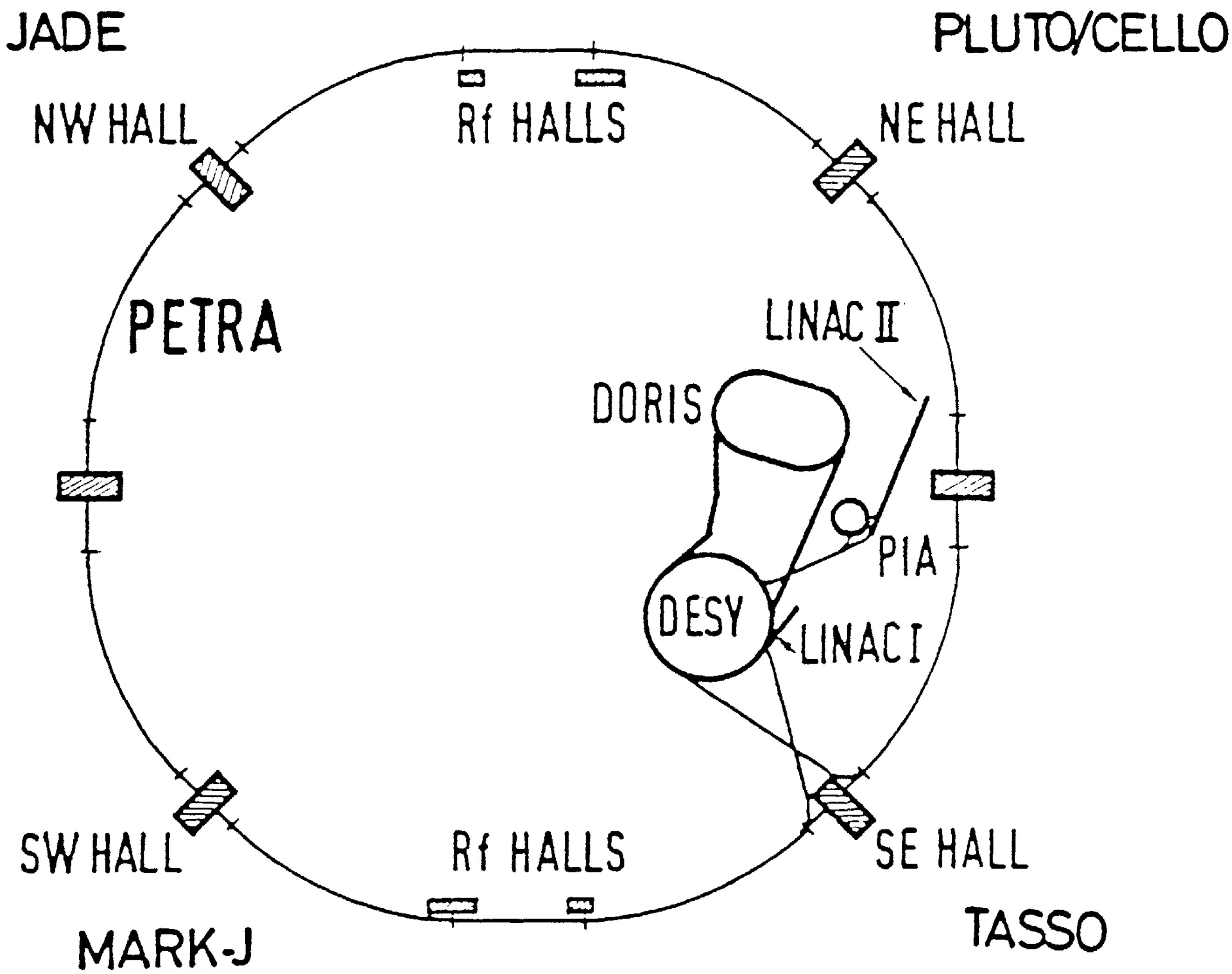
JADE
PLUTO/CELLO
NW HALL
Rf HALLS
NE HALL
PETRA
LINAC II
DORIS
PIA
DESY
LINAC I
SW HALL
Rf HALLS
SE HALL
MARK-J
TASSO

Fig. 2.1

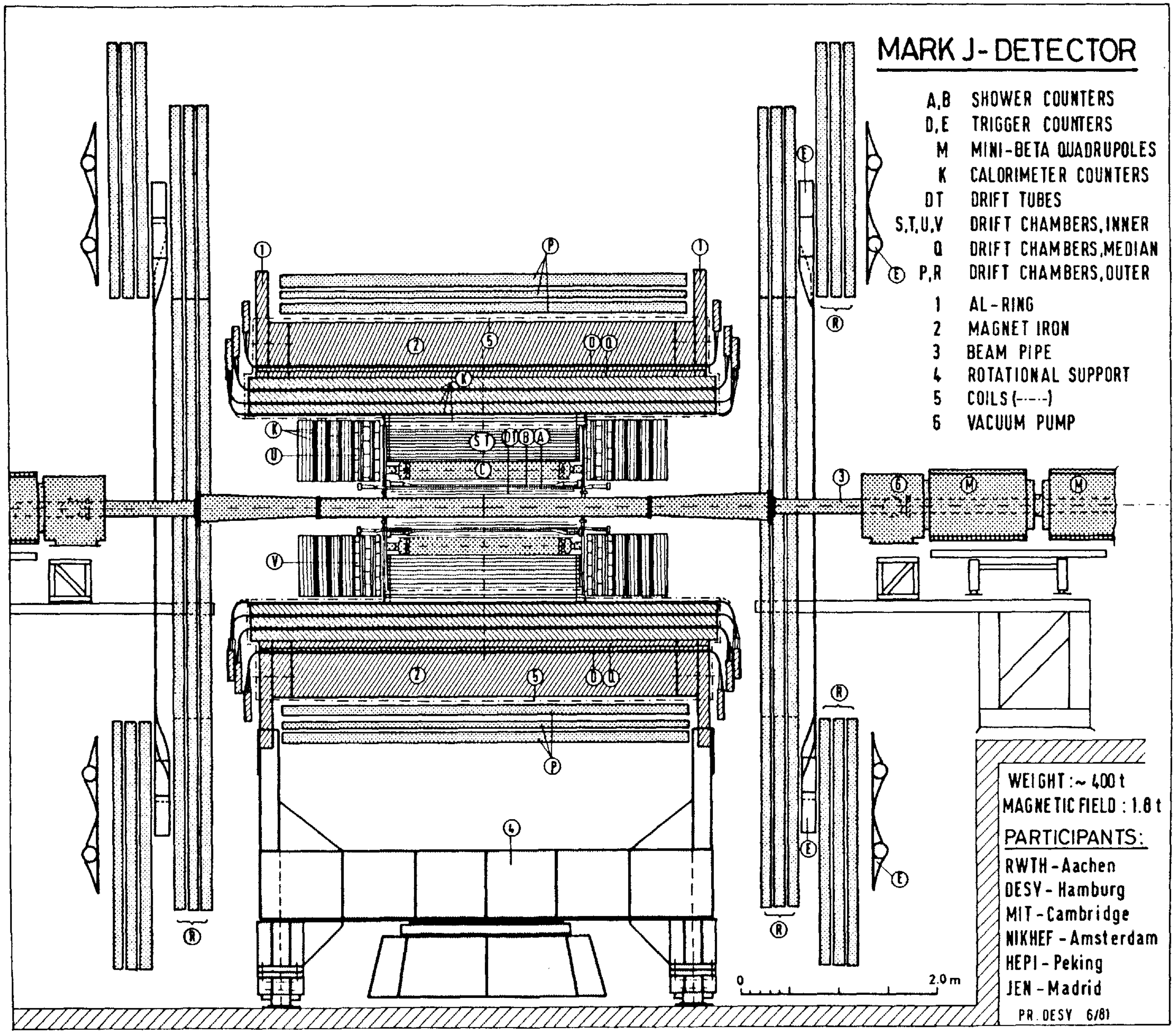
MARK J- DETECTOR
A,B SHOWER COUNTERS
D,E TRIGGER COUNTERS
M MINI-BETA QUADRUPOLES
K CALORIMETER COUNTERS
DT DRIFT TUBES
S,T,U,V DRIFT CHAMBERS, INNER
Q DRIFT CHAMBERS, MEDIAN
P,R DRIFT CHAMBERS, OUTER
1 AL-RING
2 MAGNET IRON
3 BEAM PIPE
4 ROTATIONAL SUPPORT
5 COILS (-----)
6 VACUUM PUMP
WEIGHT: ~ 400 t
MAGNETIC FIELD : 1.8 t
PARTICIPANTS:
RWTH - Aachen
DESY - Hamburg
MIT - Cambridge
NIKHEF - Amsterdam
HEPI - Peking
JEN - Madrid
PR. DESY 6/81
0
2.0 m

33676

Fig. 3.1

MARK J - DETECTOR
(Cross Section)

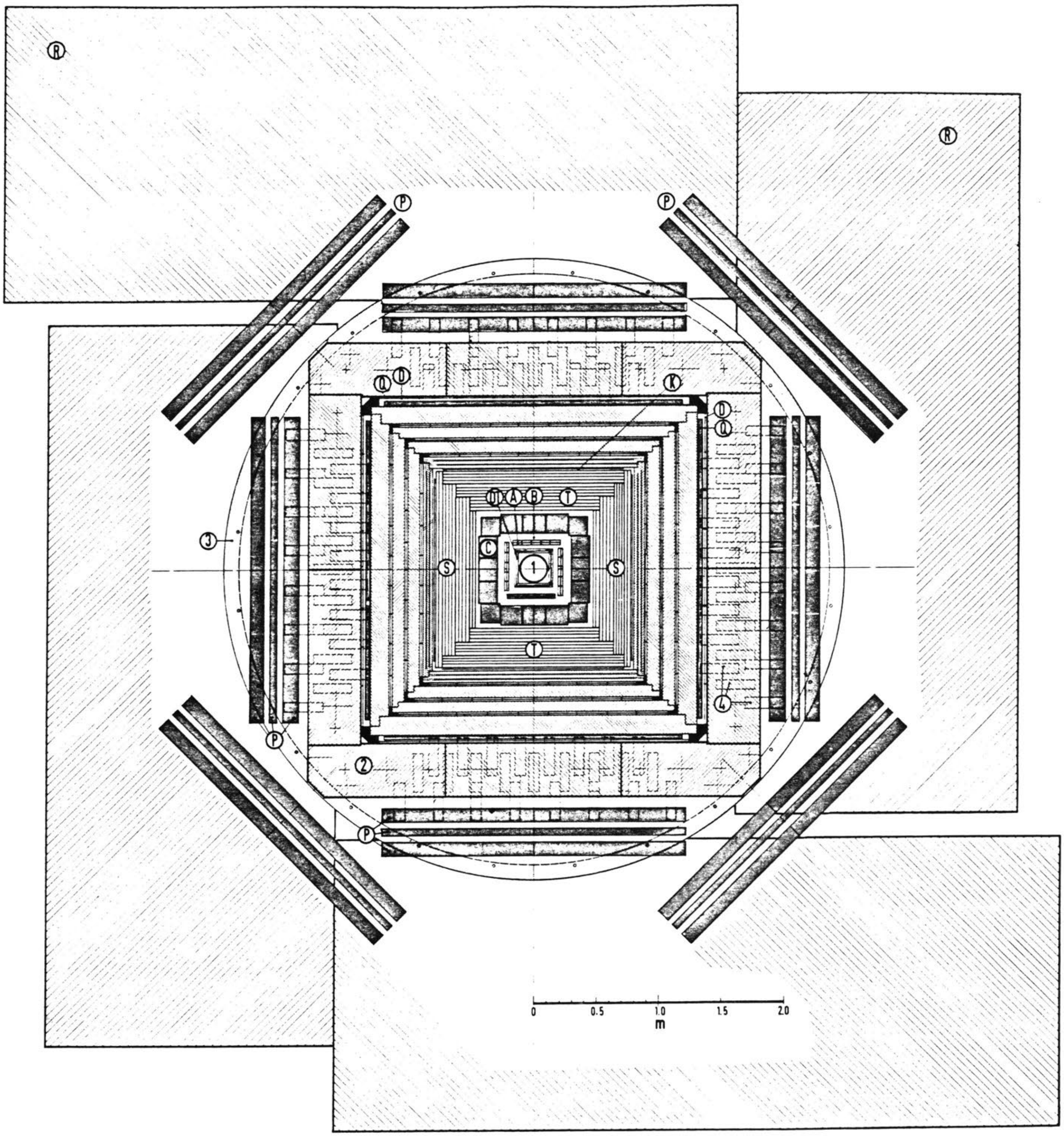

Ⓐ Ⓑ Ⓒ SHOWER COUNTERS
Ⓓ TRIGGER COUNTERS
ⒹⓉ DRIFT TUBES
Ⓠ DRIFT CHAMBERS, MEDIAN
Ⓟ Ⓡ DRIFT CHAMBERS, OUTER
Ⓢ Ⓣ DRIFT CHAMBERS, INNER

① BEAM PIPE
② MAGNET IRON
③ Al - RING
④ MULTIPLIERS

PARTICIPANTS:
RWTH - Aachen
DESY - Hamburg
MIT - Cambridge
NIKHEF - Amsterdam
HEPI - Peking
JEN - Madrid
CALTECH - Pasadena

WEIGHT (total) : ~ 400 t
MAGNETIC FIELD : 1.8 T

Fig. 3.2

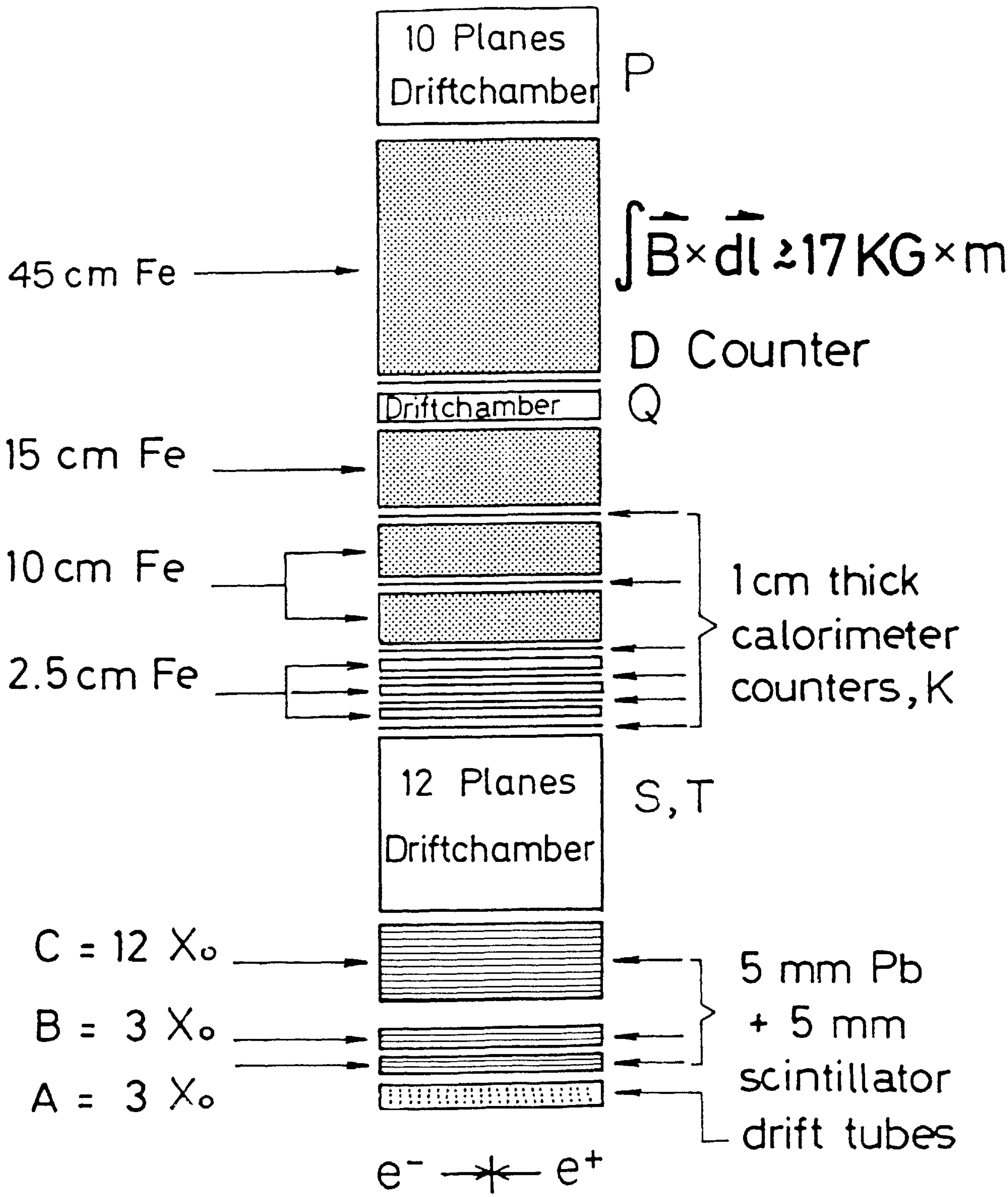
10 Planes
Driftchamber
P
45 cm Fe
$\int \vec{B} \times \vec{dl} \gtrsim 17$ KG × m
D Counter
Driftchamber
Q
15 cm Fe
10 cm Fe
2.5 cm Fe
1 cm thick
calorimeter
counters, K
12 Planes
Driftchamber
S, T
C = 12 X_0
B = 3 X_0
A = 3 X_0
5 mm Pb
+ 5 mm
scintillator
drift tubes
e^-
e^+

Fig. 3.3

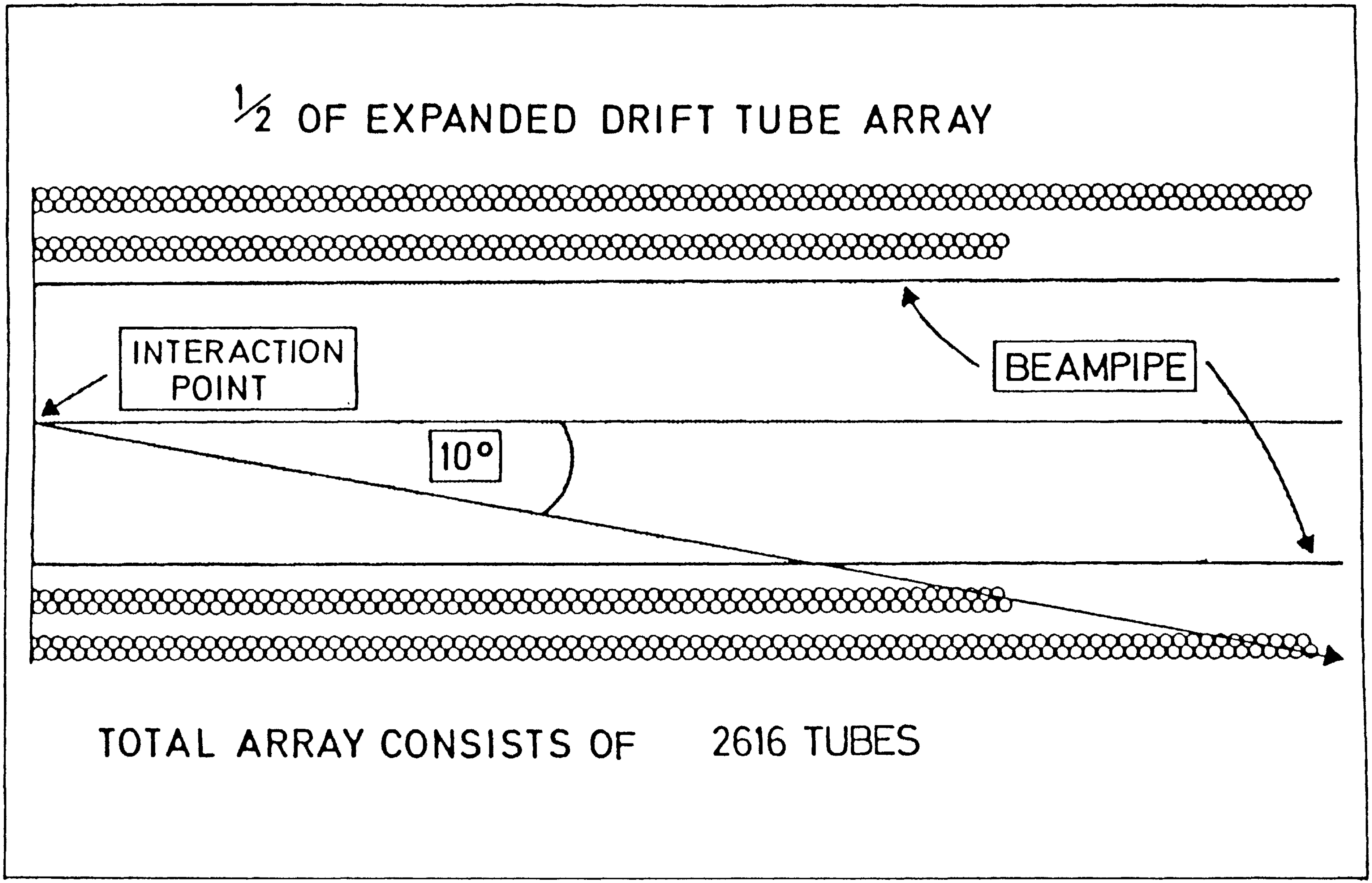

½ OF EXPANDED DRIFT TUBE ARRAY
INTERACTION POINT
BEAMPIPE
10°
TOTAL ARRAY CONSISTS OF 2616 TUBES

Fig. 3.4

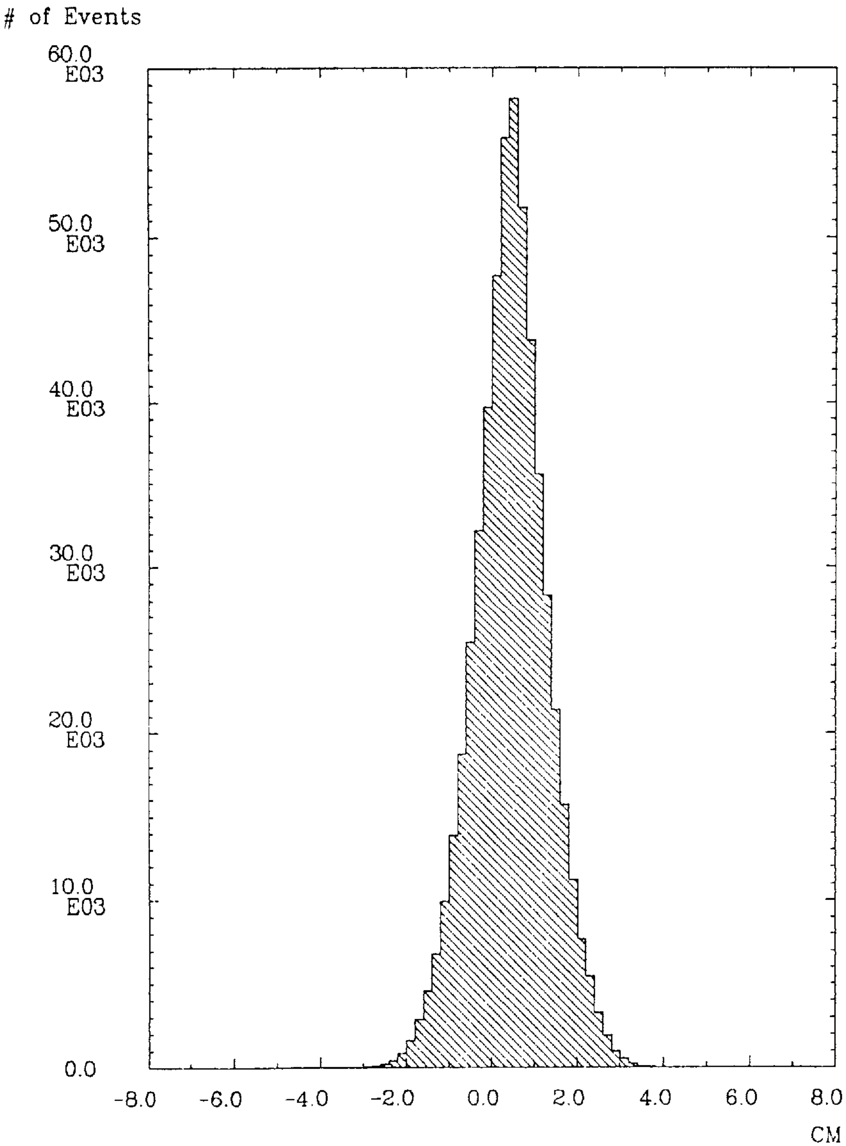

Fig. 3.5 Vertex Distribution of BHABHA Events

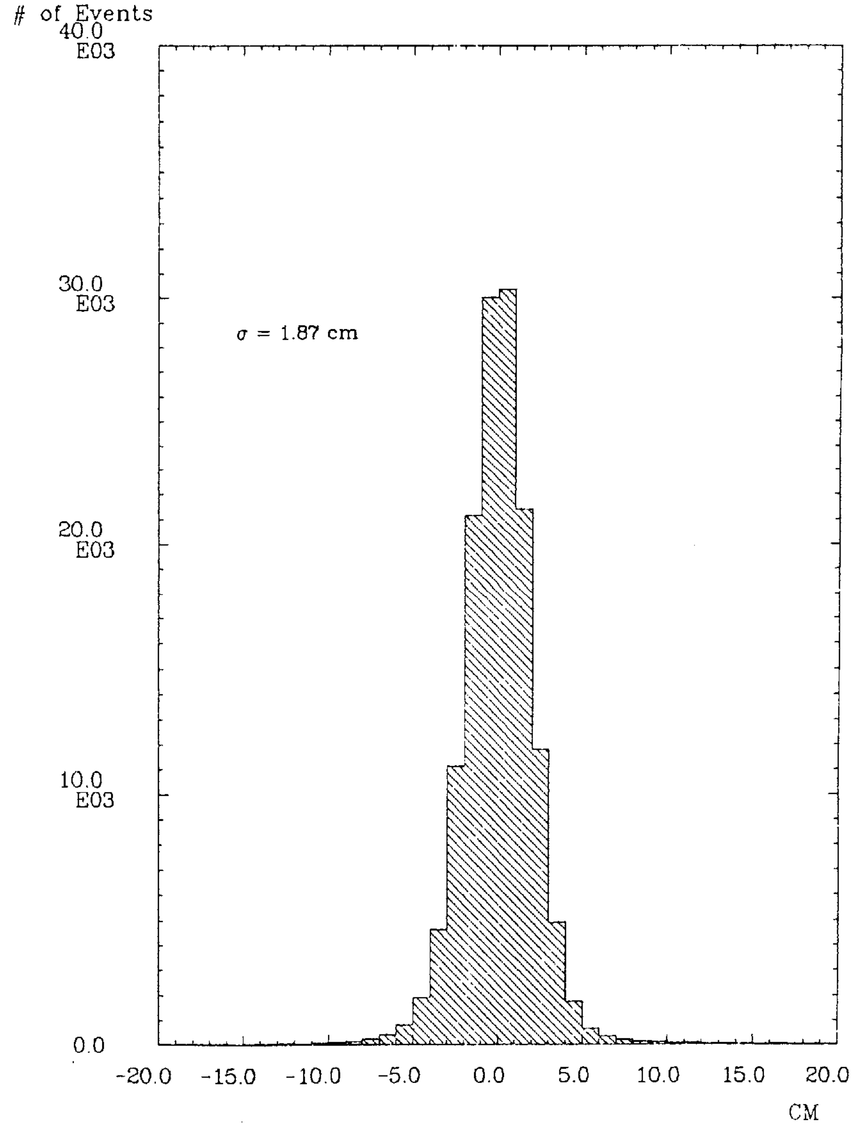

Fig. 3.6 Resolution of TDC Position of B Counters

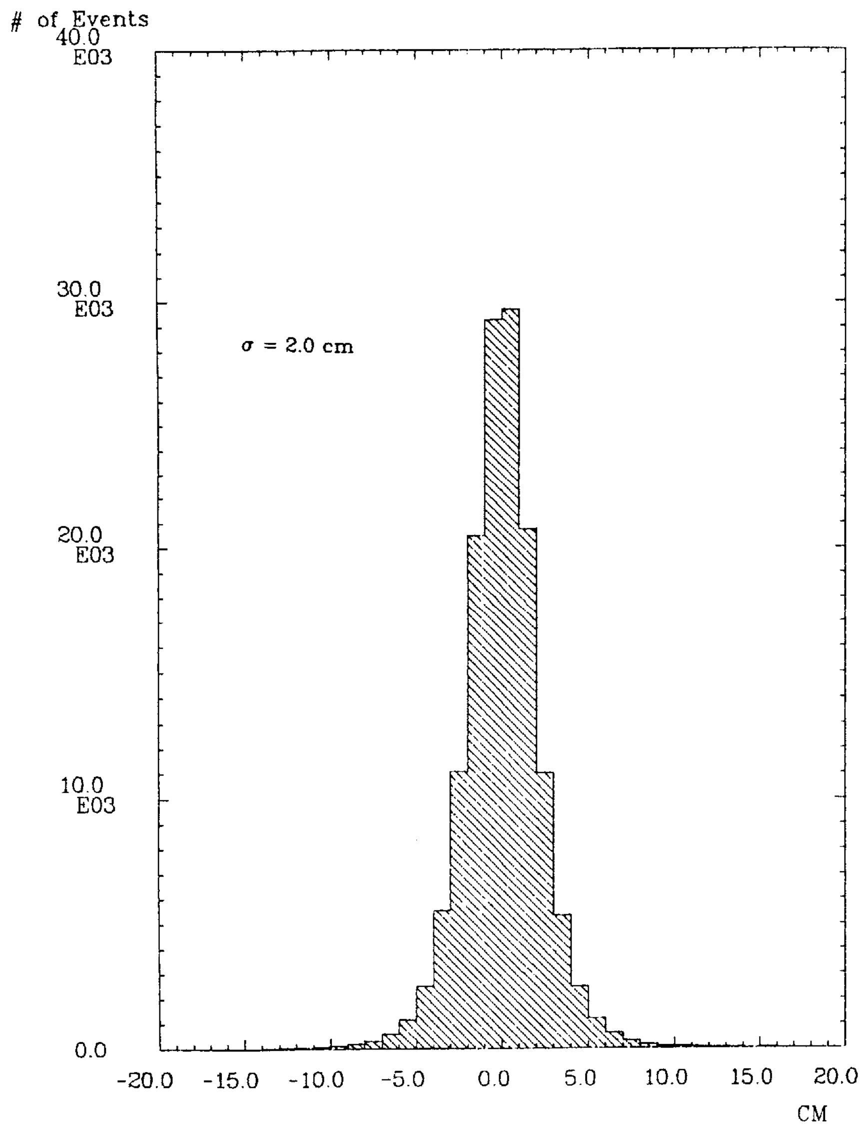

Fig. 3.7 Resolution of ADC Position of B Counters

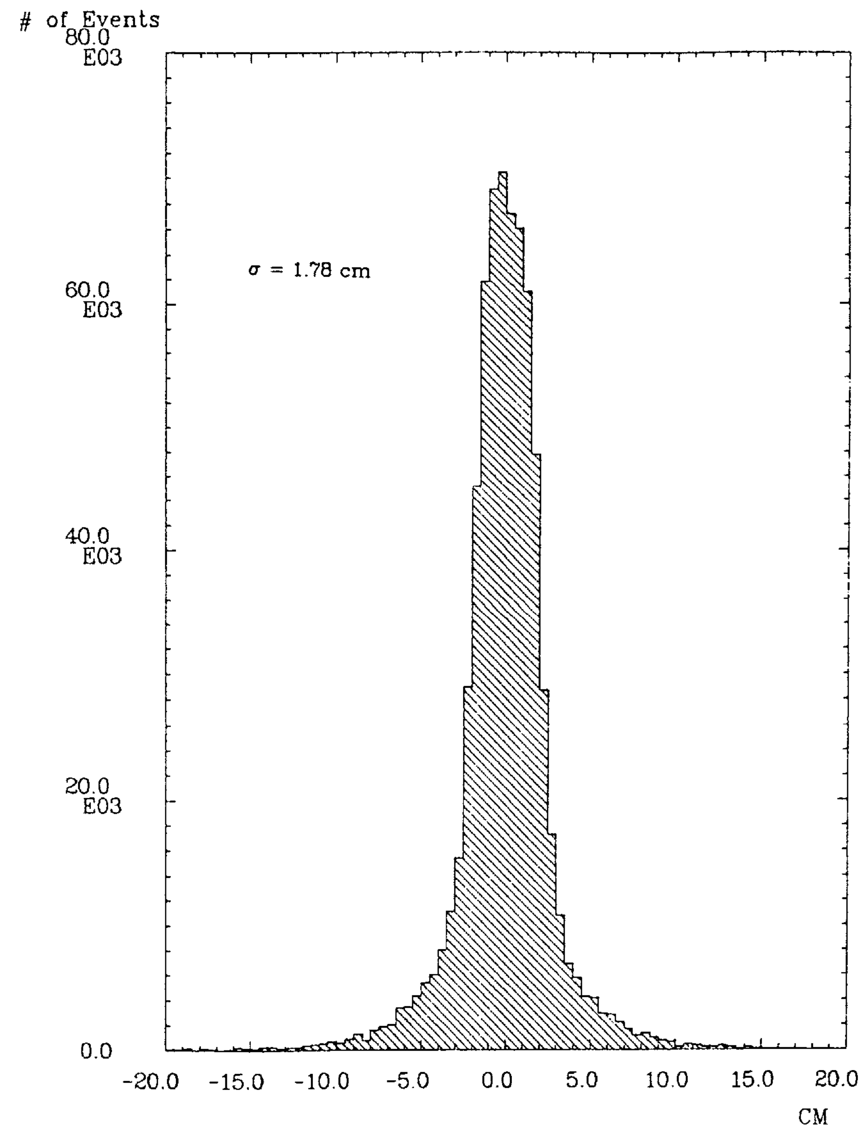

Fig. 3.8 Resolution of High Threshold TDC Position of A Counters

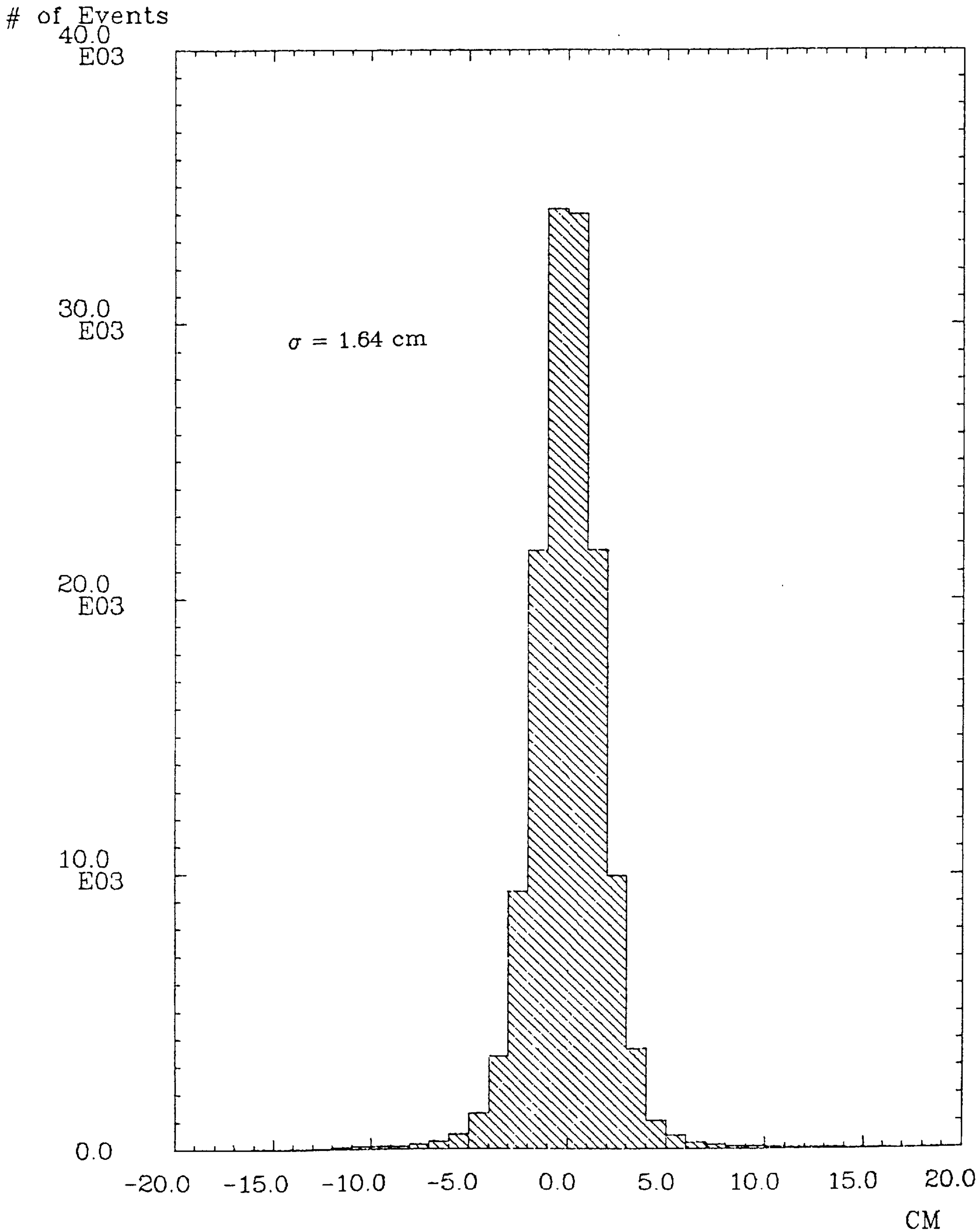

Fig. 3.9 Resolution of Weighted Position (Zbest) of B Counters

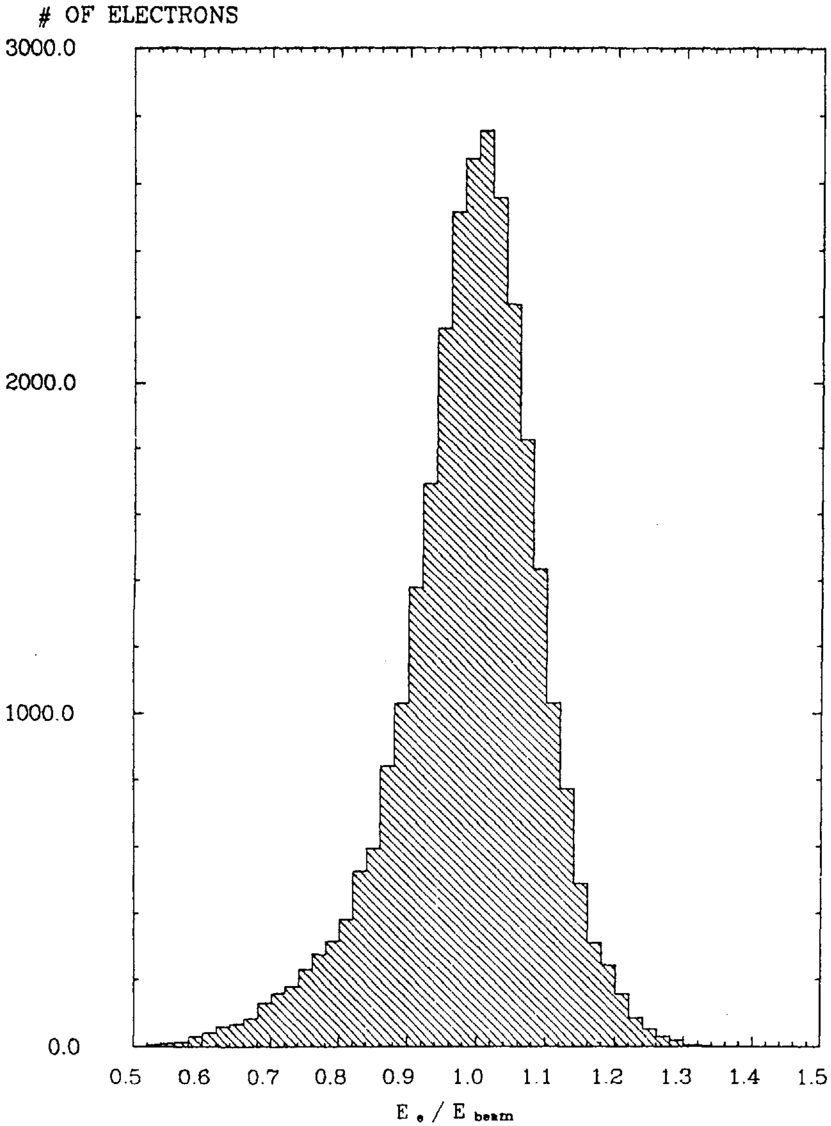

Fig. 3.10 ENERGY RESOLUTION OF THE ELECTRONS

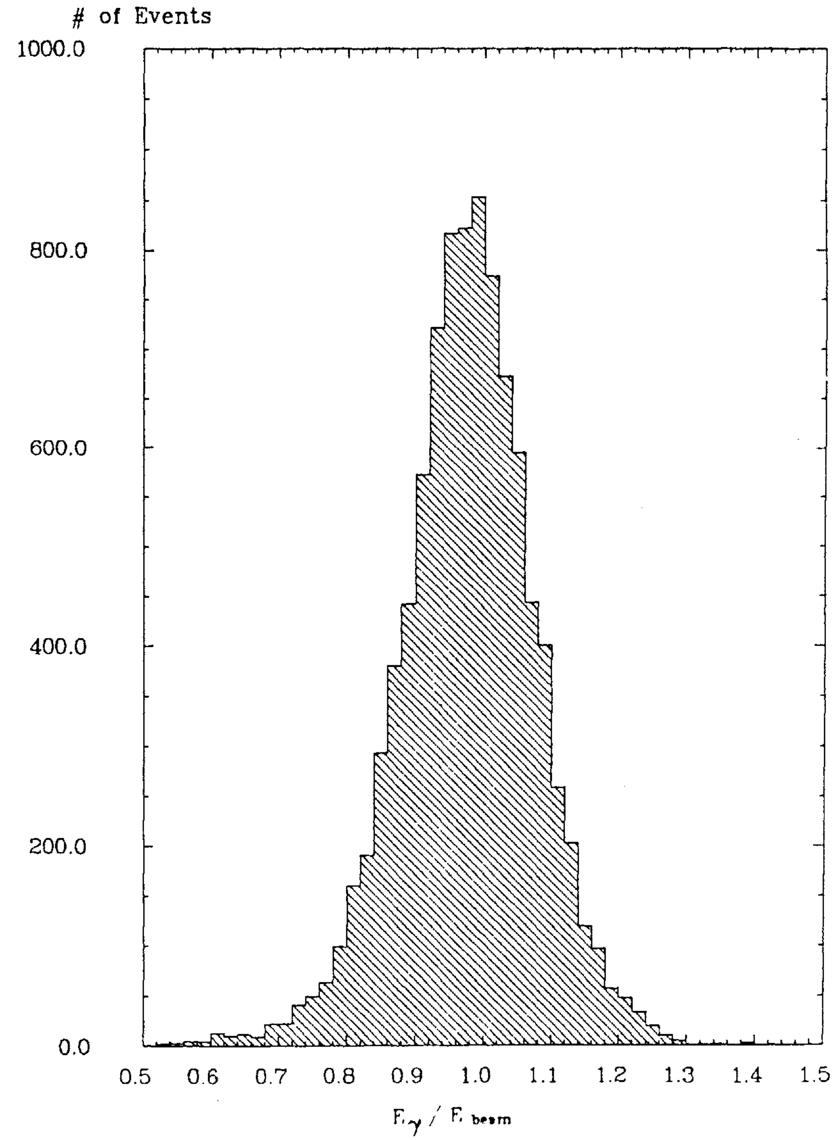

Fig. 3.11 ENERGY RESOLUTION OF PHOTONS

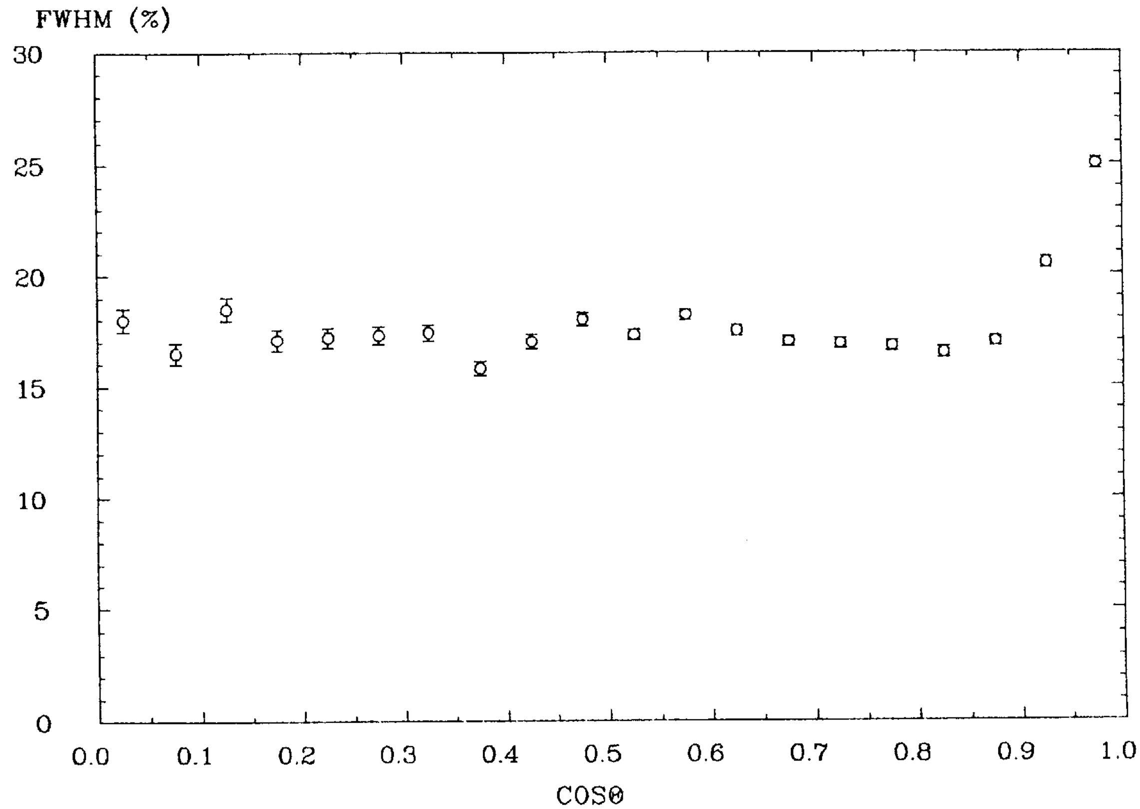

Fig. 3.12 FWHM RESOLUTION OF ELECTRON ENERGY

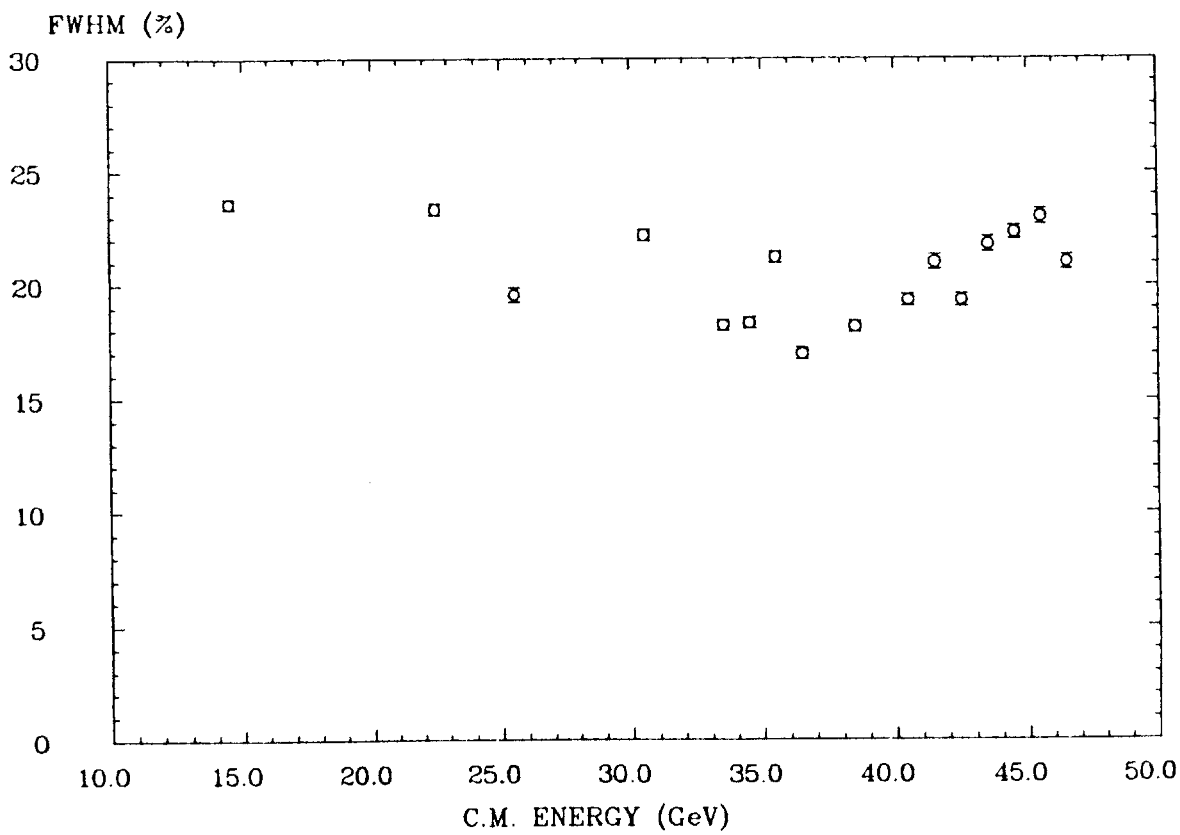

Fig. 3.13 FWHM RESOLUTION of ELECTRON vs. C.M. ENERGY

Relative difference of integrated luminosities measured with central detector (C) and luminosity monitor (G) during energy scan.

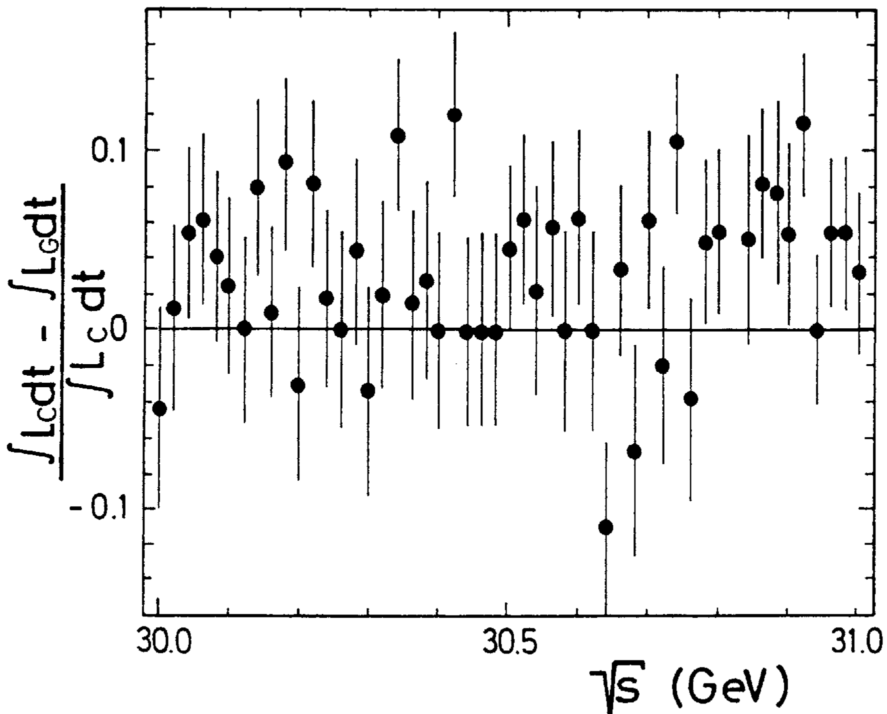

Fig. 3.14

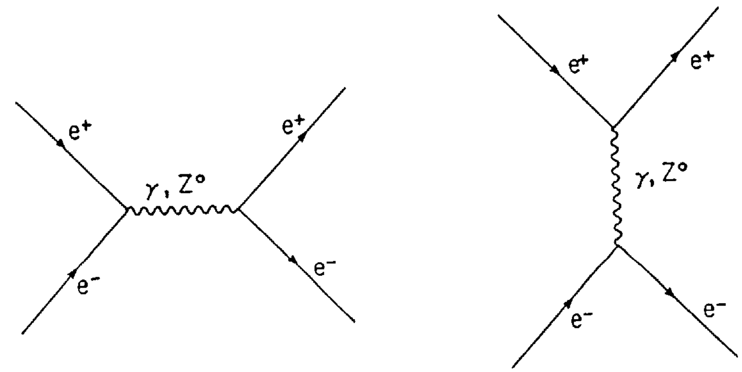

Fig. 5.1a

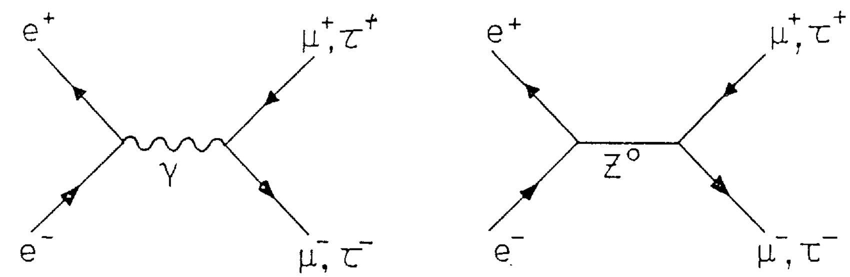

Fig. 5.1b

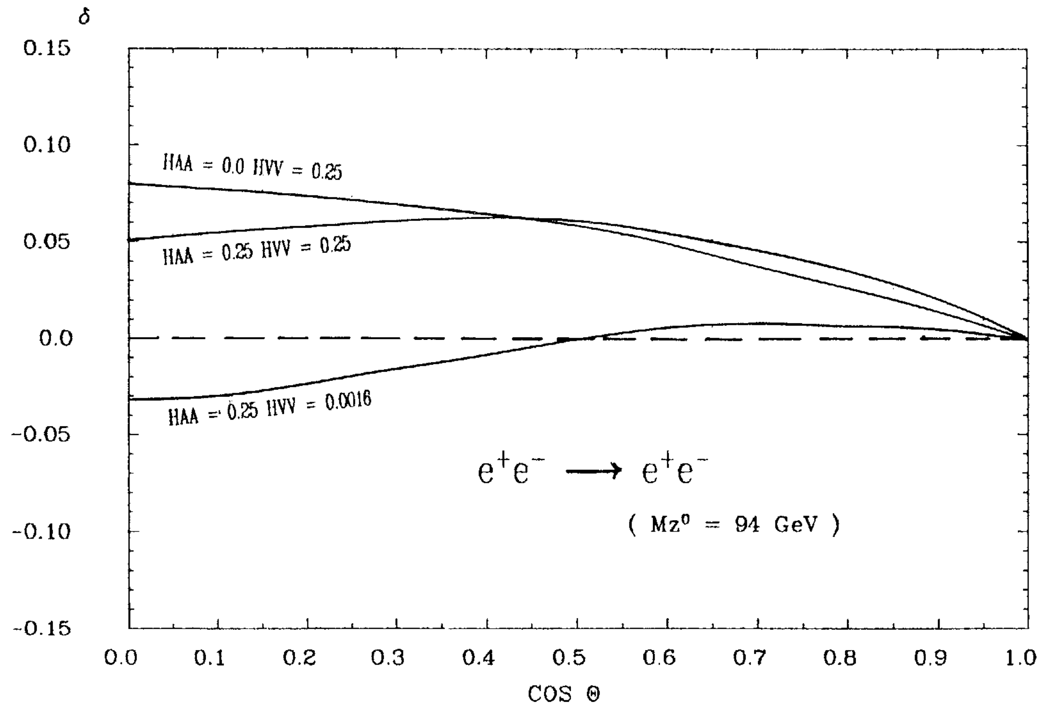
δ
0.15
0.10
0.05
0.0
-0.05
-0.10
-0.15
HAA = 0.0 HVV = 0.25
HAA = 0.25 HVV = 0.25
HAA = 0.25 HVV = 0.0016
e+e- ⟶ e+e-
(Mz0 = 94 GeV)
0.0
0.1
0.2
0.3
0.4
0.5
0.6
0.7
0.8
0.9
1.0
COS Θ

Fig. 5.2

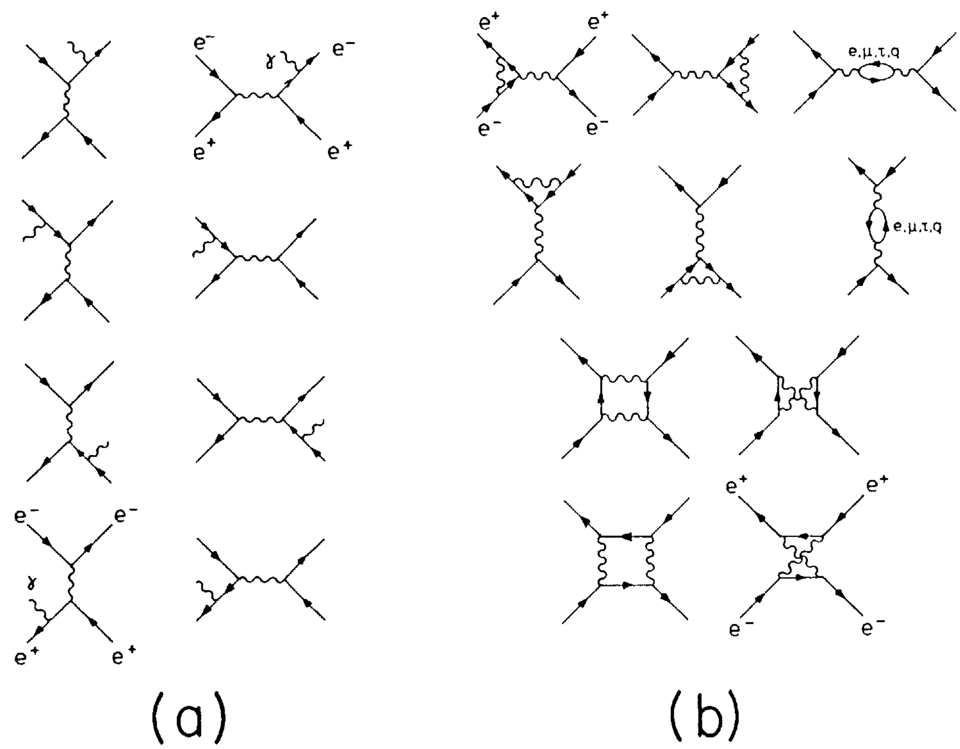
e-
e+
γ
e,μ,τ,q
(a)
(b)

Fig. 5.3

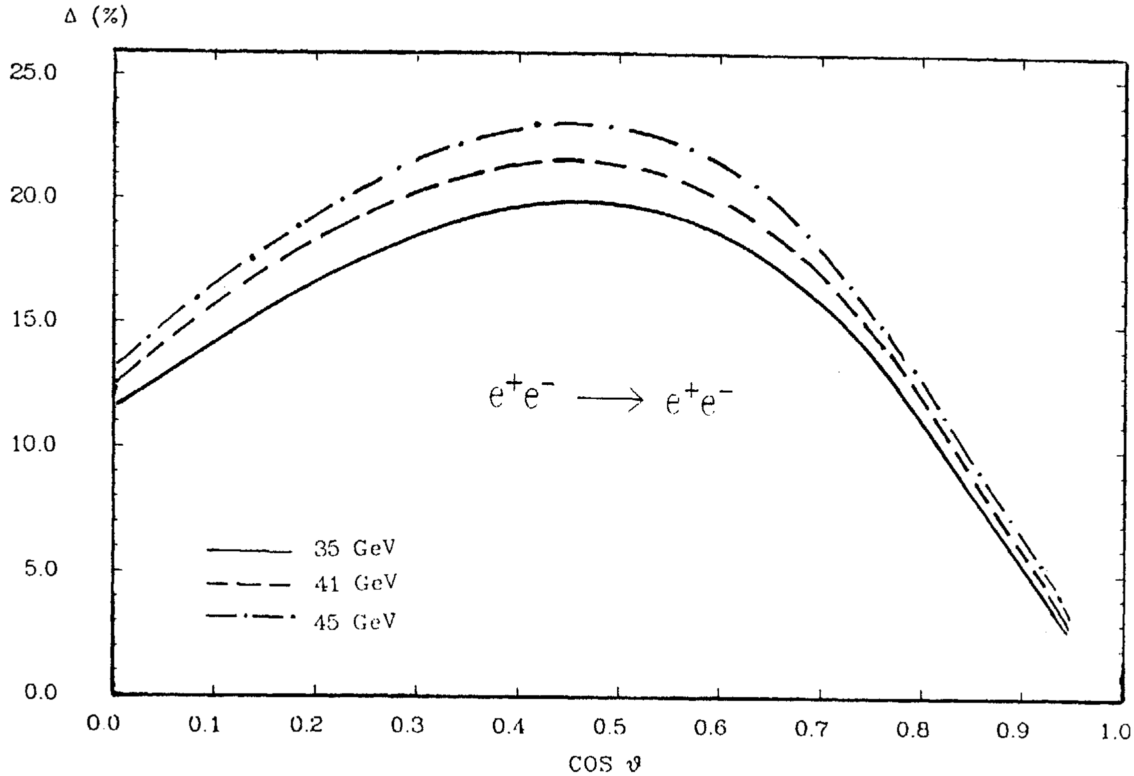

RADIATIVE CORRECTIONS OF BHABHA SCATTERING

Fig. 5.4

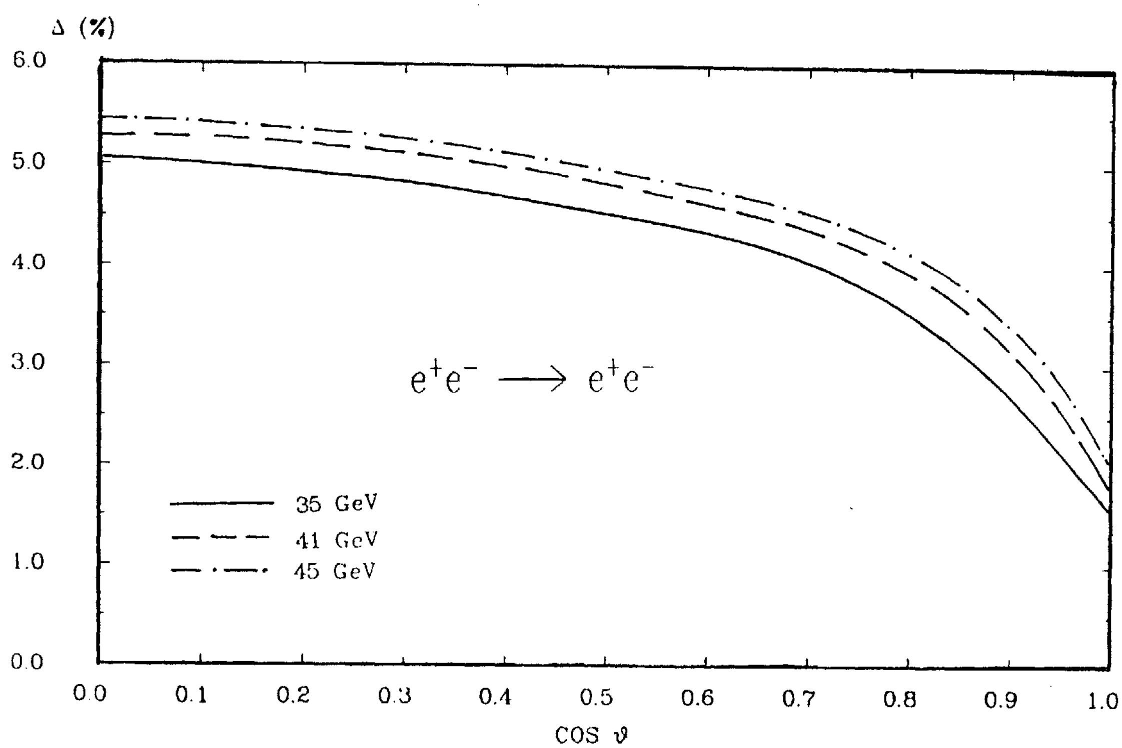

HADRON AND τ VACUUM POLARIZATION

Fig. 5.5

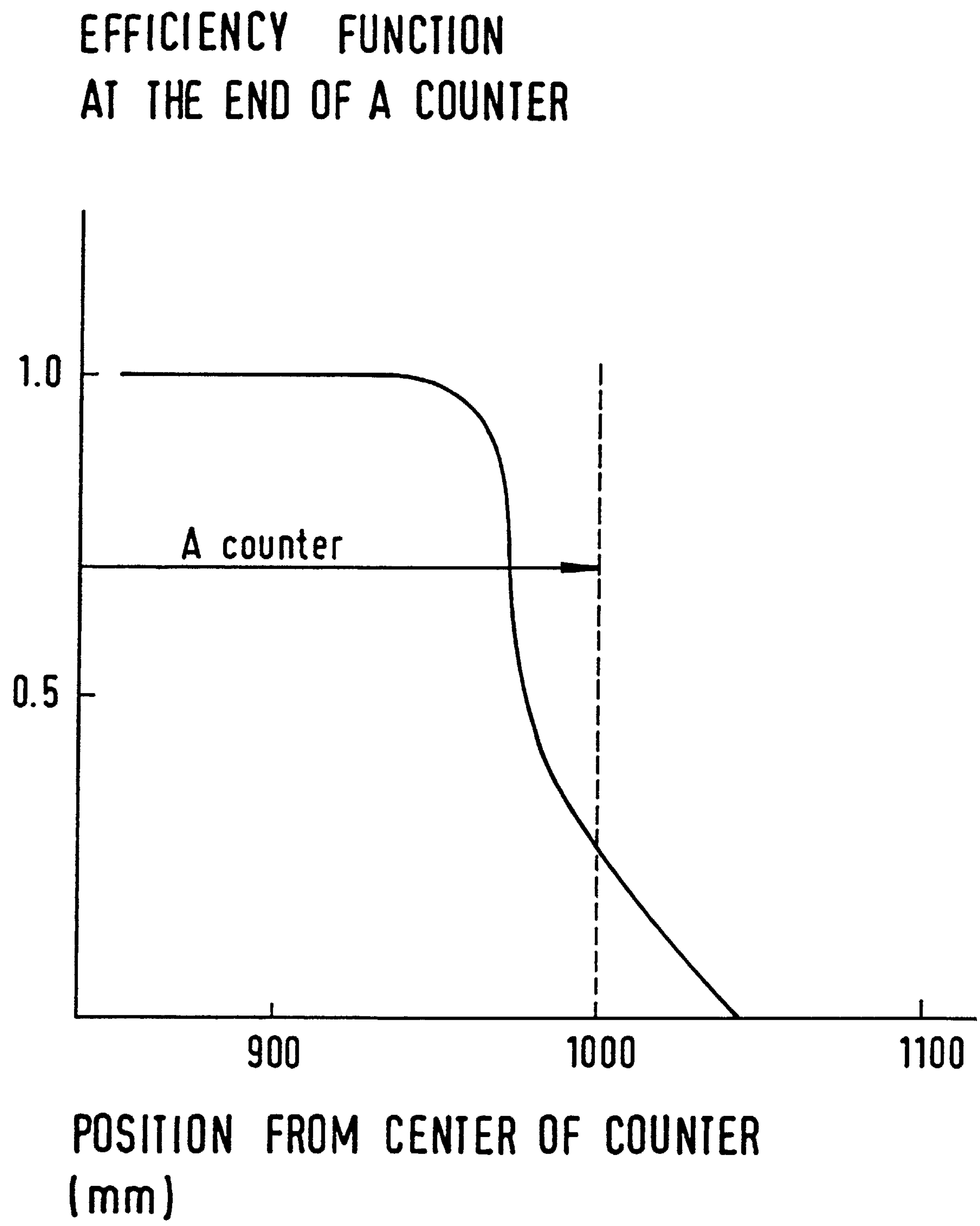
EFFICIENCY FUNCTION
AT THE END OF A COUNTER
1.0
0.5
A counter
900
1000
1100
POSITION FROM CENTER OF COUNTER
(mm)

Fig. 5.6

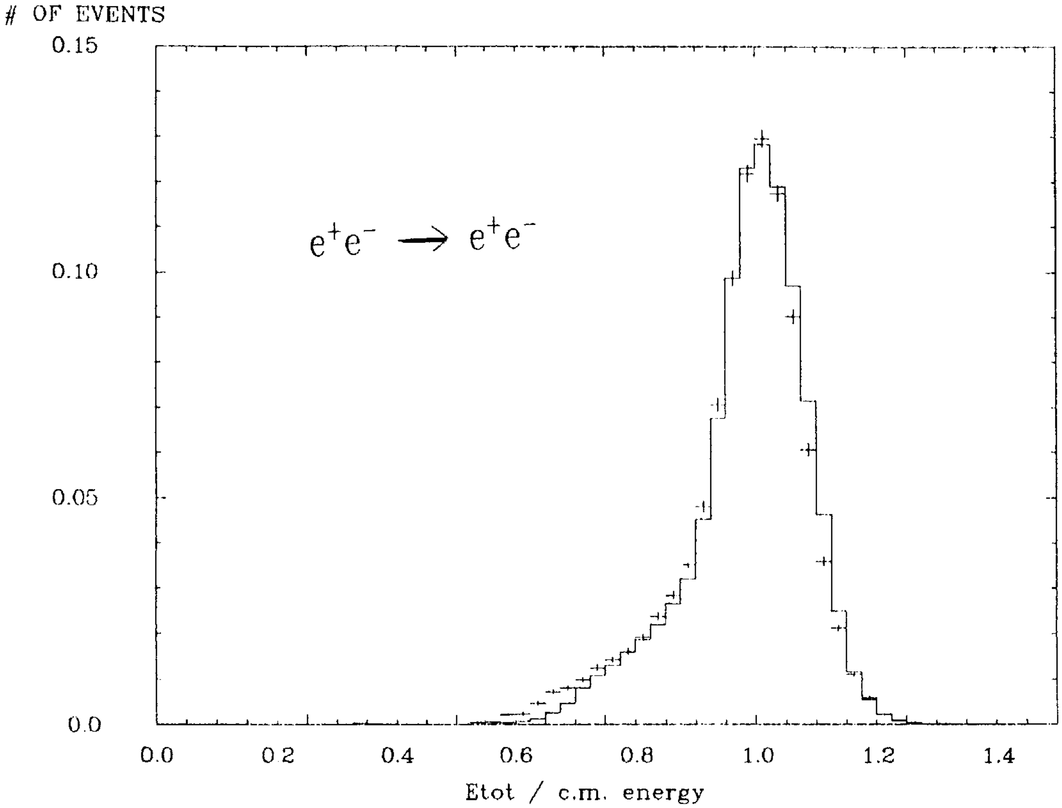

Fig. 5.7

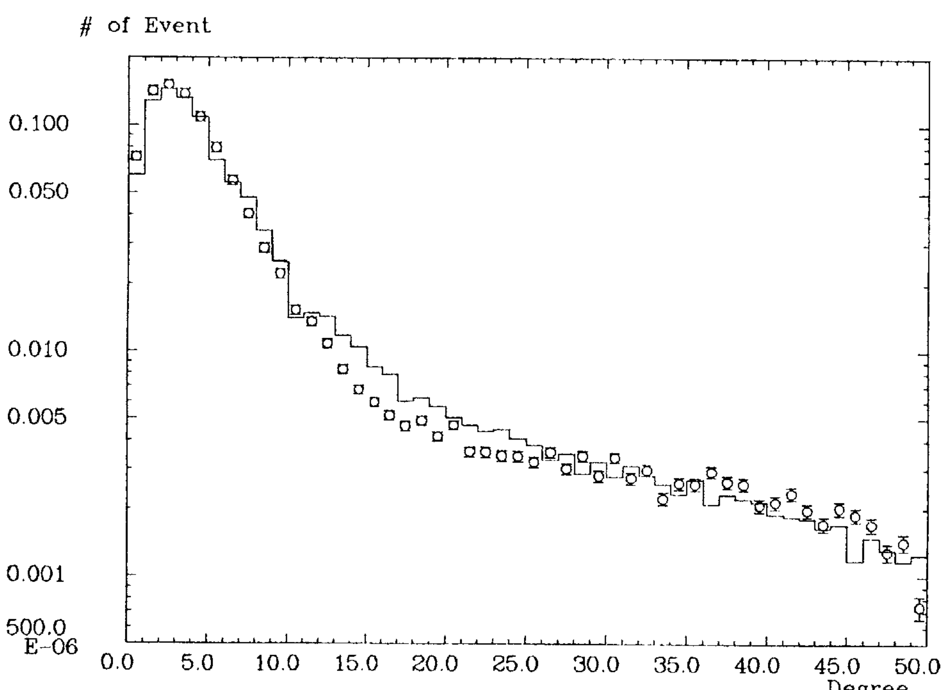

ACOLLINEARITY DISTRIBUTION OF BHABHA EVENTS

Fig. 5.8

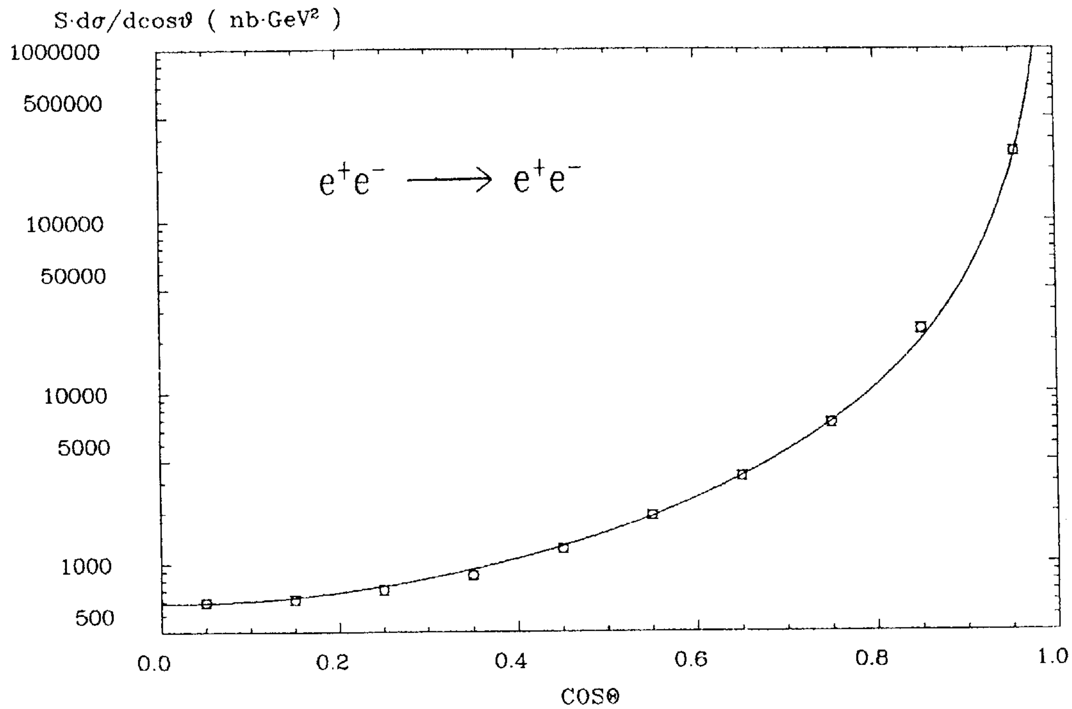

COSΘ DISTRIBUTION OF $e^+e^- \longrightarrow e^+e^-$ (14GeV)

Fig. 5.9

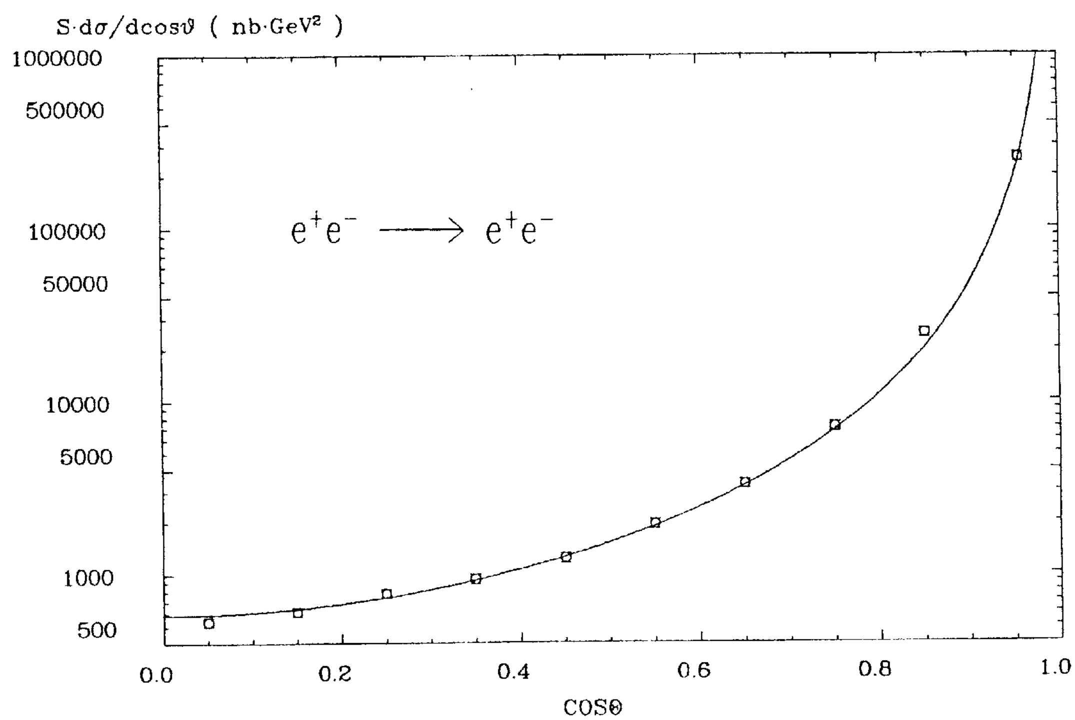

COSΘ DISTRIBUTION OF $e^+e^- \longrightarrow e^+e^-$ (22GeV)

Fig. 5.10

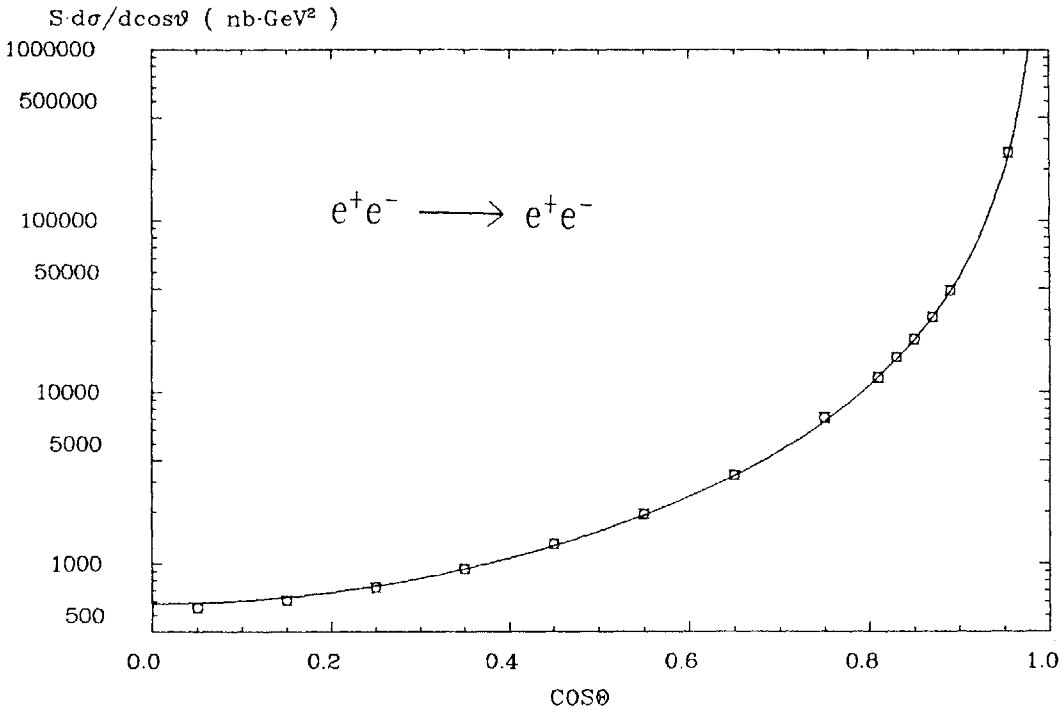

COSΘ DISTRIBUTION OF $e^+e^- \longrightarrow e^+e^-$ (35GeV)

Fig. 5.11

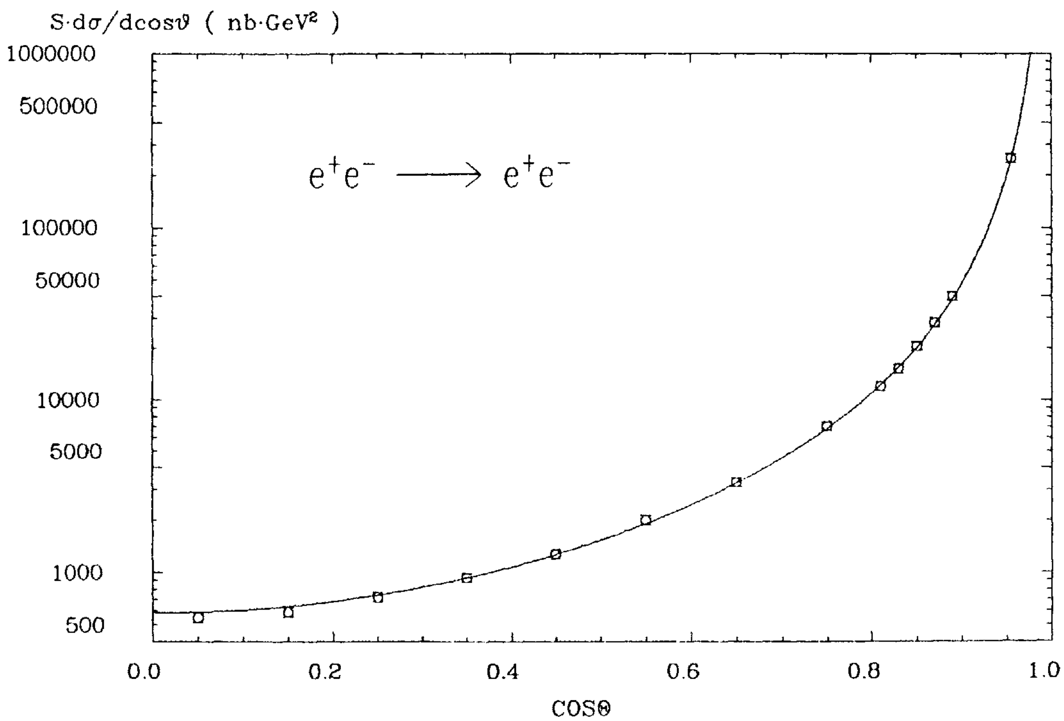

COSΘ DISTRIBUTION OF $e^+e^- \longrightarrow e^+e^-$ (43GeV)

Fig. 5.12

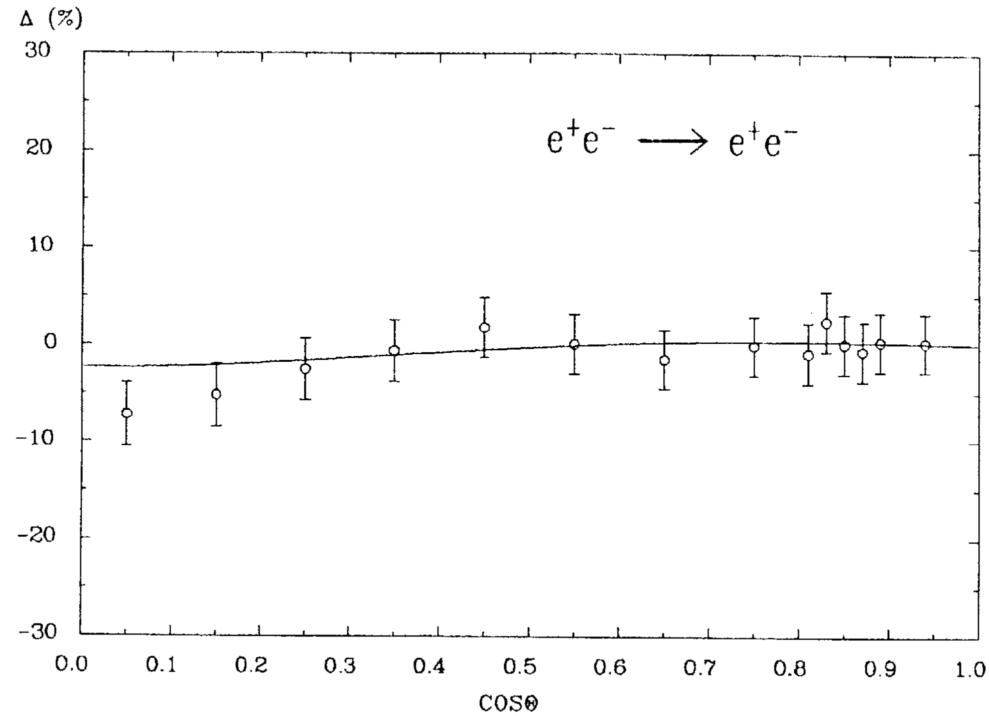

Fig. 4.13 DELTA VALUES OF $e^+e^- \longrightarrow e^+e^-$ (35GeV)

Fig. 5.13

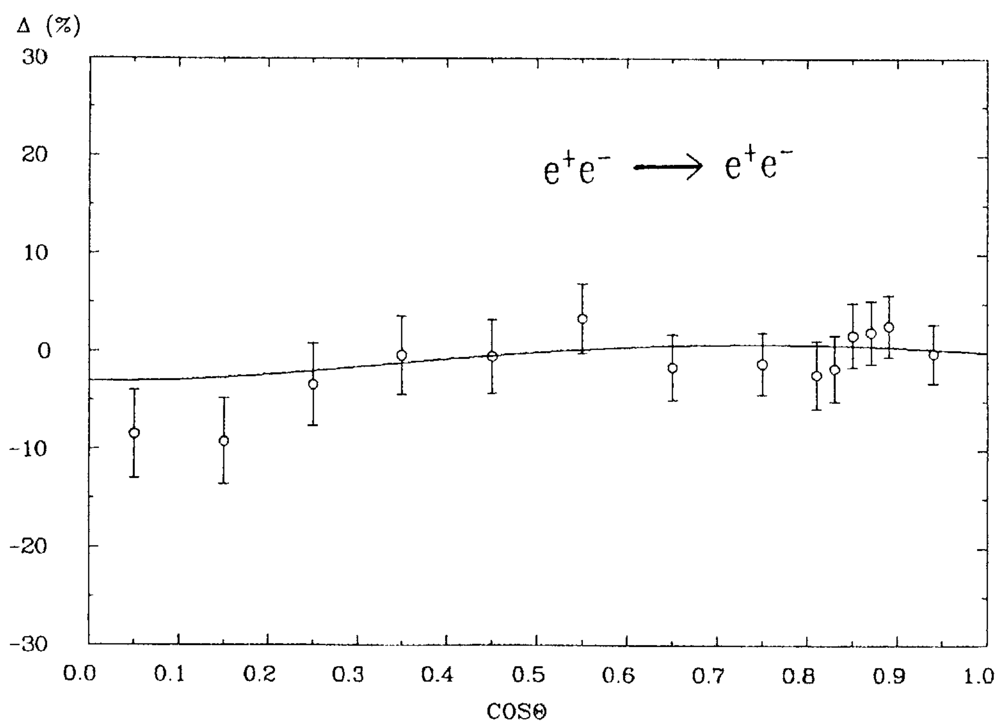

Fig. 4.14 DELTA VALUES OF $e^+e^- \longrightarrow e^+e^-$ (43GeV)

Fig. 5.14

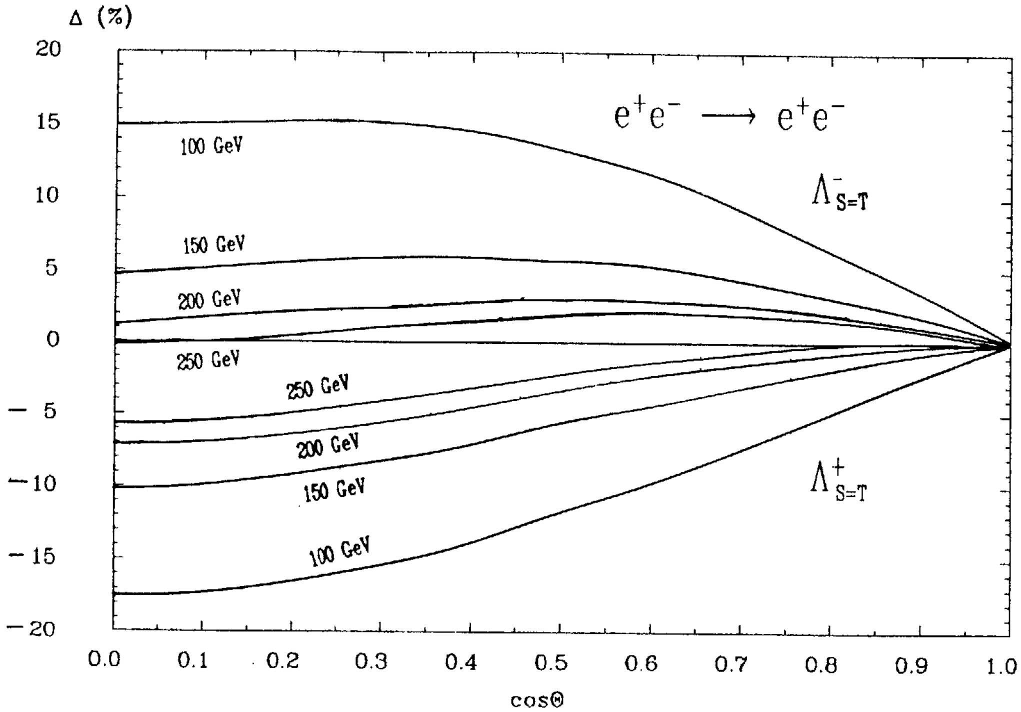

Fig. 5.15

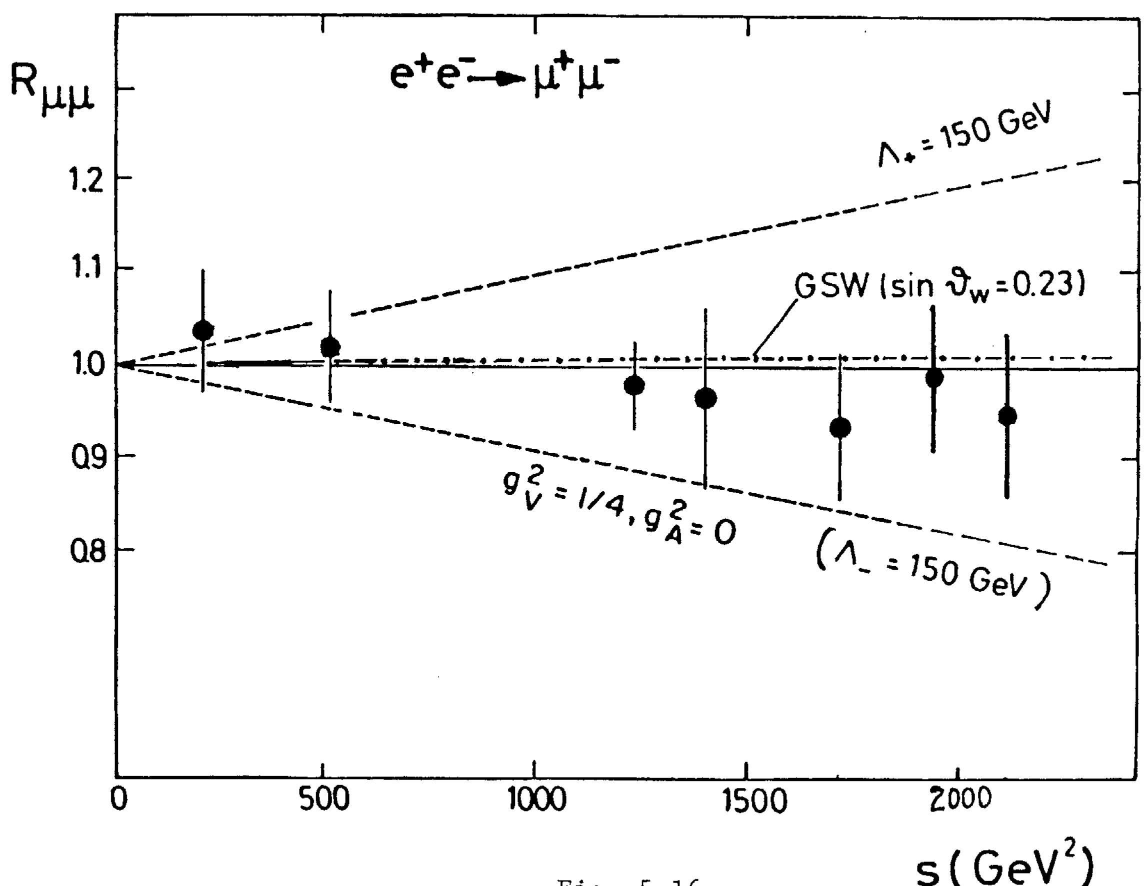

Fig. 5.16

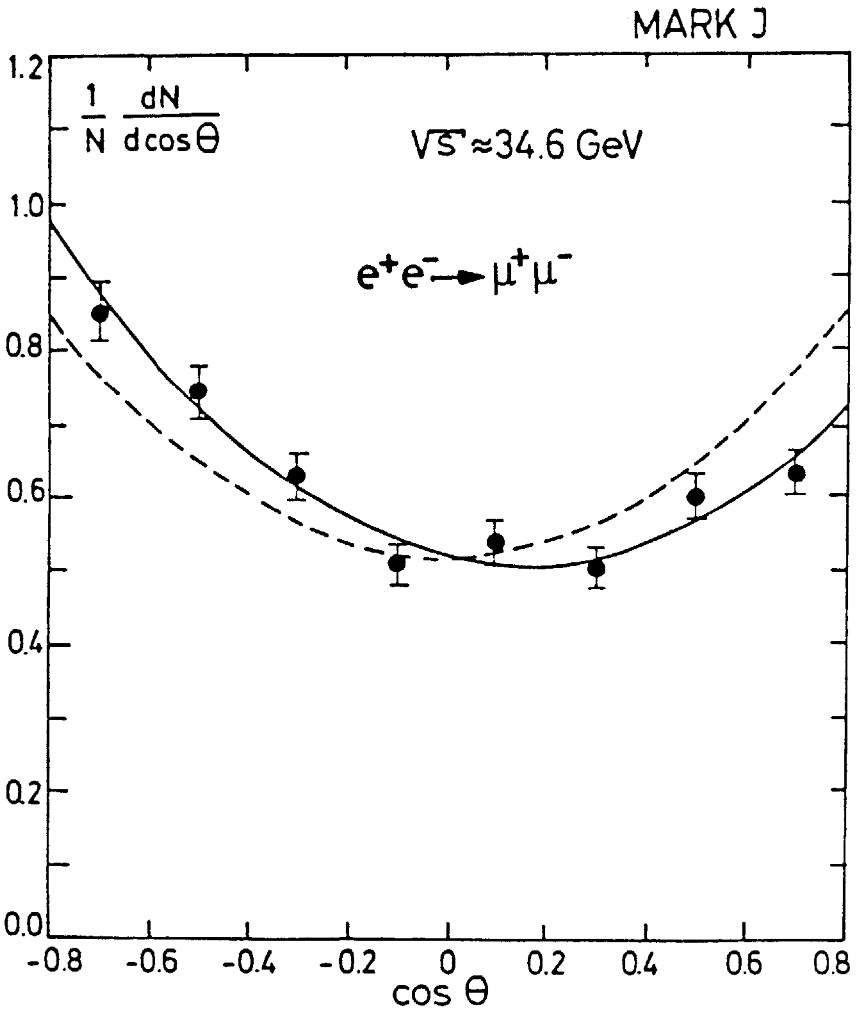

Fig. 5.17

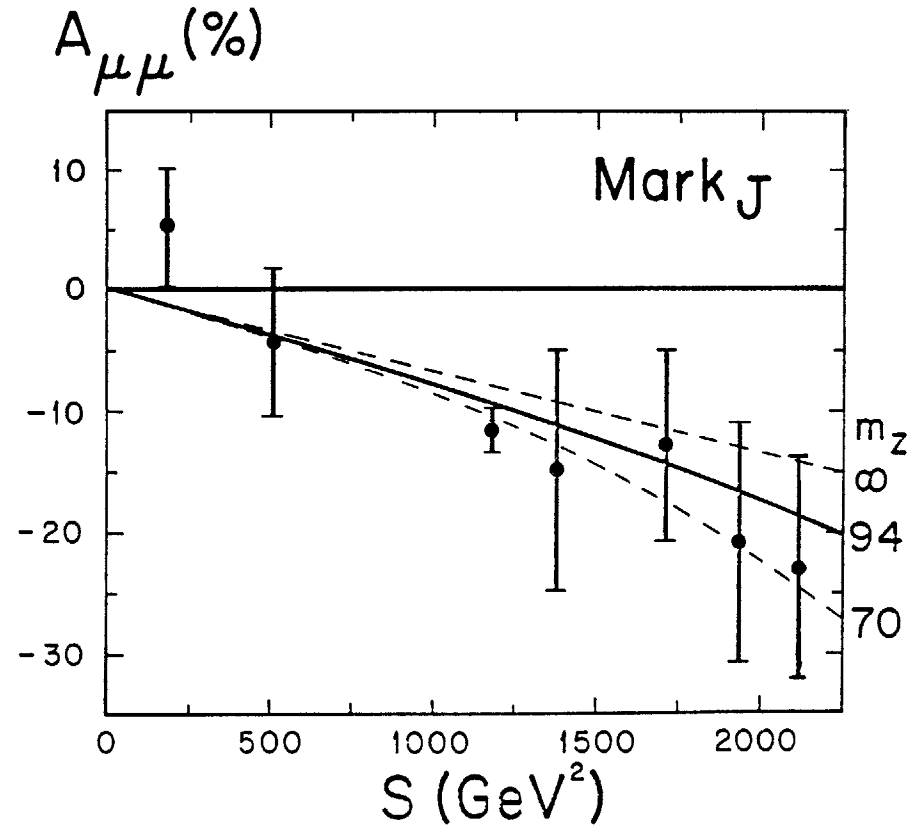

Fig. 5.18

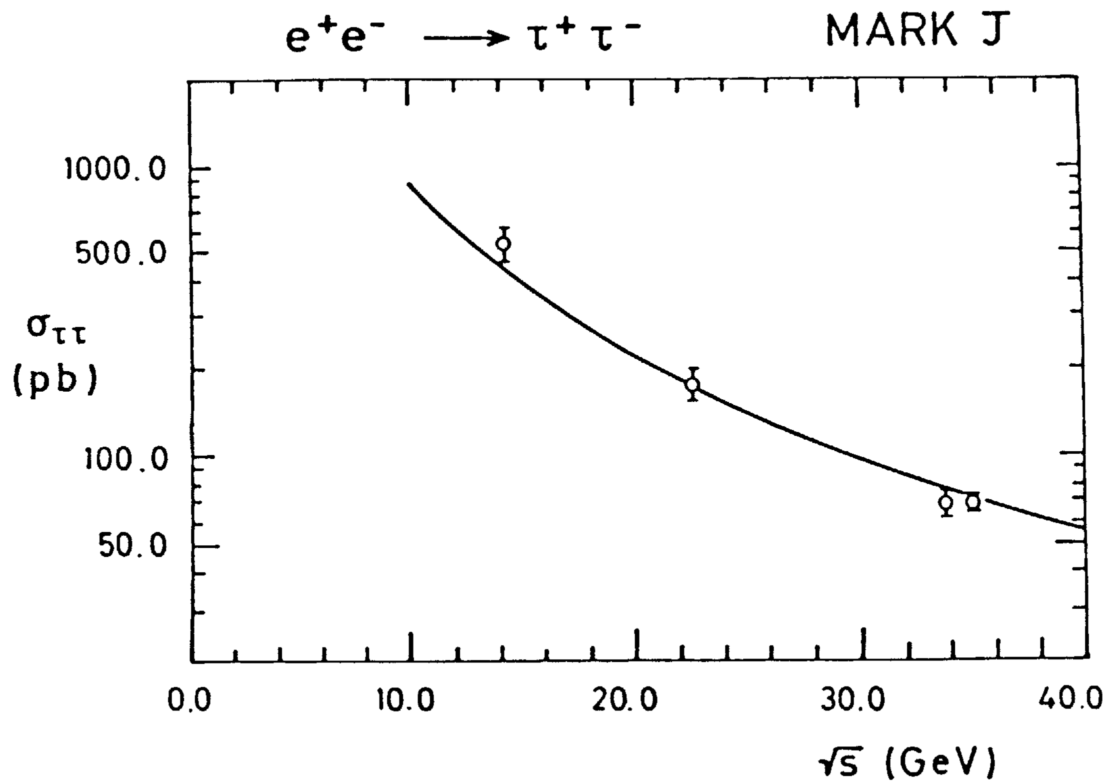

Fig. 5.19

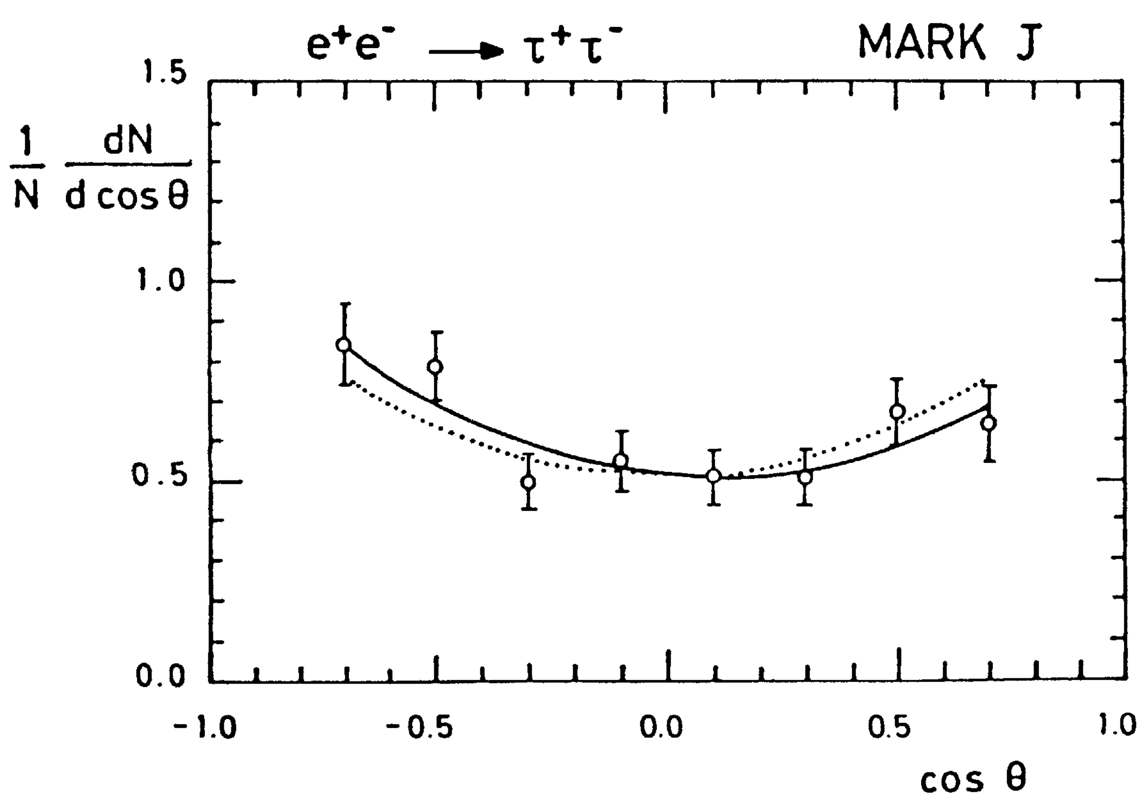

Fig. 5.20

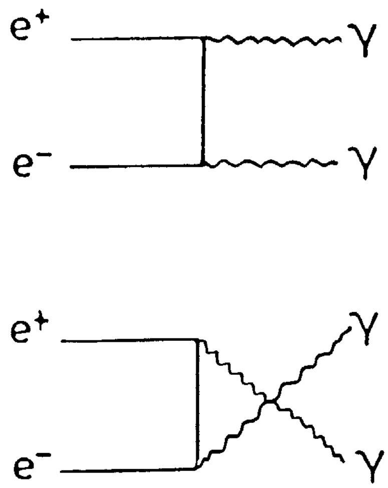

Fig. 5.21

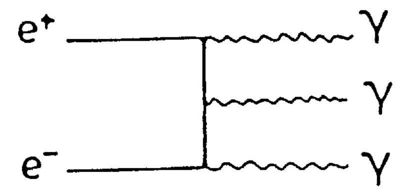

Fig. 5.22

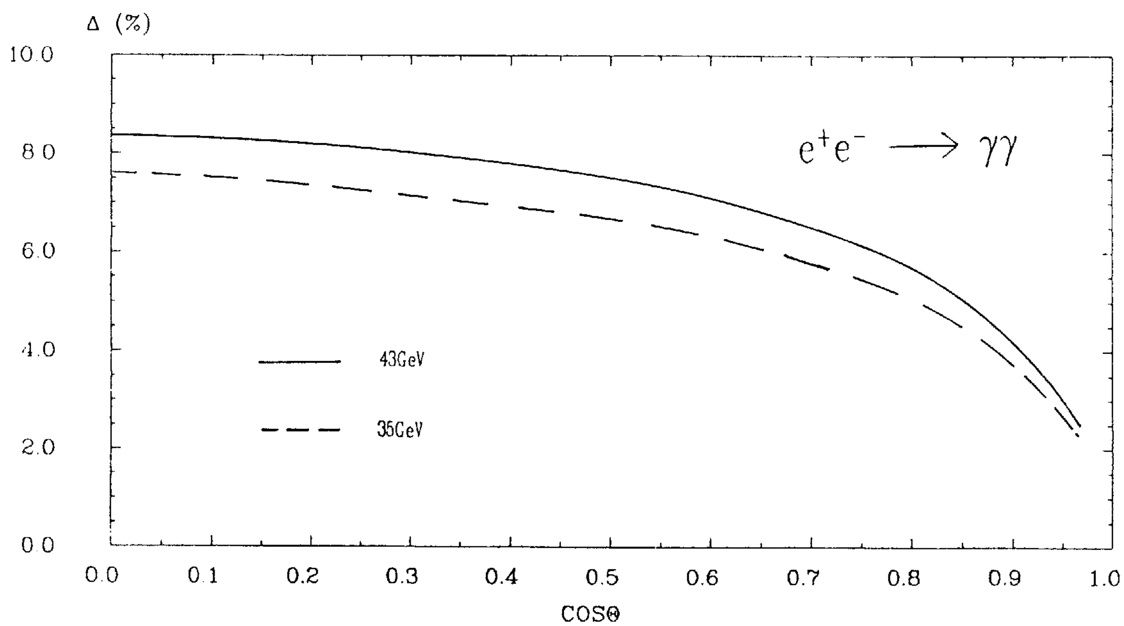

RADIATIVE CORRECTION OF $e^+e^- \longrightarrow \gamma\gamma$

Fig. 5.23

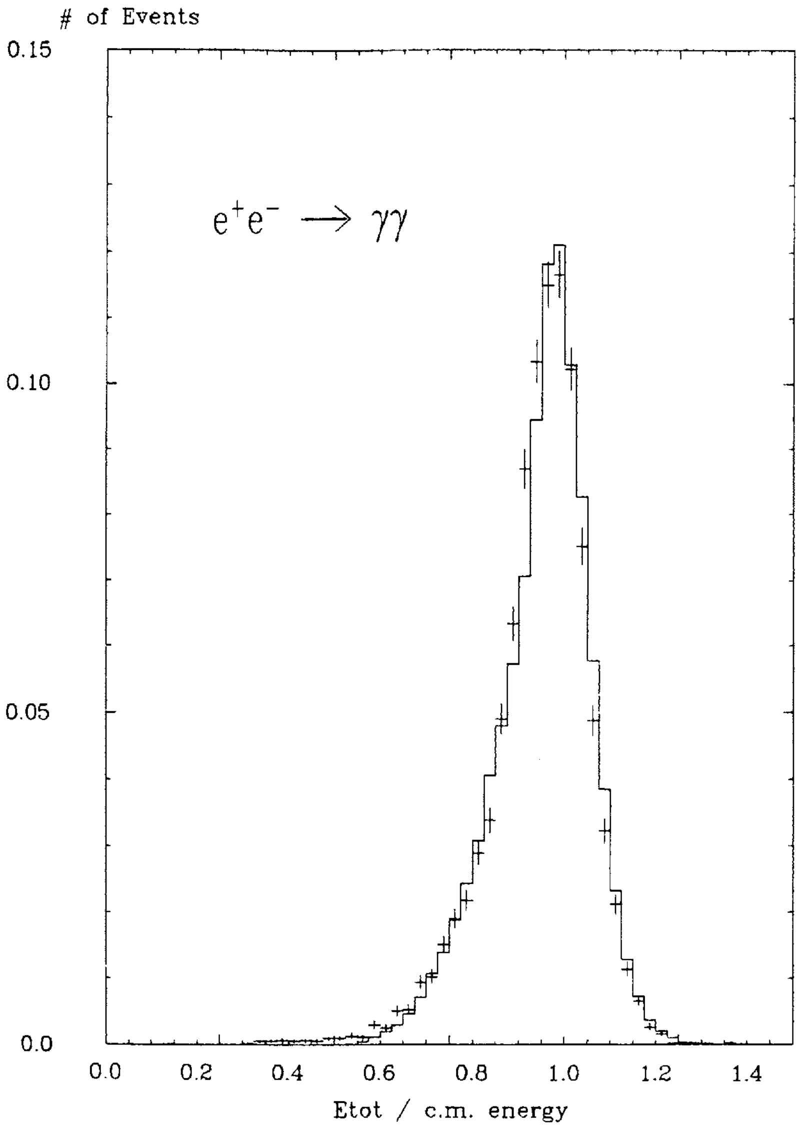

Fig. 5.24

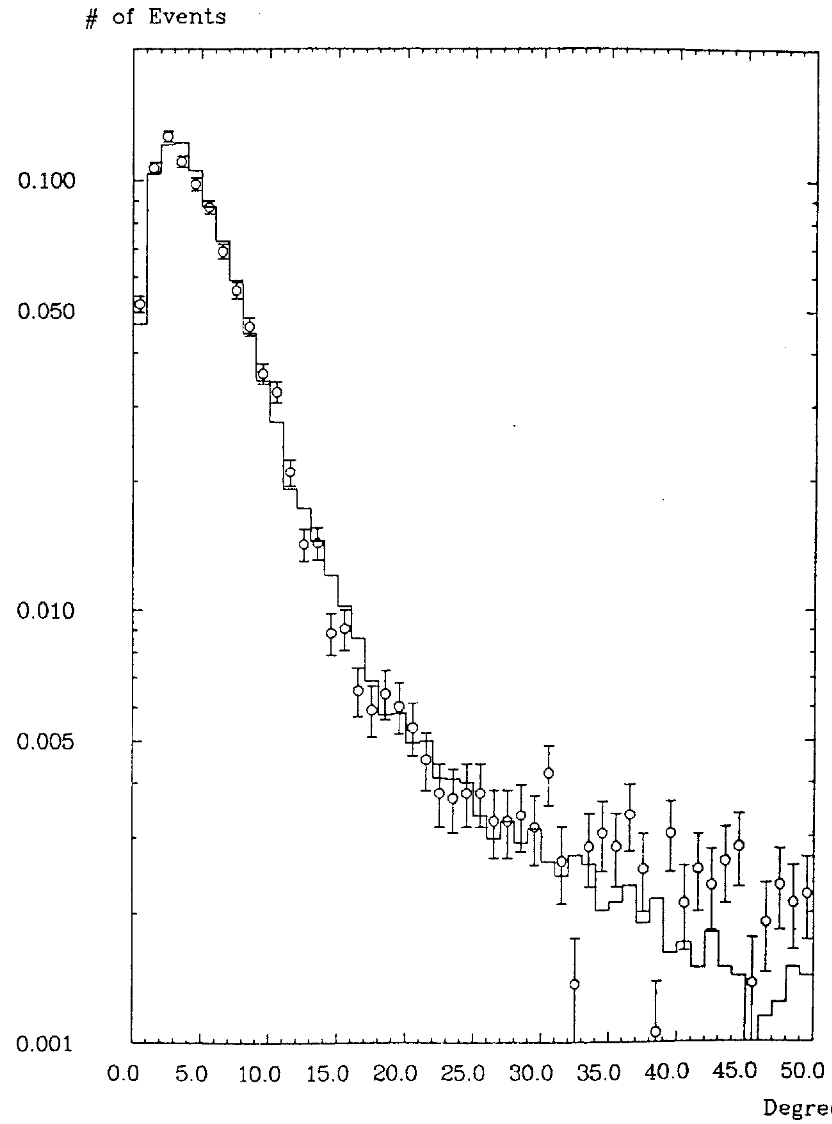

ACOLLINEARITY DISTRIBUTION OF TWO PHOTON EVENTS

Fig. 5.25

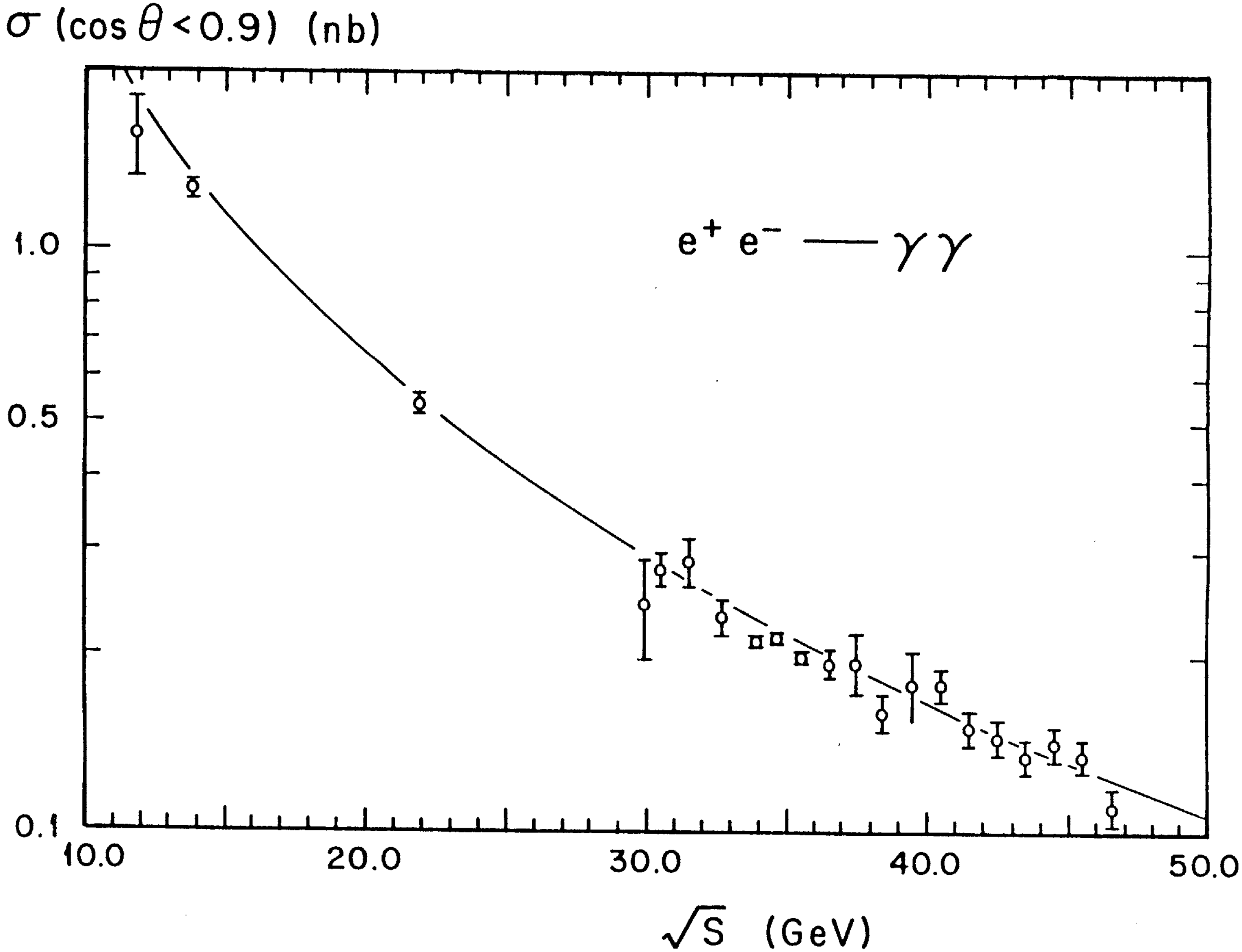

Fig. 5.26

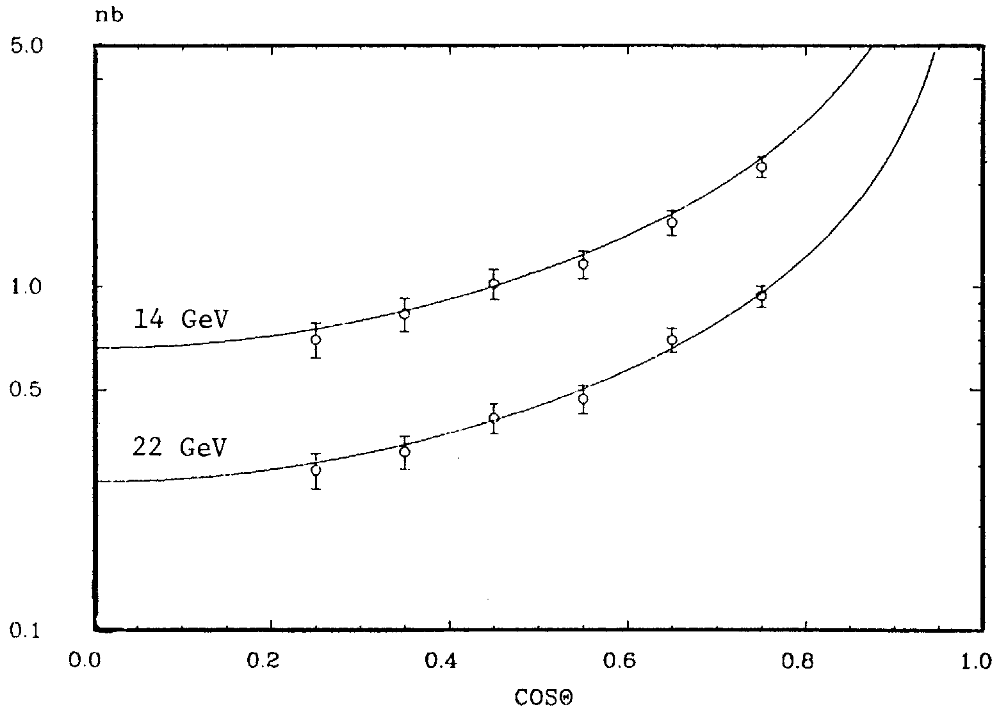

COSΘ DISTRIBUTION OF $e^+e^- \longrightarrow \gamma\gamma$ (14 & 22GeV)

Fig. 5.27a

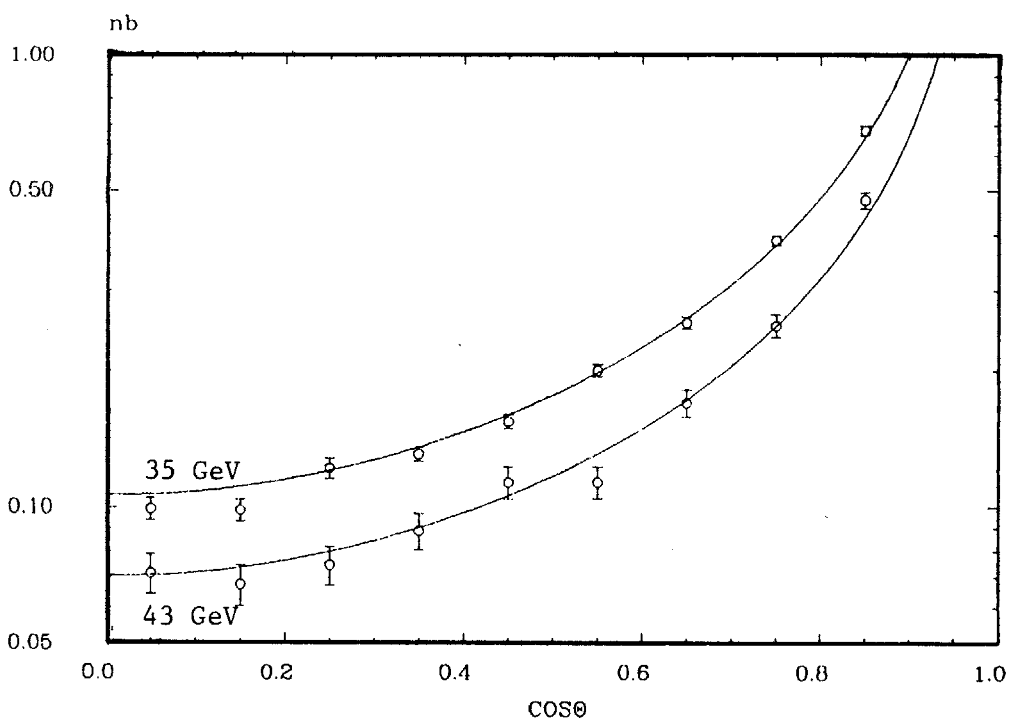

COSΘ DISTRIBUTION OF $e^+e^- \longrightarrow \gamma\gamma$ (35 & 43 GeV)

Fig. 5.27b

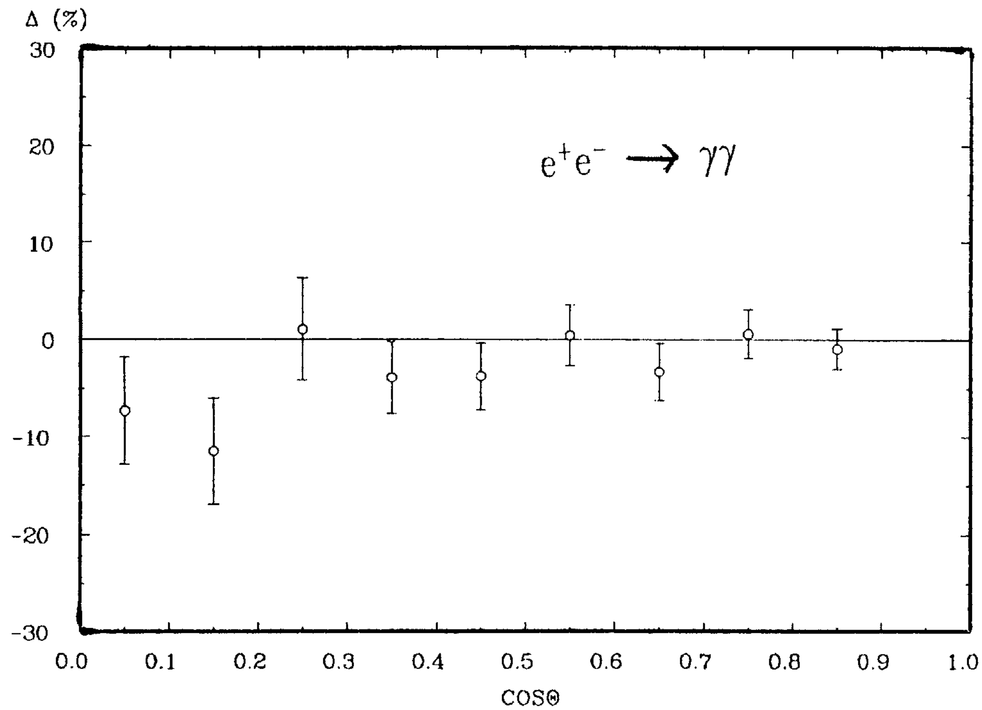

DELTA VALUES OF $e^+e^- \longrightarrow \gamma\gamma$ (35 GeV)

Fig. 5.28a

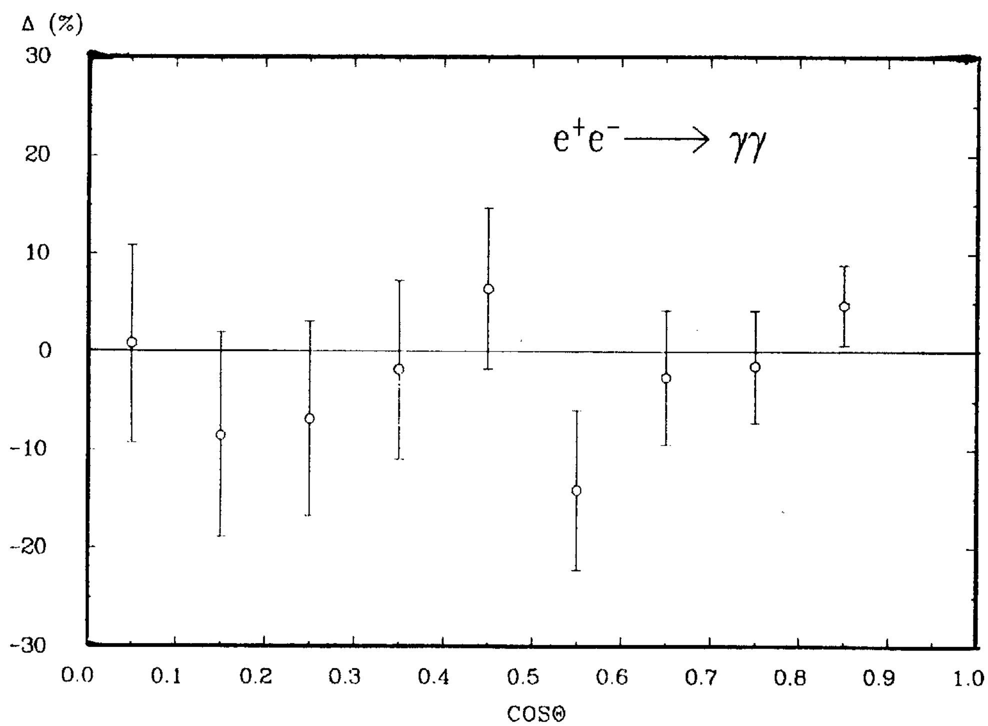

DELTA VALUES OF $e^+e^- \longrightarrow \gamma\gamma$ (43 GeV)

Fig. 5.28b

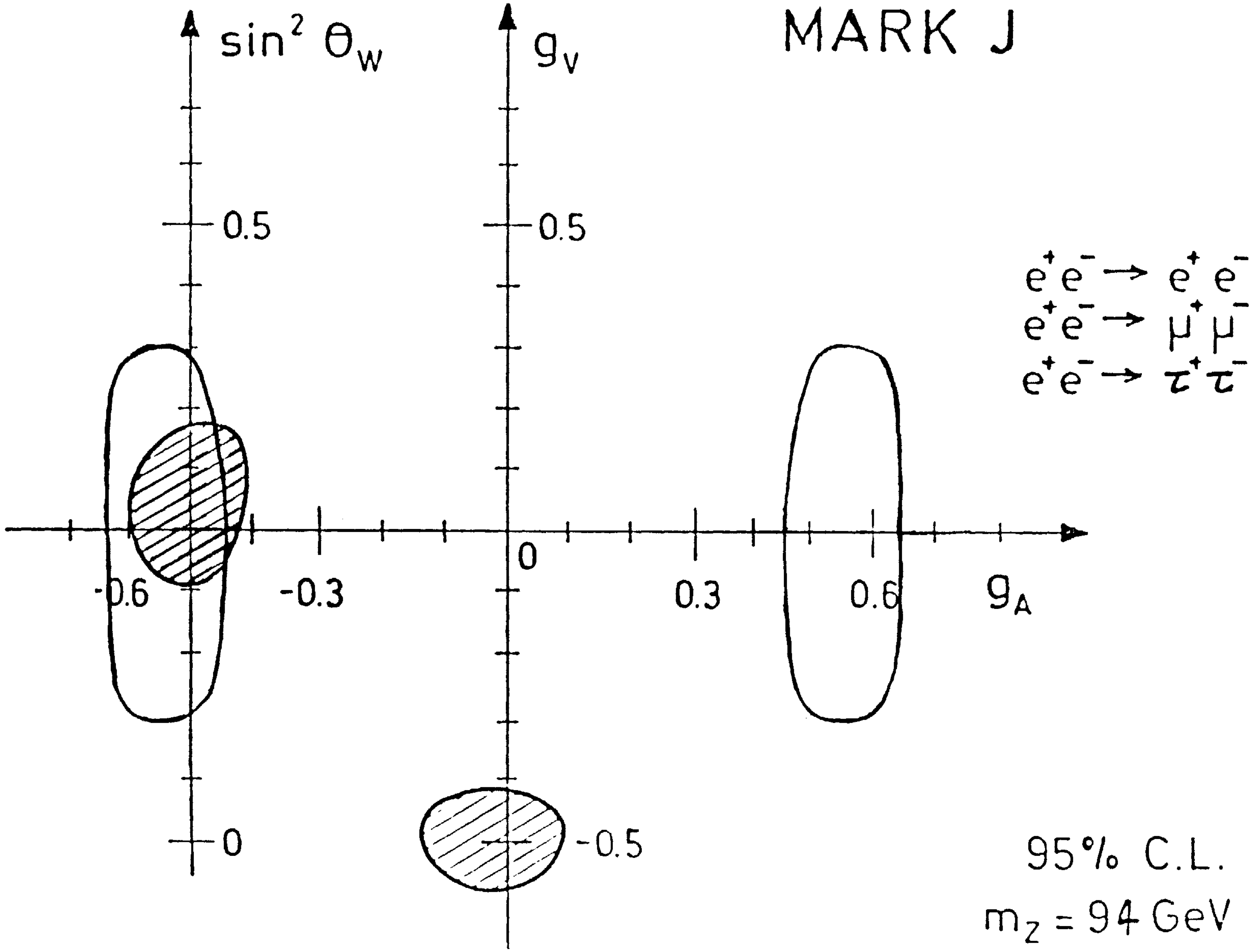

MARK J
$\sin^2 \theta_W$
g_V
0.5
0.5
$e^+e^- \to e^+e^-$
$e^+e^- \to \mu^+\mu^-$
$e^+e^- \to \tau^+\tau^-$
-0.6
-0.3
0
0.3
0.6
g_A
0
-0.5
95% C.L.
$m_Z = 94$ GeV

Fig. 5.29

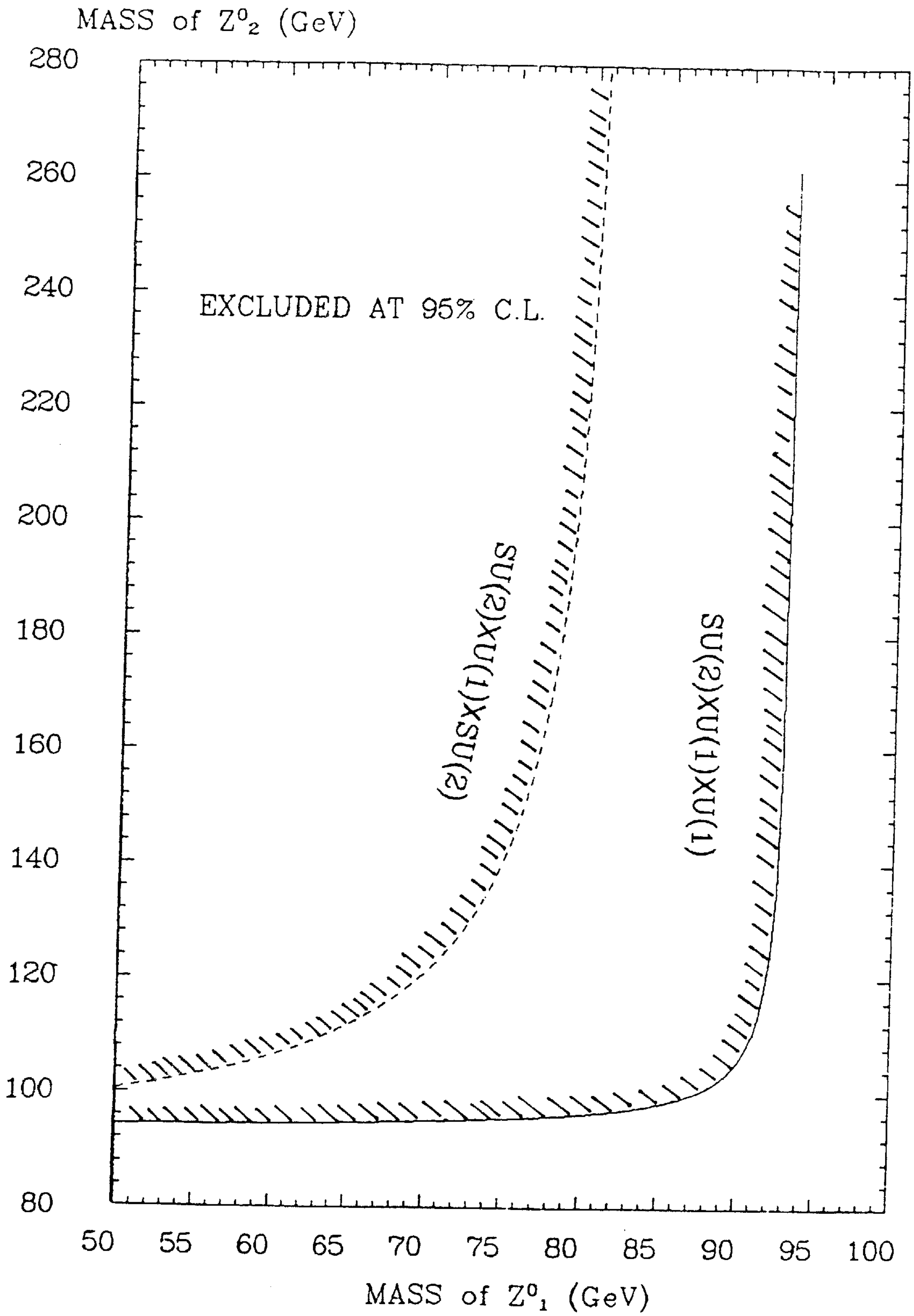

Fig. 5.30 The Mass Limits On Two Z° Models

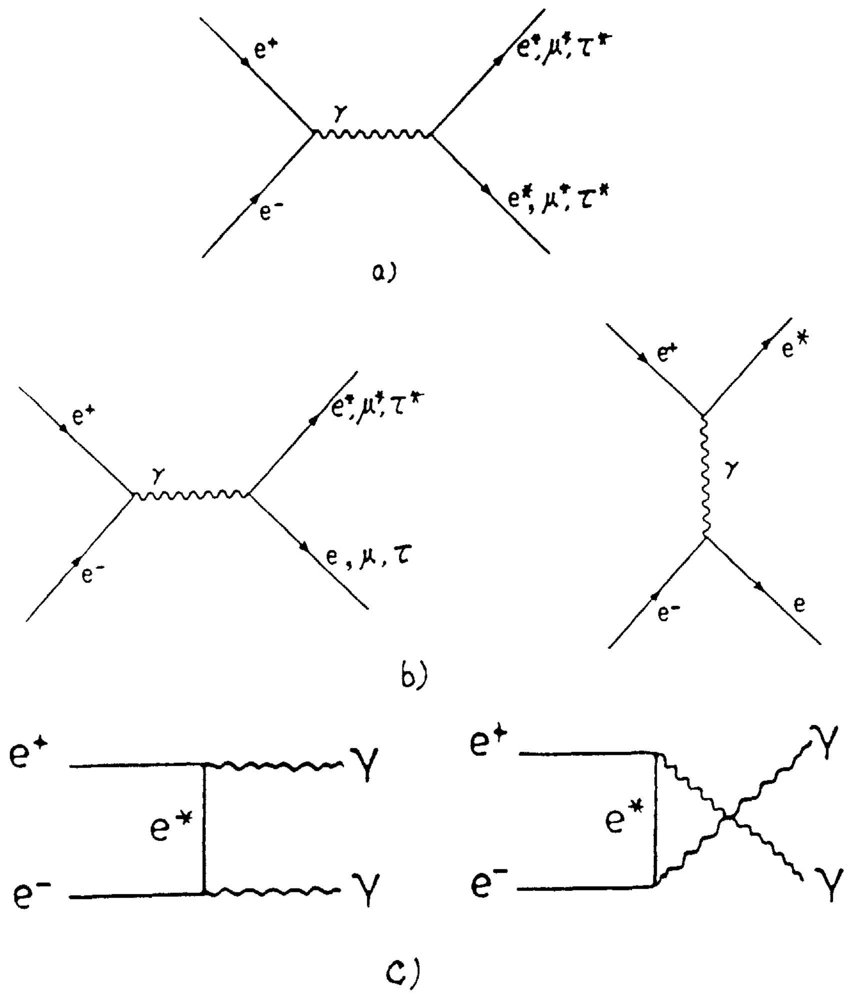

Fig. 6.1

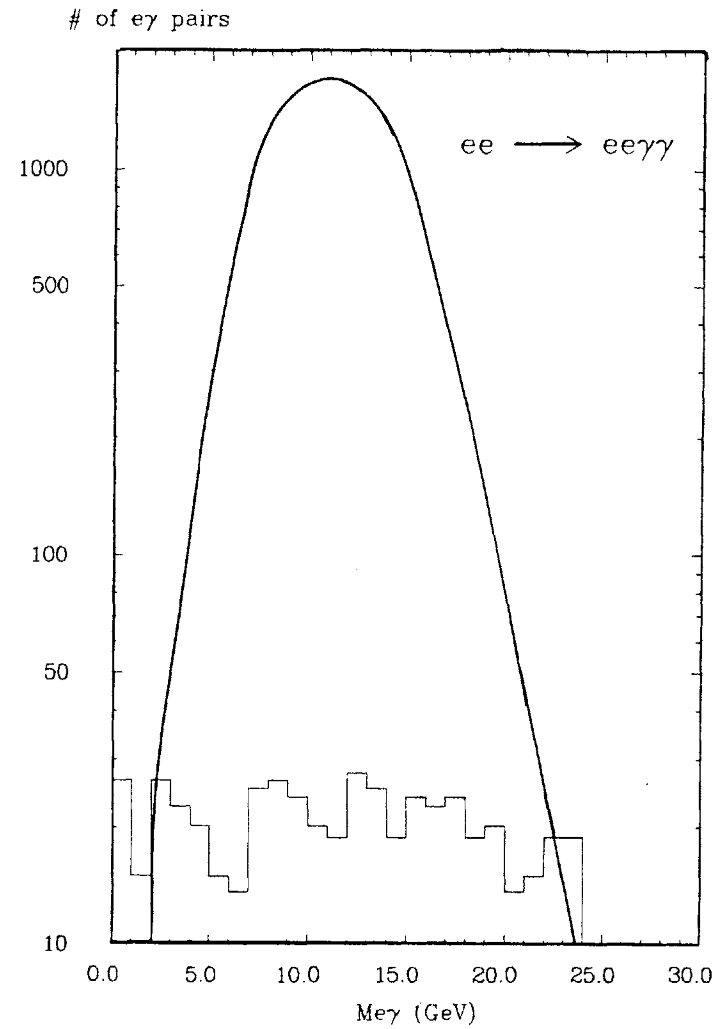

INVARIANT MASS DISTRIBUTION OF ee → eeγγ

Fig. 6.2

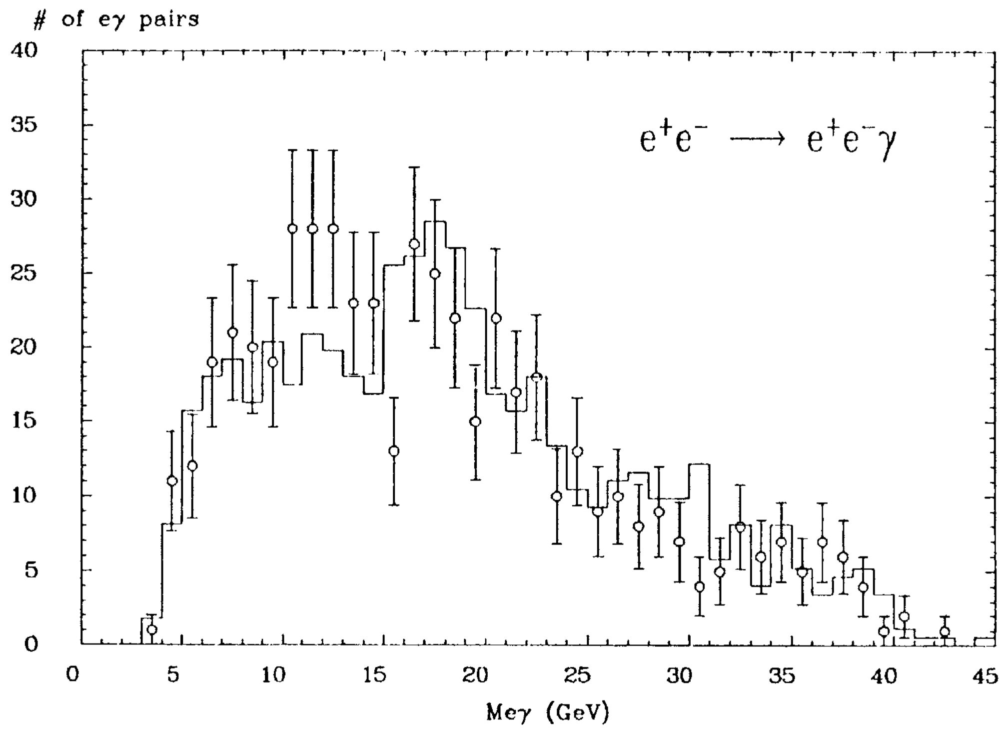

# of eγ pairs
40
35
30
25
20
15
10
5
0
0
5
10
15
20
25
30
35
40
45
Meγ (GeV)
e+e- ⟶ e+e-γ

Fig. 6.3

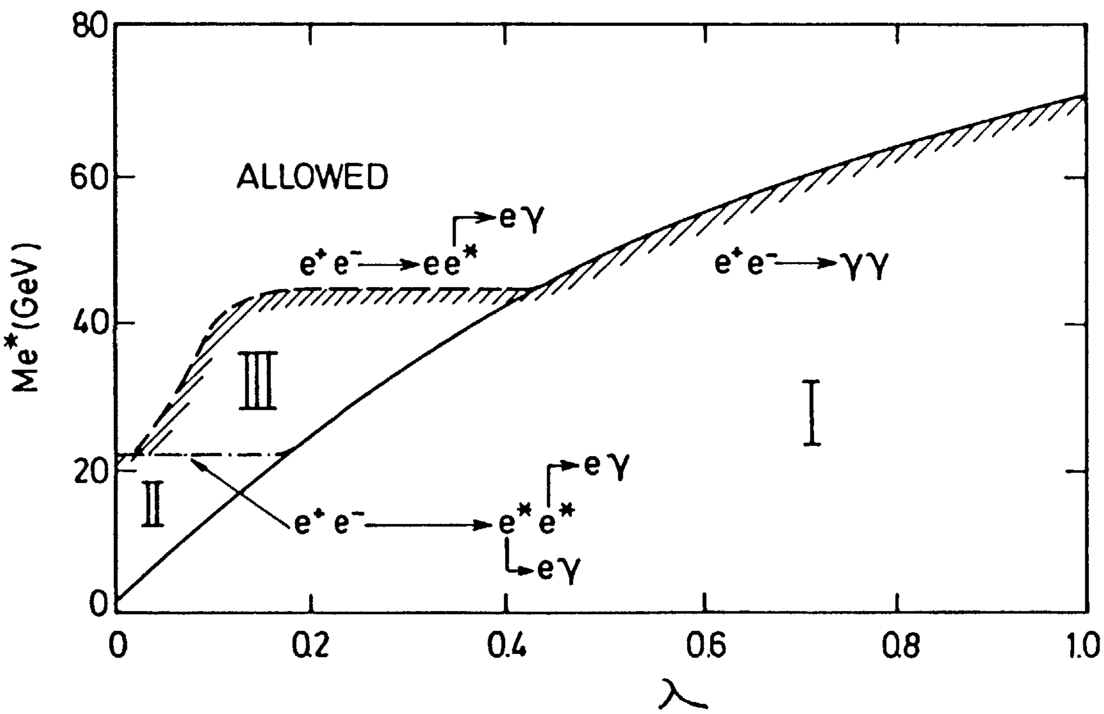

80
60
40
20
0
Me*(GeV)
0
0.2
0.4
0.6
0.8
1.0
λ
ALLOWED
e+e- → ee*
→ eγ
e+e- → γγ
III
I
II
e+e- → e*e*
→ eγ
→ eγ

Fig. 6.4

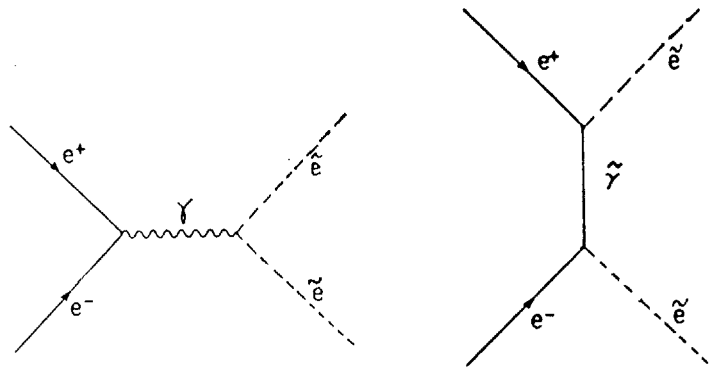

e+
e-
γ
ẽ
ẽ
e+
e-
γ̃
ẽ
ẽ

Fig. 6.5

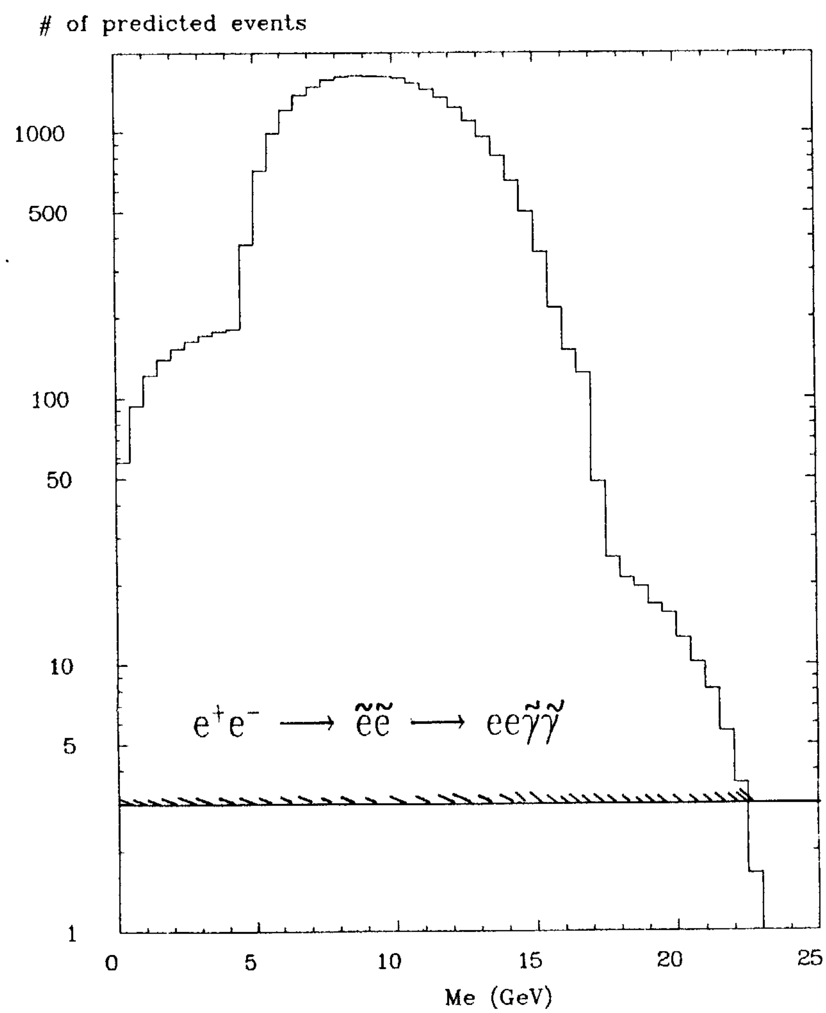

# of predicted events
1000
500
100
50
10
5
1
0
5
10
15
20
25
Me (GeV)
$e^+e^- \longrightarrow \tilde{e}\tilde{e} \longrightarrow ee\tilde{\gamma}\tilde{\gamma}$

Fig. 6.6

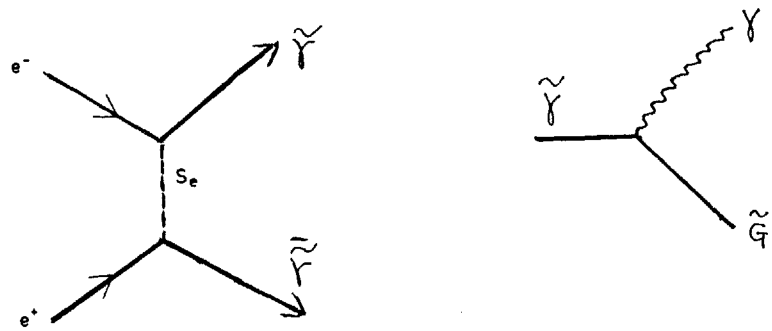

e⁻
e⁺
s_e
$\tilde{\gamma}$
$\tilde{G}$
γ

Fig. 6.7

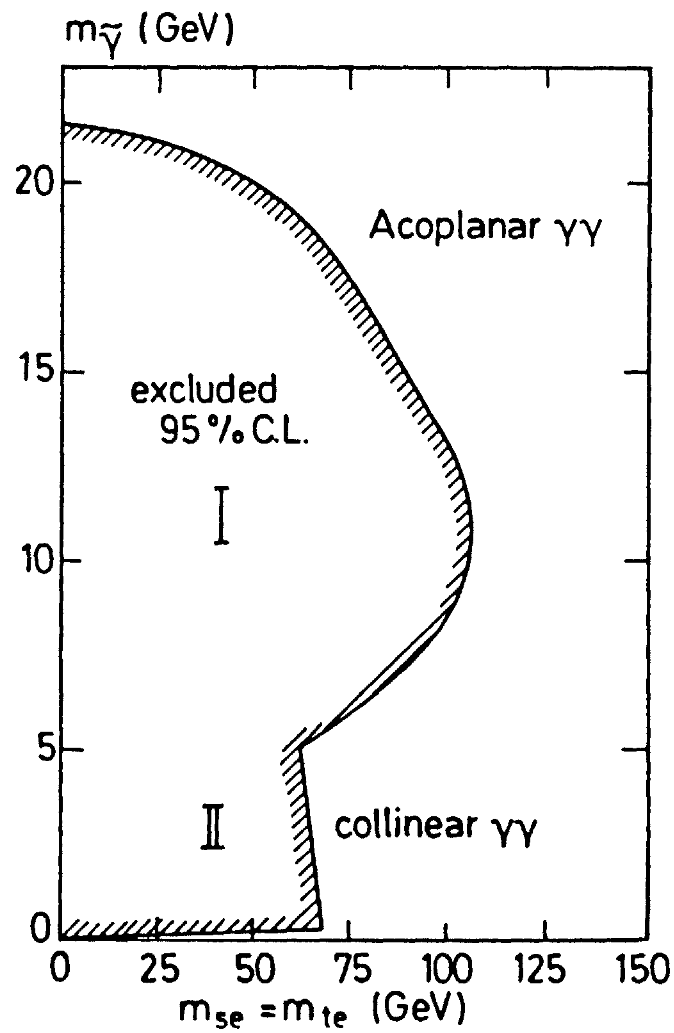

$m_{\tilde{\gamma}}$ (GeV)
Acoplanar γγ
excluded
95 % C.L.
I
II
collinear γγ
$m_{se} = m_{te}$ (GeV)
0
5
10
15
20
0
25
50
75
100
125
150

Fig. 6.8

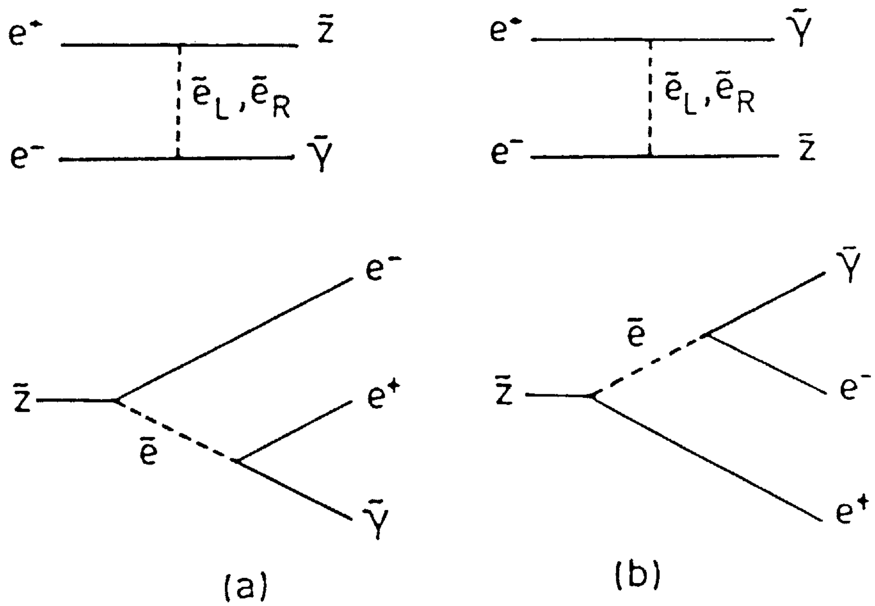

Fig. 6.9

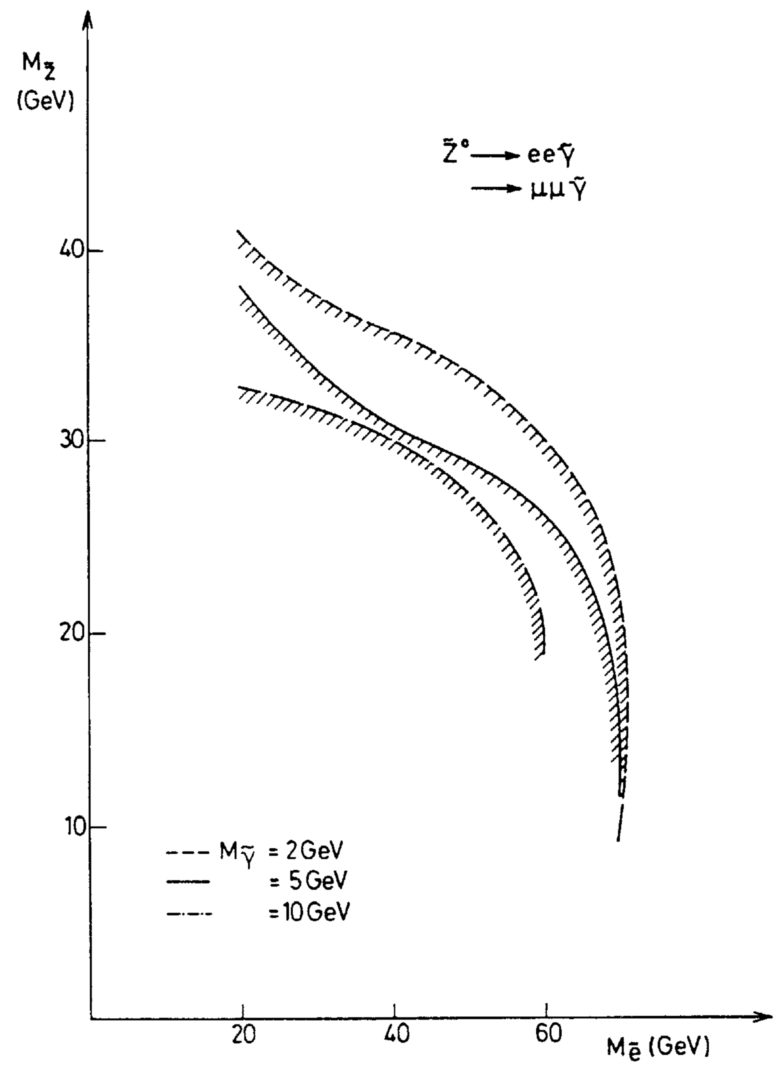

Fig. 6.10

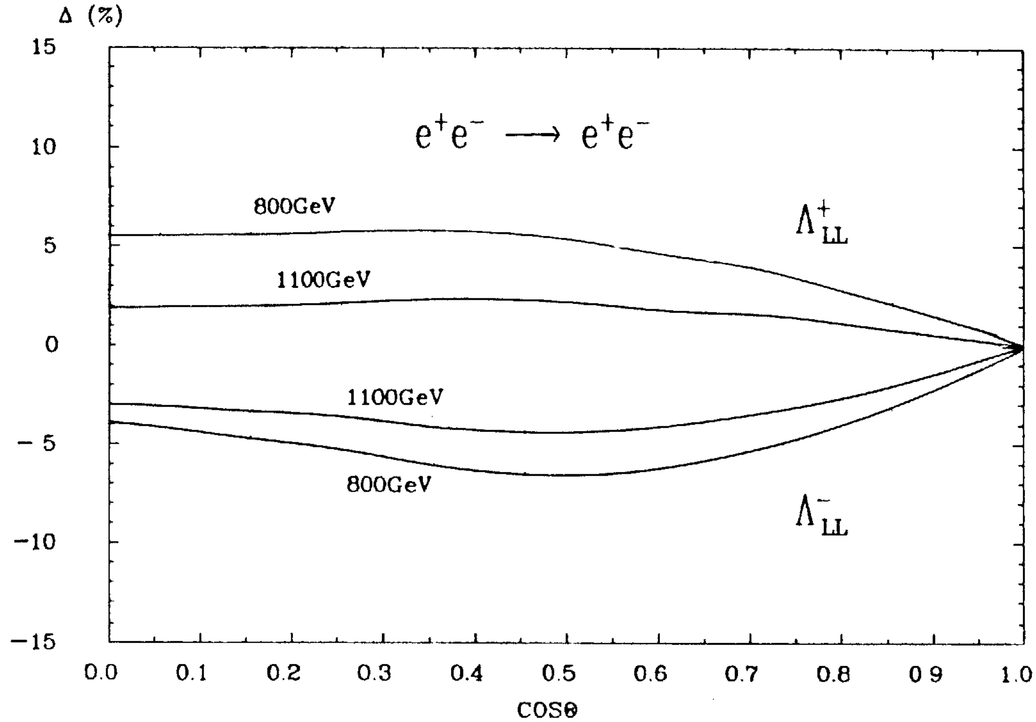

PREON MASS SCALAR

Fig. 6.11

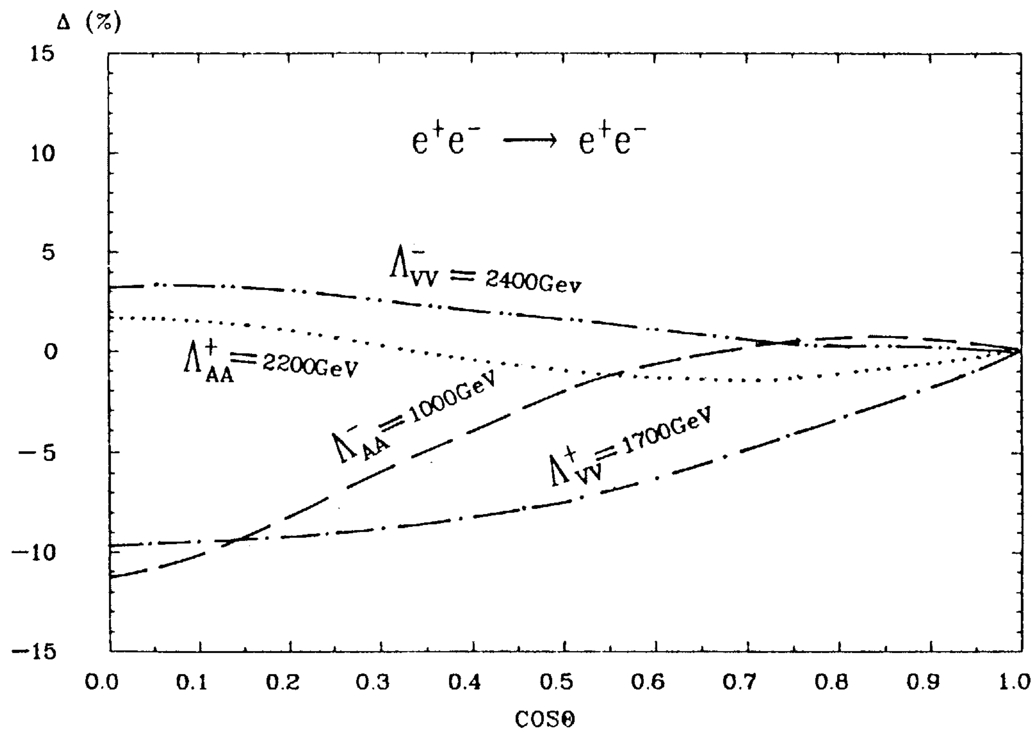

PREON MASS SCALAR

Fig. 6.12

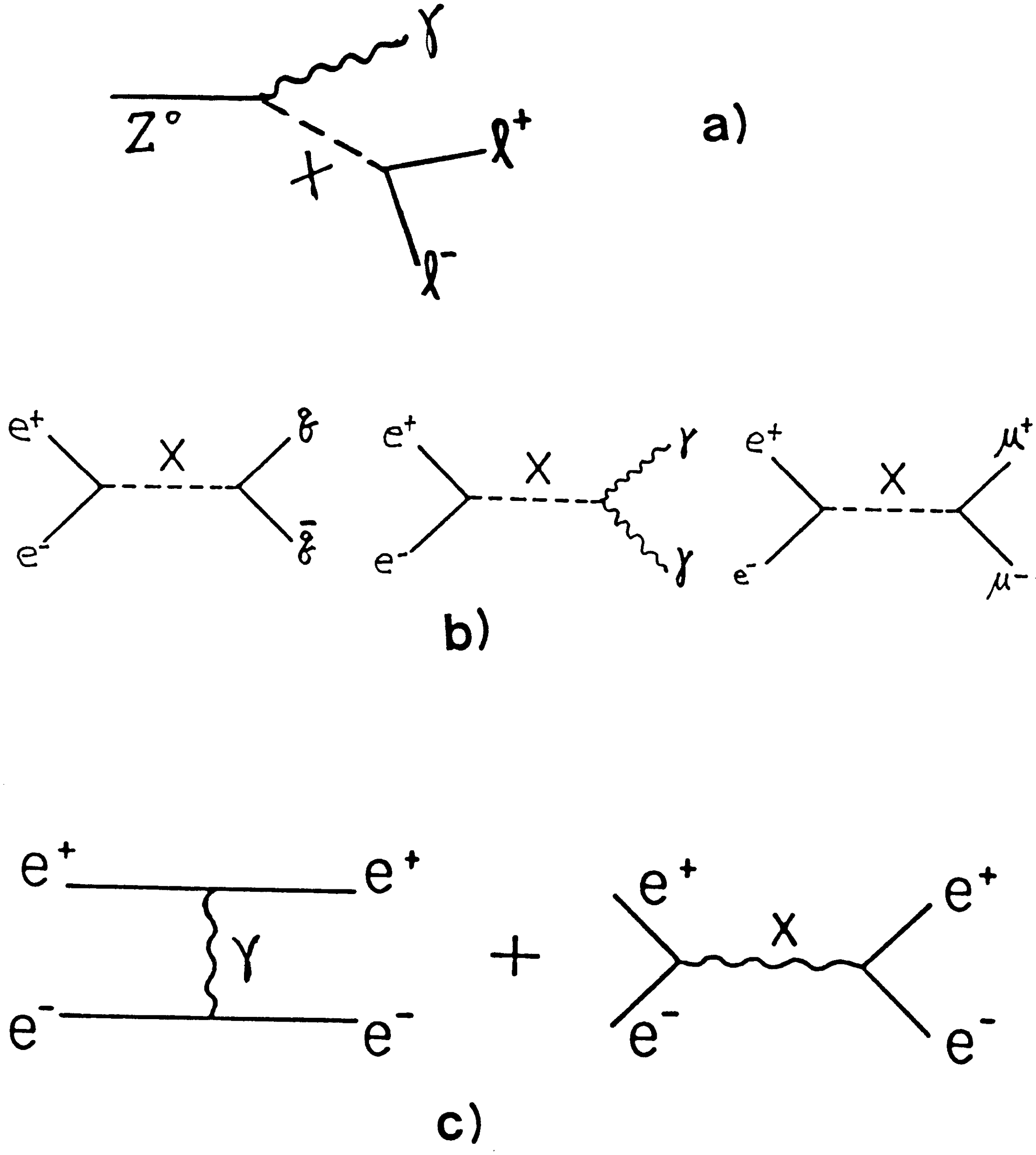

Fig. 6.13

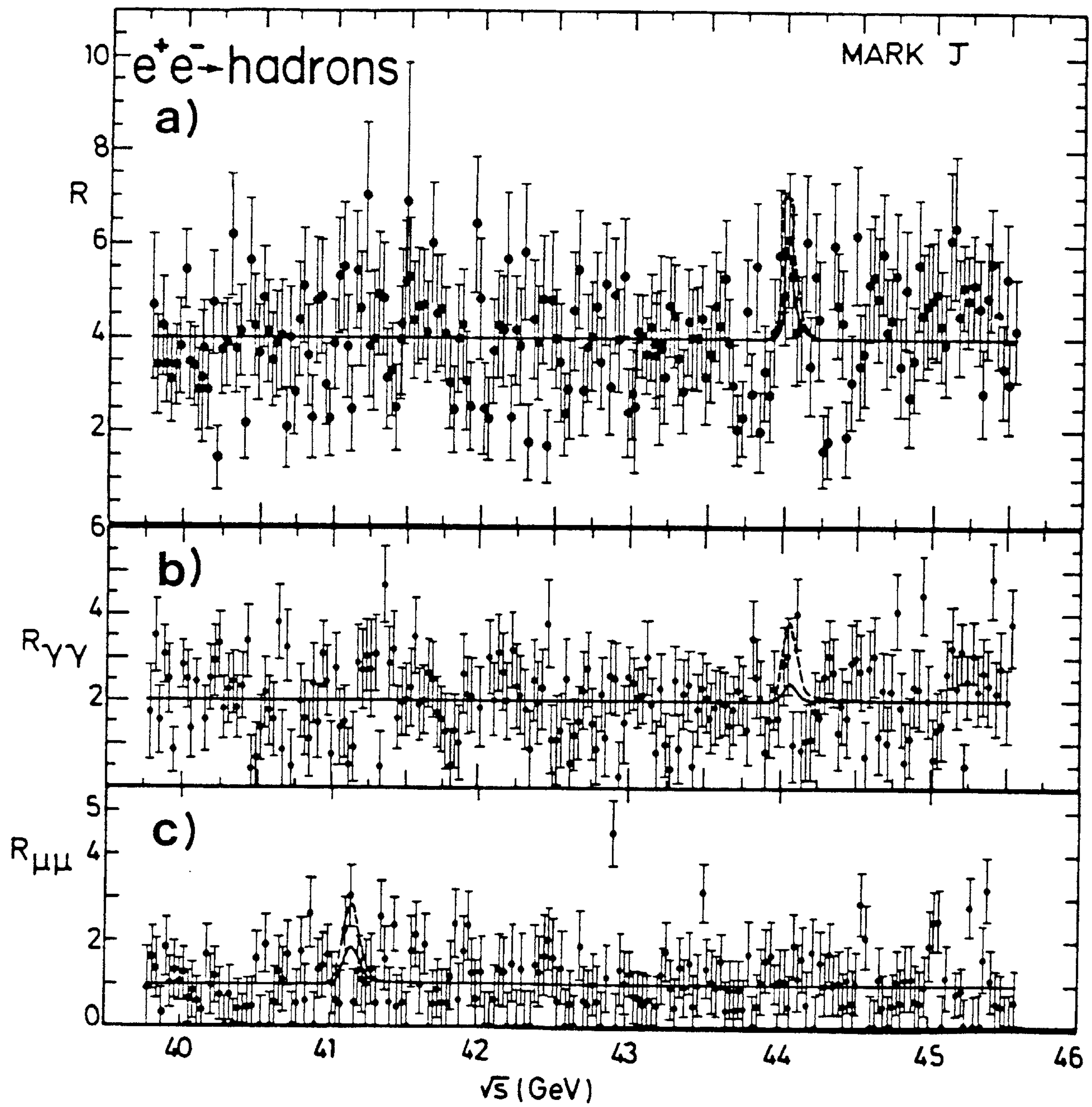

e+e-→hadrons
MARK J
a)
R
10
8
6
4
2
6
b)
Rγγ
4
2
5
c)
Rμμ
4
2
0
40
41
42
43
44
45
46
√s (GeV)

Fig. 6.14

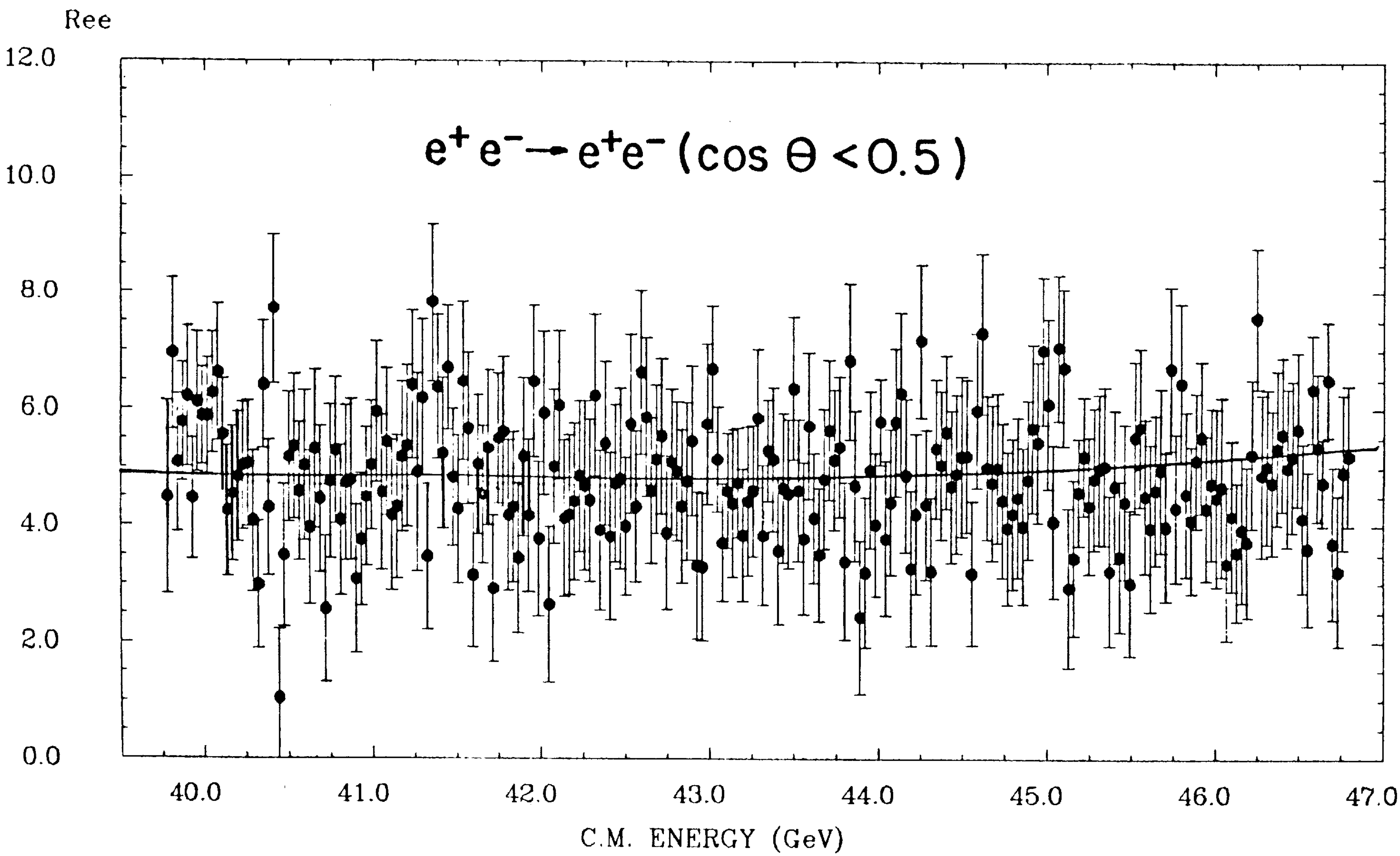

Ree
$e^+e^- \to e^+e^- (\cos\Theta < 0.5)$
12.0
10.0
8.0
6.0
4.0
2.0
0.0
40.0
41.0
42.0
43.0
44.0
45.0
46.0
47.0
C.M. ENERGY (GeV)

Fig. 6.15